

國立交通大學
光電工程學系
博士論文

超高頻光毫米波產生
與60-GHz光載微波無線訊號系統

Ultra-High Frequency Optical Millimeter-Wave
Generation and 60-GHz Radio-over-Fiber Systems

研 究 生：施伯宗
指 導 教 授：陳智弘 教授
 祁 姓 教授

中華民國九十九年九月

**Ultra-High Frequency Optical Millimeter-Wave
Generation and 60-GHz Radio-over-Fiber Systems**

by
Po-Tsung Shih

A Dissertation
Submitted to Department of Photonics
College of Electrical and Computer Engineering
Nation Chiao-Tung University
in partial Fulfillment of the Requirements
for the Degree of
Doctor of Philosophy
September, 2010

摘 要

論文標題：超高頻光毫米波產生與 60-GHz 光載微波無線訊號系統

指導教授：陳智弘 教授

祁姓 教授

國立交通大學，光電工程研究所

隨著科技的發展，毫米波訊號的產生與應用更為受到重視。毫米波訊號不只可應用於寬頻無線訊號傳輸，更可利用於雷達系統、汽車防撞系統、天文應用與毫米波顯像系統。然而，由於在空氣與銅導線之中的高傳輸損耗，毫米波訊號的產生與傳送依然存在許多挑戰。因此，利用低損耗的光纖網路並配合光倍頻技術，光毫米波訊號產生技術吸引各方的注目。

在這份論文當中，我們提出了使用四倍頻、八倍頻以及 12 倍頻的光毫米波產生技術，並使用理論以及實驗來分析及驗證系統。所提出之架構，可以產生超高頻、高純度之光毫米波訊號，提供給不同之毫米波應用使用。

基於所提出之光毫米波產生與光昇頻系統，我們可以將其利用於 60-GHz 光載微波無線訊號系統，並傳輸超過數個 Gbps 的訊號。在同時利用電與光昇頻技術，我們提出了 Tandem-Single Sideband 與六倍頻的 60-GHz 系統。在這些系統當中，我們達成了 21-Gbps 的訊號傳輸，並且在經過 25 公里光纖傳輸之後，並無明顯的訊號損耗。我們同時也提出，利用強度調變直接偵測(IMDD)的 60 GHz RoF 系統。系統架構非常簡單的 IMDD 系統，產生雙旁帶的訊號，因此將有光纖色散所造成之訊號衰退現象，在本論文中也有詳細之討論。利用 IMDD 的系統，我們達成 60-GHz 全雙工雙向 21-Gbps 訊號傳輸，並且達成 500 公尺光纖與 10 公尺無線傳輸。此 IMDD 系統，將可應用於短距離室內 60-GHz RoF 系統。

在本論文中，我們也同時提出整合有線基頻傳輸與光載微波無線訊號之整合型擷取網路系統。所提出之架構，可同時提供射頻 M-array PSK 訊號，與基頻 OOK 訊號。並且在遠端節點不需窄頻的光濾波器，將射頻與基頻訊號作分離，因此將可相容於現存的被動光纖網路(PON)架構之中。所提出之架構，在經過 25 公里光纖傳輸之後，基頻 OOK 與射頻 PSK 訊號，皆沒有明顯因光纖傳輸所造成之訊號衰減現象。



ABSTRACT

Title of Dissertation: Ultra-High Frequency Optical Millimeter-Wave Generation and 60-GHz Radio-over-Fiber Systems

Po-Tsung Shih, Ph.D., 2010

Dissertation Directed by: Jyehong Chen, Associate Professor
Sien Chi, Professor
Department of Photonics
National Chiao Tung University

With the rapidly developing of technologies, optical millimeter-wave signal generation attracts a lot of interests for various kinds of applications. Not only in broadband wireless communication systems, but high frequency millimeter-wave signals can be utilized in radar, car anti-collision system, radio astronomy and imaging. However, millimeter-wave signal generation and transmission still remain great challenges due to the high propagation loss in air and in copper cables. Based on the extremely low loss of the optical fiber, generation of optical millimeter-wave signal with frequency multiplication attracts a lot of attentions.

In this dissertation, optical millimeter-wave signal generation with frequency quadrupling, octupling and 12-tupling are proposed, theoretically analyzed and experimentally demonstrated. Optical millimeter-wave signals with ultra-high frequencies and high undesired optical sideband suppression ratios can be generated using low-frequency optical modulator, components and equipments. Because the high undesired optical sideband suppression ratios, high purity millimeter-wave signals can be generated and suitable for various kind of millimeter-wave applications.

Based on the optical millimeter-wave signal generation and up-conversion systems, 60-GHz radio-over-fiber (RoF) system which provides wireless transmission with multi-Gbps data-rate can be achieved. A asymmetrical full-duplex bidirectional RoF system based on tandem-single-sideband (TSSB) modulation technique, and an

optical up-conversion system with frequency sextupling for 60-GHz RoF links are proposed. Transmission of 25-km standard single mode fibers can be achieved without significant receiver power penalties.

A 2×21 -Gbps symmetrical bidirectional full-duplex system at 60 GHz based on intensity modulation direct detection (IMDD) technique which is a very simple architecture is also proposed. Although chromatic dispersion induced performance fading issues are observed in the IMDD systems due to the double-sideband (DSB) modulation scheme, 500-m fiber transmission and 10-m wireless transmission with acceptable receiver power penalties can be achieved without any dispersion compensation. Based on the very simple architectures and fully transparent characteristic of the bidirectional IMDD systems, the proposed systems are ideal for in-building high data-rate wireless applications, which are characterized by short fiber spans.

Multi-service hybrid access networks which supports both RoF and fiber to the x (FTTx) systems attract a lot of interests. Two multi-service hybrid access network systems which simultaneously generate and transmit radio frequency (RF) M-array phase shift keying (PSK) signal and baseband (BB) On-Off-keying (OOK) signal are proposed and experimentally demonstrated. The wired BB signal is compatible with the existing passive optical network (PON) system, and the wireless RF PSK signal can also share the same distributed infrastructure. No dispersion induced fading issues are expected and no narrow band optical filter is needed at the remote nodes in the proposed systems. After transmission over 25-km standard single mode fiber, no significant receiver power penalties are observed in both RF and BB channels in the proposed systems.

致 謝

四年的博士班終於完成了，能夠順利拿到博士學位，當然有非常多的人需要感謝。首先，要感謝指導教授 陳智弘老師與 祁姓老師，在這四年當中，提供了無數的資源、實驗設備與環境、以及無私的指導跟照顧，並且願意讓我多次出席國際學術演討會與參加為期一年的千里馬計畫，這讓我不只充實專業領域的知識，更讓我能夠感受到不同的文化與生活方式。

此外，要特別感謝林俊廷學長，在他的耐心指導之下，讓我不只學習到專業領域與實驗上的知識、觀念與技巧，更教導我學習論文寫作，並且帶著我參加各個國際研討會，讓我從甚麼都不懂到可以自己四處闖蕩。在參加千里馬計畫的初期，更幫助我很快在美國安頓下來，迅速的進入狀況，進行在美國的實驗。

由於參加國科會的千里馬計畫，讓我有機會到美國康寧公司的研究部門，參與一年的研究計畫。要非常感謝 Anthony Ng'oma 博士，在那一年當中，我不只學習到了很多專業知識、實驗技巧，更了解與體驗到了不同國家的文化與生活方式。還要感謝 Michael Sauer 博士、Connie Wang 博士、Fred Sears 博士與 Bruce Chow 博士，由於他們的幫助，才能促使這個計畫的順利進行。更要感謝 Frank Annunziata、Jason Hurley、Boh Ruffin、Becki Rappleye、Jacob Geroge、Ming Li Yee、Seldon Benjamin，由於他們的協助，才能讓我獨自在美國的實驗順利完成而且有個多采多姿的生活。

另外，還要感謝實驗室的學弟妹們，江文智、吳芳民、戴盛鵬、陳昱宏、黃漢昇、翁而姿、何燕霖、王何立穎，由於你們的協助與陪伴，才能讓我的實驗與論文順利完成。

最後，當然要感謝我的家人們，感謝多年來你們的支持與鼓勵，讓我可以無後顧之憂的專心唸書。真的非常謝謝你們。

終於要離開這個待了十年的學校了，帶著豐碩的收穫與滿滿的回憶，邁向下個人生里程，再見了交大。

施伯宗 于 風城交大 民國九十九年九月

ACKNOWLEDGEMENTS

Finally, I finished my Ph. D program in four years and got my Ph. D degree. First of all, I would like to thank my advisors, Prof. Jyehong Chen and Prof. Sien Chi, for their kind supports and advices during my Ph. D Program. They also gave me many chances to attend international conferences and to participate in the international internship program which gave me a lot of professional knowledge and experiences of many different cultures. Thank you.

I would also like to thank Prof. Chun-Ting Lin. Thank him for his kindness and patient of teaching me the professional knowledge and experimental skills. He also led me to join the international conferences and helped a lot at the beginning of the international internship program. Without him, it should be difficult for me to finish the Ph. D program within this short period. Thank you.

Because the project of Nation Science Council, I got the chance to participate in the internship program of Corning Incorporated in the US. I would like to thank Dr. Anthony Ng'oma who also taught me a lot about the professional knowledge and many experimental skills. I also would like to thank Dr. Michael Sauer, Connie Wang, Dr. Fred Sears, Dr. Bruce Chow for their help to this international cooperation. Finally, I would like to thank Frank Annunziata · Jason Hurley · Boh Ruffin · Becki Rappleye · Jacob Geroge · Ming Li Yee · Seldon Benjamin. They helped me a lot during my stay in US and make it very colorful. Thank you.

I would also like to thank all of the junior students, Wen-Jr Jiang, Fang-Ming Wu, Sheng-Peng Dai, Yu-Hung Chen, Han-Sheng Huang, Er-Zih Wong, Li-Ying Wang-He, and Yen-Lin Ho, for their great help in my experiments and dissertation. Thank you.

Finally, I would like to thank my families. Without your help and support, I cannot concentrate on my study and get my Ph. D degree. Thank you.

Po-Tsung (Boris) Shih,
at NCTU Hsinchu Taiwan, Sep. 2010.

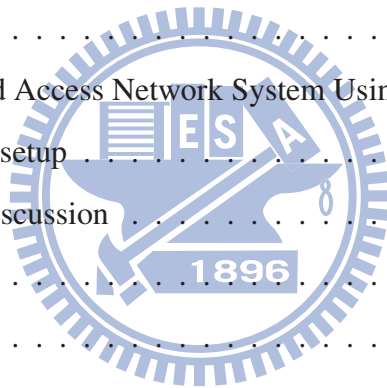
TABLE OF CONTENTS

ACKNOWLEDGMENTS	i
LIST OF FIGURES	vii
Chapter 1 INTRODUCTION	1
1.1 Introduction to Millimeter-Wave Signals	1
1.2 Generation and Transmission of Millimeter-Wave Signals	2
1.3 Radio-over-Fiber Technologies	4
1.4 60-GHz Wireless Communication Systems	5
1.5 Objective and Outlines of the Thesis	7
Chapter 2 OPTICAL MILLIMETER-WAVE GENERATION USING EXTERNAL MODULATOR AND SQUARE-LAW DETECTION	11
2.1 Double-Sideband Modulation Systems	12
2.2 Single-Sideband Modulation Systems	13
2.3 Double-Sideband with Carrier Suppression Systems	14
2.4 Square-Law Detection using Photo Diode	15
2.5 Conclusion	16
Chapter 3 OPTICAL MILLIMETER-WAVE GENERATION SYSTEM	

	WITH FREQUENCY QUADRUPLING	17
3.1	Concept and Theoretical Model	18
3.2	Impact of The PD-MZM Imbalance	22
3.3	Experimental Results	27
3.4	WDM Up-Conversion Employing Frequency Quadrupling	31
3.4.1	Concept	31
3.4.2	Experimental Setup	33
3.4.3	Results and Discussion	34
3.5	Conclusion	38
Chapter 4	OPTICAL MILLIMETER-WAVE GENERATION SYSTEM WITH HIGHER ORDER MULTIPLICATION	41
4.1	Optical Millimeter-Wave Generation with Frequency Octupling	42
4.1.1	Concept and Theoretical Model	42
4.1.2	Experimental Setup and Results	46
4.1.3	Summary	51
4.2	W-Band Wireless Communication	52
4.2.1	Device Structure And Measurement Setup	53
4.2.2	Experimental Results	56
4.2.3	Summary	59
4.3	Optical Millimeter-Wave Generation with Frequency 12-tupling	60
4.3.1	Concept and Theoretical Model	60
4.3.2	Experimental setup and results	64
4.3.3	Summary	66
4.4	Conclusion	67

Chapter 5	60-GHZ RADIO-OVER-FIBER COMMUNICATION SYSTEM	73
5.1	Orthogonal-Frequency-Division-Multiplexing Modulation Format	74
5.1.1	Introduction	74
5.1.2	OFDM signal generation	75
5.2	Tandem-Single-Sideband Modulation System	77
5.2.1	Concept	77
5.2.2	Experimental Setup	78
5.2.3	Experimental Results and Discussion	80
5.2.4	Summary	83
5.3	Modulation System with Frequency Sextupling	84
5.3.1	Concept	84
5.3.2	Experimental Setup	86
5.3.3	Experimental Results and Discussion	88
5.3.4	Summary	90
5.4	Intensity Modulation Direction Detection Systems Using a Mach-Zehnder Modulator	92
5.4.1	Experimental Setup	92
5.4.2	Results and Discussion	94
5.4.3	Summary	96
5.5	Intensity Modulation Direction Detection System Using an Electro-absorption Modulator	97
5.5.1	Experimental Setup	99
5.5.2	Results and Discussion	100
5.5.3	Summary	101
5.6	Full-Duplex Bidirectional Transmission	103

5.6.1	Experimental Setup	104
5.6.2	Results and Discussion	105
5.6.3	Summary	108
5.7	Conclusion	109
Chapter 6	MULTI-SERVICE HYBRID ACCESS NETWORK	111
6.1	Multi-Services Hybrid Access Network System Using A Dual-Electrode MZM	112
6.1.1	Concept	112
6.1.2	Experimental setup	114
6.1.3	Results and discussion	115
6.1.4	Summary	117
6.2	Multi-Services Hybrid Access Network System Using A DP-MZM . .	119
6.2.1	Experimental setup	119
6.2.2	Results and discussion	121
6.2.3	Summary	123
6.3	Conclusion	124
Chapter 7	CONCLUSIONS	125
Appendix A	IMBALANCE OF CONVENTIONAL MZM	129
Appendix B	CHROMATIC DISPERSION INDUCED RF FADING IN DSB MODULATION SCHEME	133
	REFERENCES	137
	PUBLICATION LIST	149



LIST OF FIGURES

1.1	Features of millimeter-wave signals.	2
1.2	Concept of RoF technologies.	4
1.3	Data-range versus signal coverages of various kinds of wireless systems.	6
1.4	Propagation losses at 2.4 GHz and 60 GHz.	7
2.1	Double sideband (DSB) modulation scheme	13
2.2	Single sideband (SSB) modulation scheme	14
2.3	Double sideband with carrier suppression (DSB-CS) modulation scheme	15
2.4	Double sideband with carrier suppression (DSB-CS) modulation scheme	15
3.1	Optical colorless up-conversion using a frequency multiplication technique for WDM RoF systems.	18
3.2	Setup of the optical frequency-quadrupled millimeter-wave signal generation system.	19
3.3	(a) Illustrated optical spectrum and (b) Illustrated electrical spectrum of of frequency-quadrupled optical millimeter-wave signal	20
3.4	Schematic principle of the optical millimeter-wave generation with frequency quadrupling	22
3.5	DP-MZM with Y-splitter imbalance.	23

3.6	Simulated optical spectra of 40-GHz optical millimeter-wave signals using the quadrupling system (a) with 25-dB extinction ratios; (b) with 25-dB extinction ratios and driving signal trimming.	26
3.7	Experimental results of 40-GHz optical millimeter-wave signal spectrum using maximum transmission operation mode. The resolution is 0.01 nm.	28
3.8	Measured electrical spectrum of the generated 40-GHz millimeter-wave signal without fiber transmission.	29
3.9	Electrical spectra of the generated 40-GHz millimeter-wave signals with 100-Hz span. (a) Comparison of the generated 40-GHz signal and 10-GHz driving signal, (b) Comparison of generated 40-GHz signal at back-to-back and with 50-km single mode fiber transmission . The resolution bandwidth is 1 Hz.	30
3.10	Measured optical spectrum of the generated 72-GHz optical millimeter-wave signal.	31
3.11	Conceptual diagram of a WDM up-conversion system.	32
3.12	Experimental setup of the WDM up-conversion system. (PC: polarization controller; TOF: tunable optical filter; RN: remote node; BPF: band pass filter; LPF: low pass filter; BERT: bit error rate tester.) . . .	34
3.13	Sensitivities and harmonic distortion suppression ratio versus MZ-a bias drifts, and optical spectrum with different bias drifts.	36
3.14	Sensitivities and harmonic distortion suppression ratio versus MZ-c bias drifts, and optical spectrum with different bias drift.	36

3.15	Sensitivities and harmonic distortion suppression ratio versus all sub-MZ bias drifts, and optical spectrum with different bias drift.	36
3.16	Optical spectra of the (a) BB WDM signals; (b) 20-GHz WDM signals.	37
3.17	BER curves of the 20-GHz WDM signals at (a) 20-GHz; (b) Baseband.	38
3.18	Spectra of Up-converted WDM signals at (a) 40-GHz; (b) 60-GHz. . .	39
4.1	Conceptual diagram and experimental setup of the frequency-octupled optical millimeter-wave signal generation system.	43
4.2	Principle of the frequency-octupled optical millimeter-wave signal generation system.	45
4.3	Optical spectra of (a) the 30-GHz millimeter-wave signal generated from the first stage of the frequency octupling system; (b) the generated 60-GHz millimeter-wave signal from the frequency octupling system.	47
4.4	(a) Optical carrier suppression ratio versus phase delay of two DP-MZMs and optical spectra of (b) 30 deg (c) 60 deg phase delay.	48
4.5	Time domain waveform of the generated 60-GHz millimeter-wave signal (a) BTB (b) 25-km SMF Transmission. (100 mV/div; 5 ps/div)	48
4.6	Electrical spectrum of the generated 60-GHz millimeter-wave signal. .	49
4.7	Optical spectrum of the generated 80-GHz optical millimeter-wave signal.	49
4.8	Undesired sideband suppression ratio versus first DP-MZM bias deviation ratio, and optical spectra.	50

4.9	Undesired sideband suppression ratio versus second DP-MZM bias deviation ratio, and optical spectra.	50
4.10	Undesired sideband suppression ratio versus all DP-MZM bias deviation ratio, and optical spectra.	50
4.11	(a)The top-view of the demonstrated device; (b) the measured and fitted OE frequency response of the used NBUTC-PD chip under -3V bias; (c) the conceptual diagram and (d)picture of our device for feeding WR-10 waveguide.	54
4.12	(a) the transfer curve of measured millimeter-wave power with corresponded photocurrent vs. reverse DC bias; (b) the same power trace plot in linear scale.	55
4.13	The system setup for W-band wireless QPSK or 8-QAM data transmission.	56
4.14	(a) transmission distance vs. $-\log(\text{BER})$ of 2.5Gbit/s QPSK wireless data transmission under different photocurrent and bias condition. And the constellations under (b) 15cm and (c) 180cm transmission distance with 9mA photocurrent. The inset shows the corresponded in-phase (I) and quadrature-phase (Q) eye-patterns of these constellations.	57
4.15	(a) transmission distance vs. EVM of 3.75-Gbit/s 8QAM wireless data transmission with different photocurrent and bias condition. And the constellations under (b) 25 cm and (c) 170 cm transmission distance with 9mA optimized photocurrent and optimized condition.	58

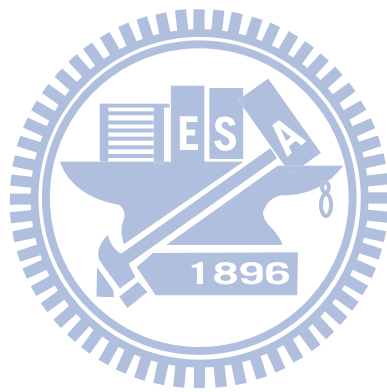
4.16	Constellation diagrams of 8QAM signals with (a) 50-km fiber transmission and 25-cm wireless transmission; (b) 100-km fiber transmission and 25-cm wireless transmission; (c) 50-km fiber transmission and 170-cm wireless transmission; (d) 100-km fiber transmission and 170-cm wireless transmission.	59
4.17	Conceptual diagram of the optical millimeter-wave signal generation with frequency 12-tupling.	61
4.18	Conceptual diagram of (a) 120-GHz and (b) 210-GHz optical millimeter-wave generations.	68
4.19	Optical spectrum of the generated optical tones separated by 40 GHz without modulation-depth trimming.	69
4.20	Optical spectrum of the generated optical tones after the FWM for 120-GHz optical millimeter-wave signal generation without modulation-depth trimming.	69
4.21	Optical spectrum of the generated optical tones separated by 40 GHz.	70
4.22	Optical spectrum of the generated optical tones after the FWM for 120-GHz optical millimeter-wave signal generation.	70
4.23	Optical spectrum of the generated optical tones separated by 120 GHz.	71
4.24	Optical spectrum of the generated optical tones separated by 70 GHz.	71
4.25	Optical spectrum of the generated optical tones after the FWM for 210-GHz optical millimeter-wave signal generation.	72
4.26	Optical spectrum of the generated optical tones separated by 210 GHz.	72

5.1	Conceptual diagrams of the OFDM signal generator and demodulator.	76
5.2	Conceptual diagram of the frequency doubling system using TSSB modulation.	78
5.3	Experimental setup of the frequency doubling system using TSSB modulation.	79
5.4	Electrical and optical spectra of the TSSB system.	80
5.5	OPR versus $-\log(\text{BER})$ of the QPSK-OFDM signal.	82
5.6	BER curves and constellation diagrams of the down-link transmission. (a) Back-to-back without one-tap equalizer; (b) back-to-back with one-tap equalizer; (c) 50-km SSMF.	82
5.7	BER curves of the OFDM system uplink 1.25-Gb/s OOK signals. . .	83
5.8	Conceptual diagram of the 60-GHz vector signal generation system with frequency sextupling.	85
5.9	The principle of the proposed RoF system with frequency sextupling.	86
5.10	Experimental setup of the frequency sextupling system.	87
5.11	Bit error rate versus optical power ratio curve and constellation diagrams of the QPSK-OFDM signal, and constellations with (a) -1-dB , (b) 6-dB , and (c) 9-dB OPR.	89
5.12	Error vector magnitude versus optical power ratio curve and constellation diagrams of the 8QAM-OFDM signal, and constellations with (a) 0-dB , (b) 5-dB , and 10-dB OPR.	90

5.13 Bit error rate curves of the QPSK-OFDM signal fiber transmission results.	91
5.14 Error vector magnitude curves of the 8QAM-OFDM signal fiber transmission results.	91
5.15 Experimental setup of the simple IMDD 60-GHz RoF system using a MZM.	93
5.16 Electrical spectrum of the down-converted OFDM signal.	95
5.17 Constellation diagrams of the recovered 21-Gbps 8QAM OFDM signals with (a) 60 m and (b) 560 m fiber transmission distances.	96
5.18 SNR vs. Received Optical Power with different fiber distances and 10-m wireless transmission distance.	97
5.19 Impact of fiber chromatic dispersion on the SNR performance of the 60 GHz IMDD RoF and 60.5-GHz sinusoidal signal.	98
5.20 Experimental setup of the simple IMDD 60-GHz RoF system using a R-EAM.	100
5.21 Electrical spectra of the down-converted OFDM system in the EAM IMDD system.	101
5.22 SNR vs. Received Optical Power with different fiber distances and 3-m wireless transmission distance.	102
5.23 Receiver sensitivities comparison between the IMDD systems using a MZM and an EAM.	102

5.24	Experimental setup of the symmetrical full-duplex bidirectional 60-GHz RoF system.	104
5.25	Receiver performance with simplex and full-duplex modes with perpendicular antenna polarization.	106
5.26	SNR curves transmission at BTB and with 500m fiber transmission for (A) down-link; (B) up-link.	107
5.27	Constellations with -6-dBm received optical power for (a) Down-link at BTB; (b) Down-link with fiber transmission; (c) Up-link at BTB; (d) Up-link with fiber transmission.	108
6.1	Conceptual diagram of a multi-service hybrid access network system.	112
6.2	Conceptual diagram of a square-law detection of the proposed system.	113
6.3	Experimental setup for RF and BB signal generation and transmission.	114
6.4	BER curves of BPSK signals.	115
6.5	Spectra (Resolution 0.01 nm) and eye diagrams of BPSK signals. (a) -6dB; (b) 0dB; (c) +6dB	116
6.6	BB OOK and RF BPSK sensitivities with different RF OOK to RF BPSK optical subcarrier power ratios.	117
6.7	Optimized BTB optical spectrum. (Resolution: 0.01 nm)	118
6.8	BER curves of BB OOK and RF BPSK BTB and after transmission over 25km.	118

6.9	Experimental setup of the multi-services hybrid access network system using a DP-MZM.	120
6.10	$-\log(\text{BER})$ versus Optical Power Ratio between PSK optical sideband and new carrier.	121
6.11	Optical Power Ratio between 8PSK and new carrier.	122
6.12	BER curves of OOK (w/ 8PSK), 8PSK, OOK (w/ QPSK) and QPSK.	123
6.13	Constellations and eye diagrams. (a) 8PSK BTB; (b) 8PSK 25km; (c) OOK w/ 8PSK BTB; (d) OOK w/ 8PSK 25km; (e) QPSK BTB; (f) QPSK 25km; (g) OOK w/ QPSK BTB; (h) OOK w/ QPSK 25km. (Eye diagrams 100 mV/div; 200 ps/div)	124
A.1	Conceptual diagram of an imbalanced MZM.	129
B.1	Conceptual diagram of a DSB optical spectrum.	133
B.2	Simulation results of dispersion induced fading of a 60.5-GHz DSB optical millimeter-wave signal.	135



Chapter 1

INTRODUCTION

1.1 Introduction to Millimeter-Wave Signals

Millimeter-waves are electro-magnetic waves with frequency range from 30 to 300 GHz. The related wavelengths of millimeter-waves are from 1 to 10 mm, and that is the origin of the name. Electro-magnetic waves with frequencies higher than 300 GHz and lower than 3 THz are usually defined as THz-waves, and the related wavelengths are range from $100\ \mu\text{m}$ to 1 mm.

Microwaves have relatively low frequency compared with millimeter-wave and THz-wave signals. Due to the relatively low atmospheric absorption loss, wireless propagation loss and generally unaffected by the weathers, the signal coverage distances of the microwave signals can range from hundred meters to several tens of kilometers. In the last few decades, microwaves have been widely utilized in our daily life mainly in long-range wireless communication applications including TV broadcasting, radio broadcasting, cell phone, and Wireless Fidelity (WiFi). However, with the developing of technologies and the rapidly growing demand for data-rate, the bandwidths of microwave signal are limited and cannot meet the new requirements.

To satisfy the requirements of the next generation wireless Gbps communications, millimeter-wave bands with higher frequency and broader bandwidth become the solution with the most potential. Several commercial available bands have been al-

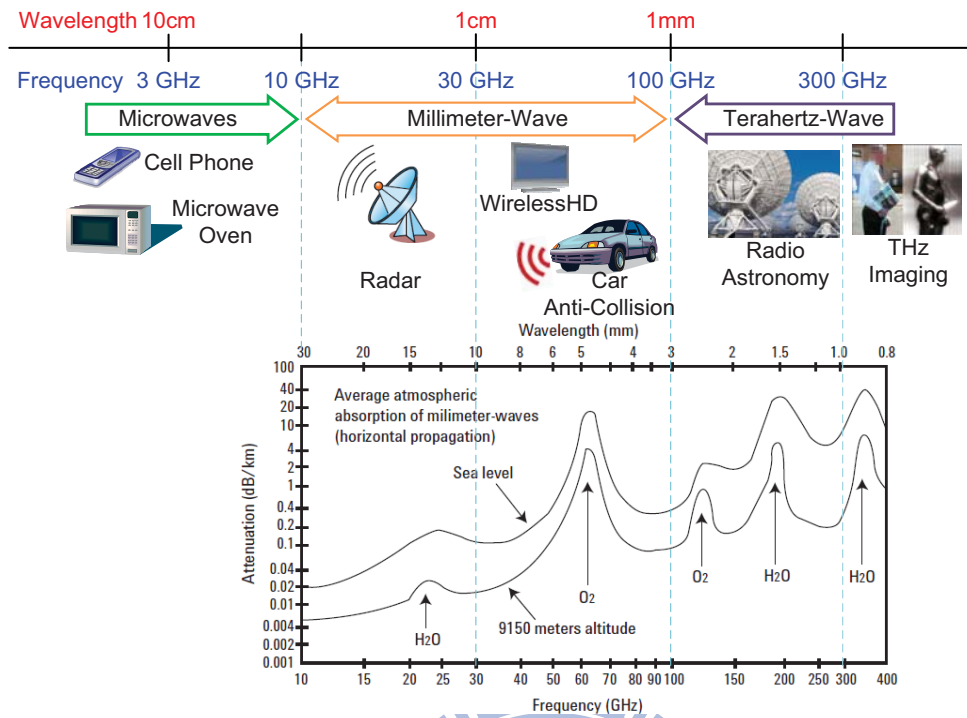


FIG. 1.1. Features of millimeter-wave signals.

located in US at 60 GHz (57-66 GHz, v-band), 70/80 GHz (71-76 GHz paired with 81-86 GHz, e-band), 90 GHz (92-94 GHz and 94.1-95 GHz, w-band) [1]. Compared with the low-frequency microwave bands, these millimeter-wave bands have very large available channel size and provide sufficient bandwidth to support Gbps wireless operation. As shown in FIG. 1.1, the millimeter-wave signals not only can be utilized in wireless communication systems, but can be used in many applications, such as radar, car anti-collision system, radio astronomy and imaging.

1.2 Generation and Transmission of Millimeter-Wave Signals

Figure 1.1 also shows the atmospheric absorption of wireless millimeter-wave signals. As can be seen, the atmospheric absorption losses increase with the increasing of the millimeter-wave frequency. Therefore, the generation and transmission of

millimeter-wave signals still remain great challenges. Although some CMOS technology can generate millimeter-wave signal beyond 60 GHz [2–5], the attenuation of millimeter-wave signal in copper wires is extremely high, which also restricts the signal transmission distance. To transmit millimeter-wave signals over a long distance, optical millimeter-wave signal based on low transmission loss optical fiber network is a cost-effective and viable solution.

Optical heterodyning using two laser sources is the most straightforward method for optical millimeter-wave signal generation. Nevertheless, optical phase-locked loop (OPLL) is required to stabilize the frequency fluctuation and minimize the phase noise of the generated optical millimeter-wave signal. The OPLL significantly increases system complexity and cost which hinder the implementation in many applications [6].

Mode-locked lasers that generate optical millimeter-wave signals with relatively low phase noise and frequencies of more than 100 GHz have been proposed [7, 8]. However, mode-locked lasers are sensitive to the environment variation including temperature fluctuation and vibrations. Therefore, a complex feedback system for long-term stabilization is usually required [9, 10].

Optical millimeter-wave signal generations using LiNbO₃ Mach-Zehnder modulator (MZM) are the most reliable approaches. Optical millimeter-wave signal generations based on single-sideband (SSB), double side-band (DSB) and double-sideband with carrier suppression (DSB-CS) have been widely investigated and demonstrated. Nevertheless, the generated optical millimeter-wave frequencies are still restricted by the bandwidth of conventional LiNbO₃ modulators, which is typically less than 40 GHz. Moreover, radio-frequency (RF) components with frequency response over 26 GHz are considerably more expensive than those below 26 GHz. In order to achieve optical millimeter-wave generation with frequency beyond 60 GHz cost-effectively, optical millimeter-wave signal generations with frequency multiplication are highly

desirable [11–13].

1.3 Radio-over-Fiber Technologies

Radio-over-Fiber (RoF) technologies utilize optical fiber networks to distribute RF signals from the central station (Head End Unit, HEU) to base stations (Remote Antenna Units, RAU). In conventional wireless system, RF signal processing such as frequency up-conversion, carrier modulation, and multiplexing are performed at the RAU and make the RAU become complex. As shown in FIG. 1.1, with the increasing of the wireless carrier frequency, the atmospheric absorptions and propagation losses increase, too. The signal coverage of each RAU is limited and referred as a pico-cell unit. To provide sufficient signal coverage, more RAUs are required in wireless millimeter-wave communication systems. If the RF signal processing is still performed at each RAU, the system expense might increase. In addition, the synchronization between all of the RAU also becomes a great challenge.

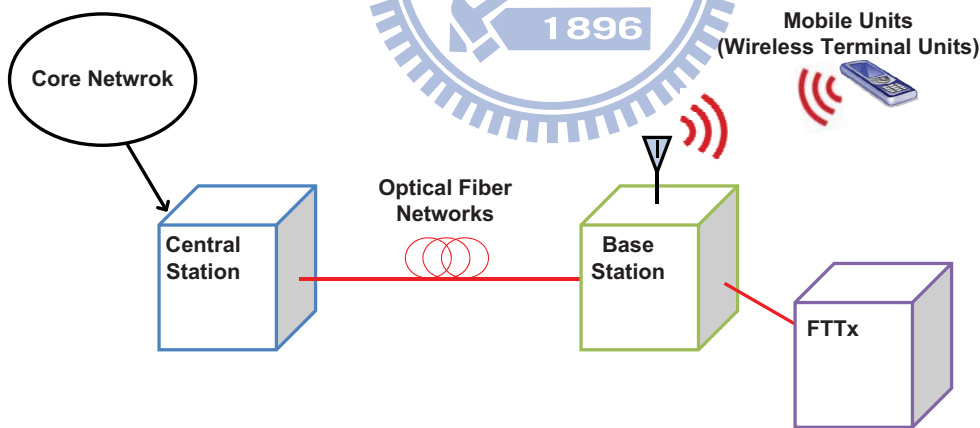


FIG. 1.2. Concept of RoF technologies.

As shown in FIG. 1.2, RoF technologies provide the feasibility of centralizing all of the RF signal processing in the shared HEU and transmit the millimeter-wave signal to the RAUs based on the low loss optical fibers (0.2 dB/km at 1550 nm). By doing

so, the RAUs become dummy antenna units which receive the optical signal, amplify the millimeter-wave signal, and feed into the antenna for wireless transmission. Due to the centralization of the RF signal processing, the high frequency equipments and components can be shared at the HEU, and the system installation and maintenance expense can be reduced.

In addition to the wireless millimeter-wave communication system, the RoF optical network can be integrated with the baseband (BB) Fiber To The x (FTTx) applications and become a multi-service hybrid access network system, as shown in FIG. 1.2. Therefore, simultaneous generation and transmission of wireless millimeter-wave signal and wired BB signals become of great interests [14–17]. By sharing one optical fiber networks for the FTTx and RoF application, the system installation and maintenance can also be reduced.

1.4 60-GHz Wireless Communication Systems

With the rapidly developing of communication and consumer electronics, the bandwidth requirement of wireless transmission become broader and broader. For example, the new standard, WirelessHD [18], which is focused on the wireless uncompressed video transmission. For an uncompressed video signal with 1920×1080 resolution, 3 colors per pixels, 32-bit high color, and 60-GHz frame rate, the total data-rate is about 12 Gbps. The target data-rate of the WirelessHD standard is up to 25 Gbps. Another standard which requires very high data-rate is the 802.15.3c Wireless Personal Area Network (WPAN) [19]. The WPAN allows very high data rate over 2 Gbit/s applications such as high speed internet access, streaming content download (Video on Demand, VoD) , real time streaming and wireless data bus for cable replacement. The optional data rates in excess of 3 Gbit/s will be provided.

Figure 1.3 shows the provided data-rate versus the signal coverage of various

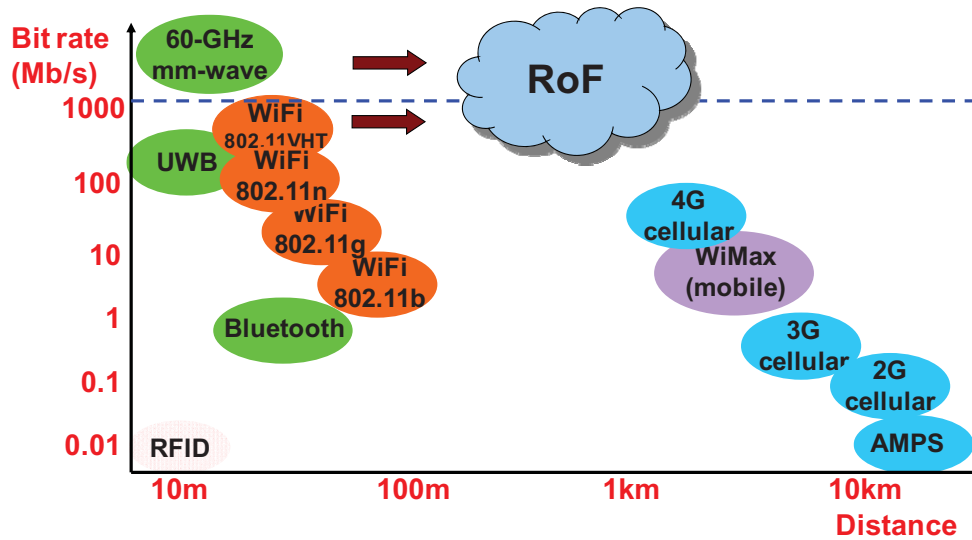


FIG. 1.3. Data-rate versus signal coverages of various kinds of wireless systems.

kinds of wireless standards. Most of the wireless standards cannot provide a wireless transmission with data-rate higher than 1 Gbps and meet the bandwidth requirements of the new applications. Thanks to the 7-GHz license-free band, 60-GHz millimeter-wave communication has a lot of attention to support multi-Gbps wireless applications [20–34]. In addition to the broad bandwidth at 60-GHz, the antennas can be much smaller than WiFi antennas because of the much shorter wavelength of the millimeter-wave signal.

Although the 60-GHz band millimeter-wave communication system can provide wireless links with very high data-rate and other benefits, there are still many challenges in the 60-GHz system. First, the frequency response of the 60-GHz RF components are very difficult to keep the flatness because of the broad bandwidth. Second, to support the transmission with ultra-high data-rate (more than 10 Gbps) within the 7-GHz license-free band, data modulation formats with high spectral efficiency is required. Figure 1.4 shows the propagation loss comparison between the WiFi and the 60-GHz wireless signals. Compared with the 2.4-GHz WiFi wireless signals, the

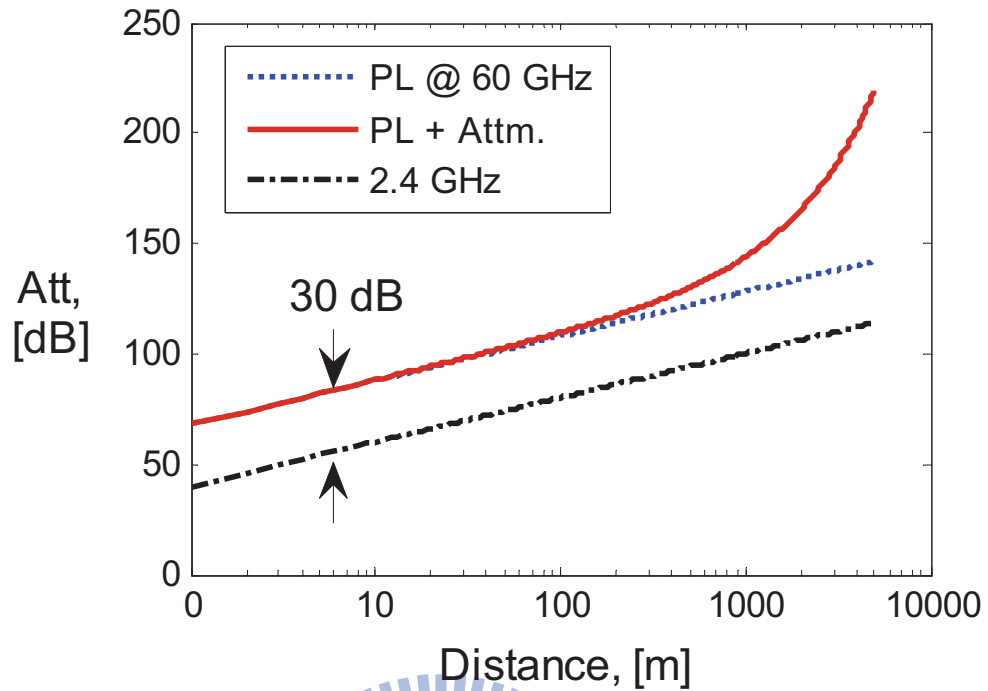


FIG. 1.4. Propagation losses at 2.4 GHz and 60 GHz.

propagation loss of the 60-GHz wireless signals is about 30 dB higher. In addition, the attenuation through the building walls is also much higher. To maintain the signal coverage compared with the 2.4-GHz WiFi signals, at least one RAU is needed at each room in the building and RoF technologies should be utilized to connect all of the RAUs. Moreover, special antenna design is needed to overcome the high directionality of the 60-GHz signals.

1.5 Objective and Outlines of the Thesis

The application and the challenge of the generation of the optical millimeter-wave signal have been discussed in this chapter. The desire of the optical millimeter-wave generations using reliable external modulators with frequency multiplication are also discussed. Moreover, the advantages of wireless communication at millimeter-wave bands are stated. Therefore, the optical millimeter-wave signal generation along

with millimeter-wave RoF communication systems are of great interests. In this thesis, optical millimeter-wave signal generation with high order multiplication will be proposed. Theoretical and experimental demonstration will be performed. 60-GHz RoF technologies based on different optical millimeter-wave generation system and multiplication system will be proposed. To demonstrate ultra-high data-rate transmission, high spectral efficiency orthogonal-frequency-division-multiplication (OFDM) modulation formats will be utilized.

In Chapter 2, the basic idea of optical millimeter-wave signal generation based on conventional double-sideband (DSB), single-sideband (SSB), and double-sideband with carrier suppression (DSB-CS) modulation schemes will be discussed. The advantage and disadvantages among these modulation schemes will be discussed. The basic idea of the optical millimeter-wave signal detection will also be discussed in Chapter 2.

A novel frequency-quadrupled optical millimeter-wave signal generation system without narrow-band optical filtering will be proposed in Chapter 3. Theoretical analysis and experimental demonstration of this system will be performed. The impact of the MZM imbalance will also be investigated. Since no narrow band optical filter is needed in this system, Wavelength-Division-Multiplexed (WDM) optical up-conversion system with frequency quadrupling can be realized based on the proposed system.

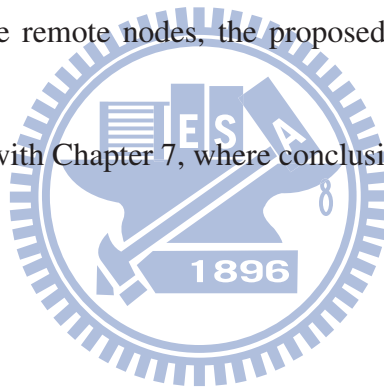
To meet ultra-high frequency millimeter-wave applications, two optical millimeter-wave signal generation system with frequency octupling and 12-tupling will be proposed in Chapter 4. 80-GHz optical millimeter-wave signal generation using the frequency-octupled optical millimeter-wave generation system will be experimentally demonstrated. W-band wireless communication system using the generated 100-GHz optical millimeter-wave signal along with a Near-Ballistic Uni-Traveling Carrier Photodiode (NBUTC-PD) will also be demonstrated. 210-GHz optical millimeter-wave

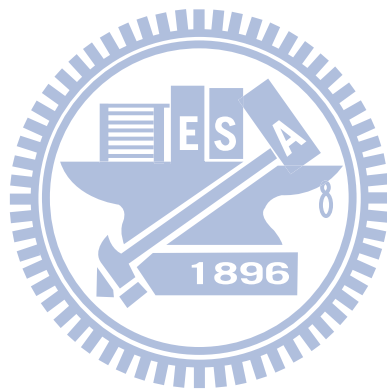
signal generation using a frequency-12-tupled system will also be proposed in this chapter.

In Chapter 5, 60-GHz RoF technologies will be discussed. To achieve high data-rate transmission and overcome the uneven frequency response, OFDM signal generation and modulation techniques will be developed. 60-GHz RoF systems based on Tandem-Single-Sideband(TSSB) with frequency doubling, optical up-conversion with frequency sextupling and Intensity Modulation Direct Detection (IMDD) systems will be proposed. Experimental demonstration of bidirectional full-duplex system at 60-GHz based on IMDD system will experimentally demonstrated.

In Chapter 6, two multi-service hybrid access network systems without narrow-band optical filter at remote nodes will be proposed. Since no narrow band optical filter is required at the remote nodes, the proposed system can be implemented in WDM systems.

This thesis ends with Chapter 7, where conclusions will be drawn.





Chapter 2

OPTICAL MILLIMETER-WAVE GENERATION USING EXTERNAL MODULATOR AND SQUARE-LAW DETECTION

Millimeter-wave signals have been extensively utilized in various applications, such as broadband wireless communication [35], Atacama large millimeter arrays (ALMA) [36], radars, millimeter-wave imaging [37], radio-over-fiber systems [38], and tera-hertz applications. With the increasing of the millimeter-wave signal frequency, the transmission loss in copper wire becomes extremely high and restricts the signal coverage. In addition, all-electronic millimeter-wave signal generation beyond 100 GHz remains a serious challenge because of restrictions on frequency responses of electronic devices and equipments. Accordingly, optical millimeter-wave signal generation techniques have become extremely attractive, due to the ability to generate optical millimeter-wave signals with frequencies of higher than 100 GHz. Moreover, the coverage of the optical millimeter-wave signal can be readily extended thanks to the low transmission loss of optical fibers. Many optical millimeter-wave generation approaches have recently been developed, including optical heterodyning with two laser sources [36], mode-locked lasers [39–41], and external modulation using electro-absorption modulators (EAM), phase modulators (PM), or Mach-Zehnder modulators

(MZM) with a single wavelength laser source [13, 38, 42–48].

Using external optical modulators represent the most reliable solutions for optical millimeter-wave signal generation because these modulators have been extensively used in telecommunication system with proven stability and reliability. There are three main conventional modulation schemes which generate optical millimeter-wave signals, including Double-Sideband (DSB), Single-Sideband (SSB), and Double-Sideband with Carrier Suppression (DSB-CS) [42, 43]. In this chapter, optical millimeter-wave signal generations using external electro-optical modulators base on these three modulation schemes will be discussed and compared. When the optical millimeter-wave signals are obtained, high speed Photo-Diodes (PD) are usually utilized for Optical/Electrical conversion. The basic concept of PD square-law detection will also be introduced in this chapter.

2.1 Double-Sideband Modulation Systems

DSB modulation scheme is the most direct method to generate an optical millimeter-wave signal. Figure 2.1 shows an example of 40 GHz DSB optical signal generation using a single-electrode MZM. The MZM is biased at quadrature point ($0.5 V_{\pi}$), and a 40 GHz sinusoidal signal is utilized to drive the MZM. After the MZM, a DSB signal as shown in FIG. 2.1 is obtained.

Although the DSB signal can be easily generated, there are several disadvantage in DSB modulation schemes, such as chromatic dispersion induced performance fading issue, higher modulator bandwidth requirement, and limited Optical Modulation Index (OMI). Since there are two identical optical sidebands with different wavelength in the DSB signal, the generated Radio-Frequency (RF) power might fade with different fiber transmission distance due to chromatic dispersion. The detail of the chromatic dispersion induced RF fading issue will be discussed in Appendix B. Be-

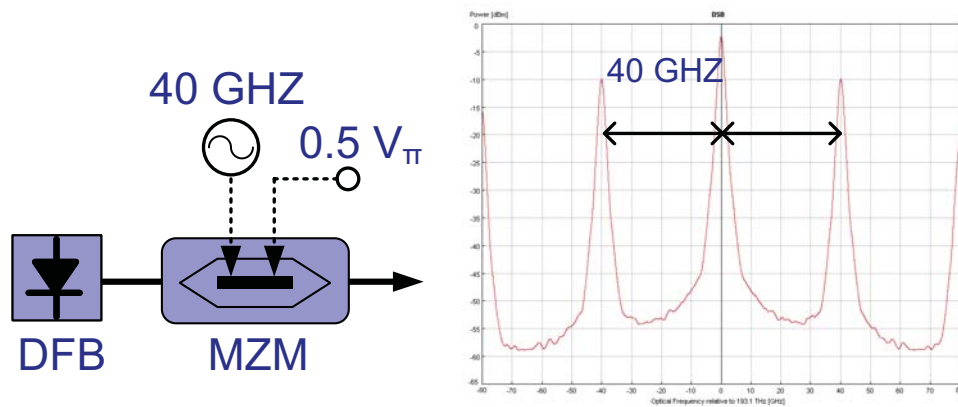


FIG. 2.1. Double sideband (DSB) modulation scheme

cause no frequency multiplication is achieved in DSB modulation scheme, the transmitter bandwidth requirement is higher compared with the modulation schemes with frequency multiplication. In addition, the optical carrier in a DSB signal is usually higher than the optical sidebands which leads to a limited OMI and provides limited signal conversion efficiency after the PD square-law detection.

2.2 Single-Sideband Modulation Systems

To overcome the chromatic dispersion induced RF fading issue, optical millimeter-wave generation based on SSB modulation scheme is proposed. FIG 2.2 shows an example of 40 GHz SSB optical signal generation. To generate the SSB optical signal, a dual-electrode MZM is utilized. The MZM is biased at quadrature point ($0.5 V_{\pi}$). The 40 GHz driving signal is divided into two paths to drive to upper and lower arm of the dual-electrode MZM. An additional $\pi/2$ phase difference is added on the lower arm driving signal. After the MZM, a SSB signal as shown in Fig. 2.2 is obtained.

Since only one optical sideband is obtained, there is no chromatic dispersion induced RF fading issue in the SSB signal. However, the Modulation Index (MI) in SSB modulation scheme is limited to prevent the nonlinear effects from MZM. Therefore,

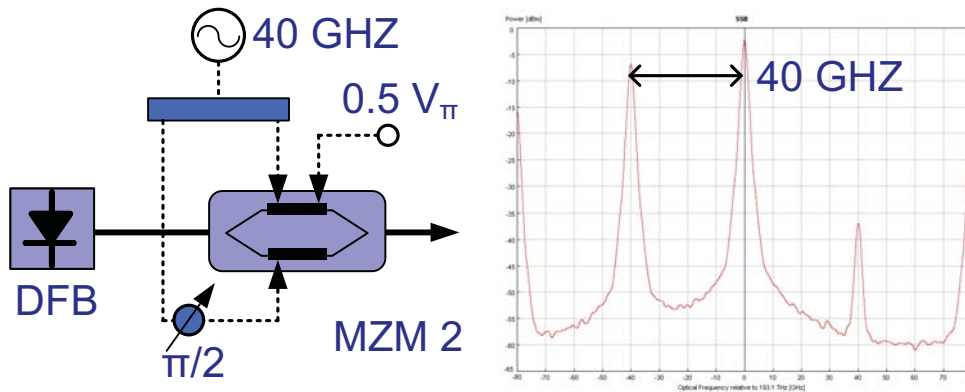


FIG. 2.2. Single sideband (SSB) modulation scheme

the optical carrier is higher than the optical sideband and the OMI is also limited. To increase the OMI, a fiber Bragg grating is usually utilized to suppress the optical carrier power. In addition, no frequency multiplication is achieved in SSB modulation scheme. Moreover, the modulation system is much more complex compared to DSB modulation scheme.

2.3 Double-Sideband with Carrier Suppression Systems

To generate optical millimeter-wave signal using external modulators with frequency doubling and without chromatic dispersion induced RF fading issue, DSB-CS modulation scheme was proposed. FIG. 2.3 shows the setup of a 40 GHz DSB-CS signal generation using a single-electrode MZM. To achieve the DSB-CS modulation scheme, the MZM is biased at null point (V_{π}), and a 20 GHz sinusoidal signal is utilized to drive the MZM. After the MZM, a DSB-CS signal as shown in Fig. 2.3 is obtained.

Since the RF signal is generated from the two second order optical sidebands after the PD square-law detection, there is no chromatic dispersion induced RF fading issue in DSB-CS modulation scheme. The optical power between these two optical side-

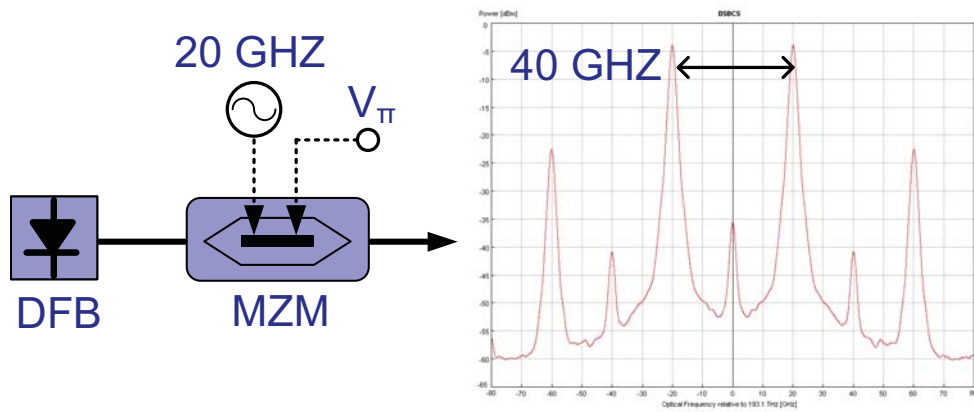


FIG. 2.3. Double sideband with carrier suppression (DSB-CS) modulation scheme

bands are equal to each other, the DSB-CS signal provides an OMI of one. Moreover, optical frequency doubling is achieved in DSB-CS modulation scheme. Therefore, the DSB-CS modulation scheme is one of the most popular choice for high frequency optical millimeter-wave signal generation.

2.4 Square-Law Detection using Photo Diode

When the optical millimeter-wave signals are generated, a PD is usually utilized to receive the optical signal and perform the O/E conversion. In this section the basic concept of the O/E conversion using a PD will be discussed.

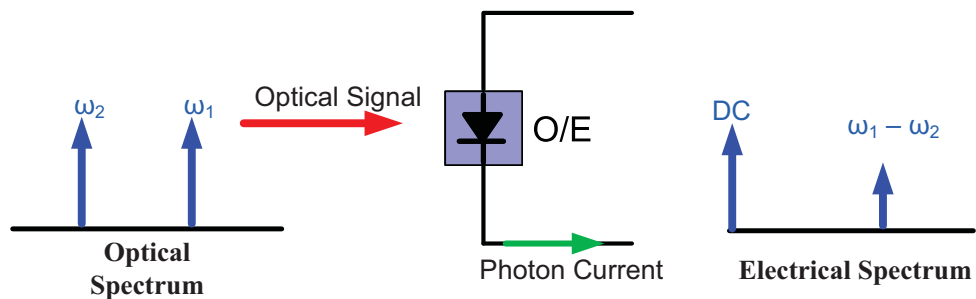


FIG. 2.4. Double sideband with carrier suppression (DSB-CS) modulation scheme

Figure 2.4 shows the conceptual diagram of the O/E conversion. A two tone optical millimeter-wave signal with angular frequencies of ω_1 and ω_2 is received using a PD. The electrical fields of the two tone signal can be expressed as $E_1 = A_1 \cos(\omega_1 t)$ and $E_2 = A_2 \cos(\omega_2 t)$, where A_1 and A_2 represent the amplitude of the electrical fields. After the square-law detection of the PD, the generated photo current can be expressed as

$$\begin{aligned} i_{PD} &= R \cdot (E_1 + E_2)^2 \\ &= R \cdot A_1 \cdot A_2 \cdot \cos[(\omega_1 - \omega_2)t] + R \cdot A_1 \cdot A_2 \cos[(\omega_1 + \omega_2)t] + DC \text{ Terms} \end{aligned} \quad (2.1)$$

Ignore the DC terms, the generated millimeter-wave signal is related to the first term of equation (2.1). Therefore, the electrical field of the generated millimeter-wave signal can be proportional to the first term of equation (2.1) and can be expressed as

$$V_{RF} \propto R \cdot A_1 \cdot A_2 \cdot \cos[(\omega_1 - \omega_2)t] \quad (2.2)$$

2.5 Conclusion

Optical millimeter-wave signal generation using external modulator is one of the most reliable technique. Optical millimeter-wave signal generation based on DSB, SSB and DSB-CS modulation schemes were discussed in this chapter. DSB modulation is the simplest architecture, but chromatic dispersion induced RF fading issue restricts the fiber transmission distance. SSB modulation scheme has no chromatic dispersion induced RF fading issue. However, the weak MI and high optical carrier power limit the OMI of SSB signal. Because the high OMI and no chromatic dispersion induced RF fading issue, DSB-CS modulation scheme becomes a popular choice for optical millimeter-wave signal generation. Moreover, frequency doubling is achieved in DSB-CS modulation scheme.

Chapter 3

OPTICAL MILLIMETER-WAVE GENERATION SYSTEM WITH FREQUENCY QUADRUPLING

Optical millimeter-wave signal generation at frequencies beyond 40 GHz remains a major challenge because of the frequency response of LiNbO₃ Mach-Zehnder modulator (MZM) or phase modulator are usually less than 40 GHz. Moreover, the electrical components and equipment at frequencies beyond 40 GHz, such as amplifiers, mixers, and synthesizers, are very expensive. Therefore, a cost-effective means of generating high frequency optical millimeter-wave signal is of great interest.

Many optical millimeter-wave signal generation schemes based on MZM or phase modulator to achieve frequency multiplication have recently been demonstrated [13, 48–56]. However, these proposed systems with frequency multiplication of more than two times either depend on more than one optical filter to remove undesired optical sidebands [13, 48, 50–56] or need two cascaded external modulators [13], which significantly increase the complexity and cost of the system. Besides, the required optical filtering severely hinders the implementation of optical up-conversion in a wavelength-division-multiplexer (WDM) radio-over-fiber (RoF) system as shown in FIG. 3.1. Although WDM up-conversion using only one external modulator with optical filters is demonstrated in [11], only frequency doubling is achieved.

In this chapter, a carrier-suppressed optical millimeter-wave signal generation

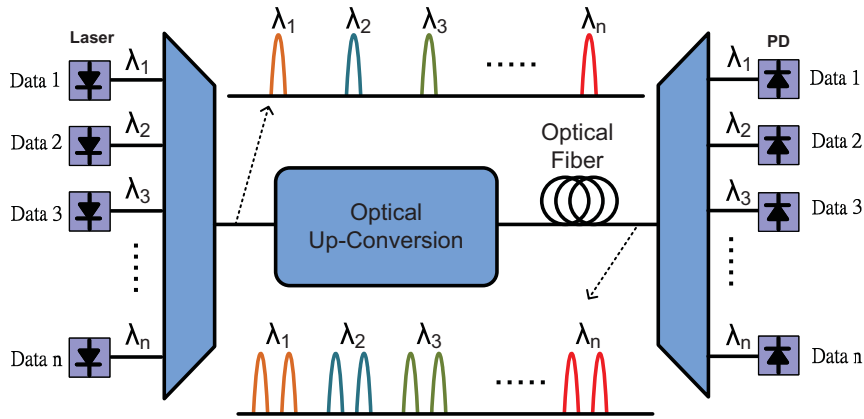


FIG. 3.1. Optical colorless up-conversion using a frequency multiplication technique for WDM RoF systems.

with frequency quadrupling is proposed. No narrow band optical filter is required to suppress the undesired optical sidebands, and only one dual-parallel (DP-MZM) is utilized in the architecture. High undesired optical sideband suppression ratio can be achieved, and the high-purity two-tone optical millimeter-wave signal does not suffer from impairment due to fiber dispersion. In addition, WDM optical up-conversion with frequency quadrupling will also be demonstrated in this chapter.

3.1 Concept and Theoretical Model

Figure 3.2 shows a conceptual diagram of the optical millimeter-wave generation with frequency quadrupling. A DP-MZM that comprises of three sub-MZMs is key to generating optical millimeter-wave signals. One sub-MZM (MZ-a or MZ-b) is embedded in each arm of the main modulator (MZ-c). The optical field at the input of the integrated MZM is defined as

$$E_{in}(t) = E_o \cos(\omega_o t) \quad (3.1)$$

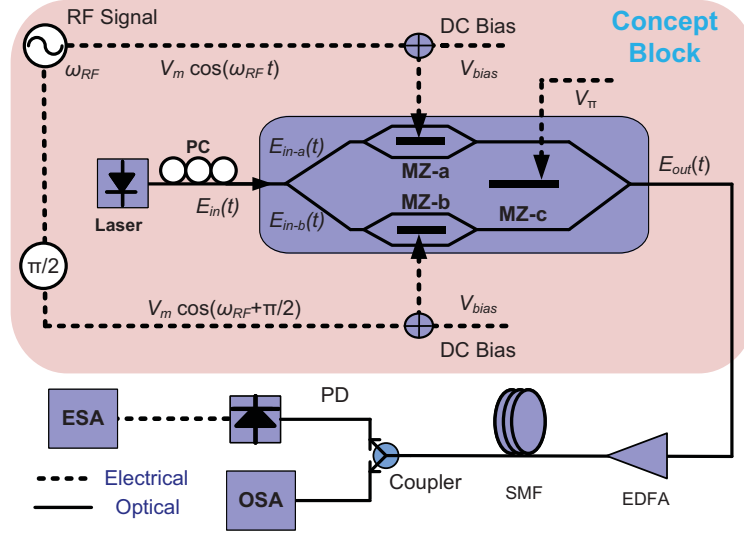


FIG. 3.2. Setup of the optical frequency-quadrupled millimeter-wave signal generation system.

, where E_o is the amplitude and ω_o is the angular frequency of the optical field.

In the DP-MZM, both MZ-a and MZ-b are biased at the full point. The driving signal is generated from a RF signal generator, and separated into two ways. An additional $\pi/2$ phase delay is added on the lower path. Therefore, the electrical driving modulation signals sent into MZ-a and MZ-b can be expressed as $V_a(t) = V_m \cos(\omega_{RF}t)$ and $V_b(t) = V_m \cos(\omega_{RF}t + \pi/2)$, respectively. After the modulation of MZ-a and MZ-b, the output signal from MZ-a and MZ-b can be expressed as

$$\begin{aligned} E_{out-a} &= \frac{1}{\sqrt{2}} \cdot E_o \cdot \cos\left[\frac{\pi}{2V_\pi} \cdot V_m \cdot \cos(\omega_{RF}t)\right] \cdot \cos(\omega_o t) \\ &= \frac{1}{\sqrt{2}} \cdot E_o \cdot \cos[m \cdot \cos(\omega_{RF}t)] \cdot \cos(\omega_o t) \end{aligned} \quad (3.2)$$

and

$$\begin{aligned} E_{out-b} &= \frac{1}{\sqrt{2}} \cdot E_o \cdot \cos\left[\frac{\pi}{2V_\pi} \cdot V_m \cdot \cos(\omega_{RF}t + \frac{\pi}{2})\right] \cdot \cos(\omega_o t) \\ &= \frac{1}{\sqrt{2}} \cdot E_o \cdot \cos[m \cdot \sin(\omega_{RF}t)] \cdot \cos(\omega_o t) \end{aligned} \quad (3.3)$$

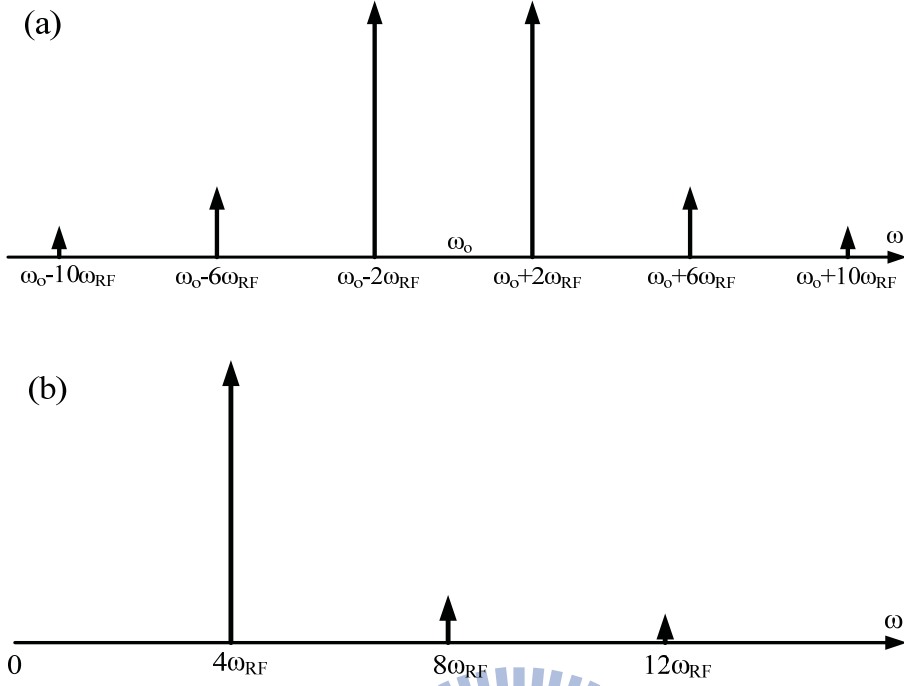


FIG. 3.3. (a) Illustrated optical spectrum and (b) Illustrated electrical spectrum of of frequency-quadrupled optical millimeter-wave signal

,where V_π is the half-wave voltage of the MZM and m is the modulation index. Expanding $E_o \cdot \cos[m \cdot \cos(\omega_{RF}t)]$ and $E_o \cdot \cos[m \cdot \sin(\omega_{RF}t)]$ using Bessel function enables the output optical field to be rewritten as

$$\begin{aligned}
 E_{out} &= \frac{E_o}{2} \cdot \cos(\omega_o t) \cdot \left\{ 2 \cdot \sum_{n=1}^{\infty} J_{2n}(m) \cdot (-1)^n \cos(2n \cdot \omega_{RF}t) \right. \\
 &\quad \left. - 2 \cdot \sum_{n=1}^{\infty} J_{2n}(m) \cdot \cos(2n \cdot \omega_{RF}t) \right\} \\
 &= -E_o \cdot \sum_{n=1}^{\infty} J_{4n-2}(m) \cdot \left\{ \cos[(\omega_o + (4n - 2)\omega_{RF})t] \right. \\
 &\quad \left. + \cos[(\omega_o - (4n - 2)\omega_{RF})t] \right\}
 \end{aligned} \tag{3.4}$$

,where J_n is the Bessel function of the first kind with order n . From equation (3.4), only optical sidebands with the order of $4n - 2$ will be obtained after the DP-MZM

as shown in FIG. 3.3 (a). Due to the properties of Bessel function, without causing significant errors, it is reasonable to ignore sidebands with orders higher than the second one. Therefore, the optical field at the output of the first DP-MZM can be further simplified as

$$E_{out} = -E_o \cdot \{J_2(m) \cos[(\omega_o + 2\omega_{RF})t] + J_2(m) \cos[(\omega_o - 2\omega_{RF})t] + J_6(m) \cos[(\omega_o + 6\omega_{RF})t] + J_6(m) \cos[(\omega_o - 6\omega_{RF})t]\} \quad (3.5)$$

Then, the generated optical millimeter-wave signal is detected using a PD with a responsivity of R . The generated photocurrent can be expressed as

$$\begin{aligned} i_{4\omega_{RF}} &= R \cdot E_o^2 \cdot [J_2(m) \cdot J_2(m) + 2 \cdot J_2(m) \cdot J_6(m)] \cdot \cos(4\omega_{RF}t) \\ i_{8\omega_{RF}} &= R \cdot E_o^2 \cdot [2 \cdot J_2(m) \cdot J_6(m)] \cdot \cos(8\omega_{RF}t) \\ i_{12\omega_{RF}} &= R \cdot E_o^2 \cdot [J_6(m) \cdot J_6(m)] \cdot \cos(12\omega_{RF}t) \end{aligned} \quad (3.6)$$

FIG. 3.3 (b) displays the electrical spectrum of the generated millimeter-wave signal after the square-law PD detection. Only the desired millimeter-wave signal with frequency of $4\omega_{RF}$ and the harmonic distortion signals with frequency of $4n\omega_{RF}$ are observed in the electrical spectrum, where n is an integer that exceeds two.

Figure 3.4 schematically depicts the principle of optical millimeter-wave generation with frequency quadrupling. Since MZ-a and MZ-b are biased at full point, the optical carrier and even-order sidebands are observed, as shown in insets (ii) and (iii) of FIG. 3.4. The optical sidebands with orders of more than two are neglected for simplicity. The 90° phase difference between the sinusoidal signals that drive MZ-a and MZ-b causes the polarities of the two second-order sidebands at the output of MZ-a to oppose those at the output of MZ-b. As the MZ-c is biased at the null point, an extra 180° phase difference is added to all optical sidebands of the lower arms of MZ-c, as shown in insets (iv) and (v) of FIG. 3.4. Notably, the two optical carriers are

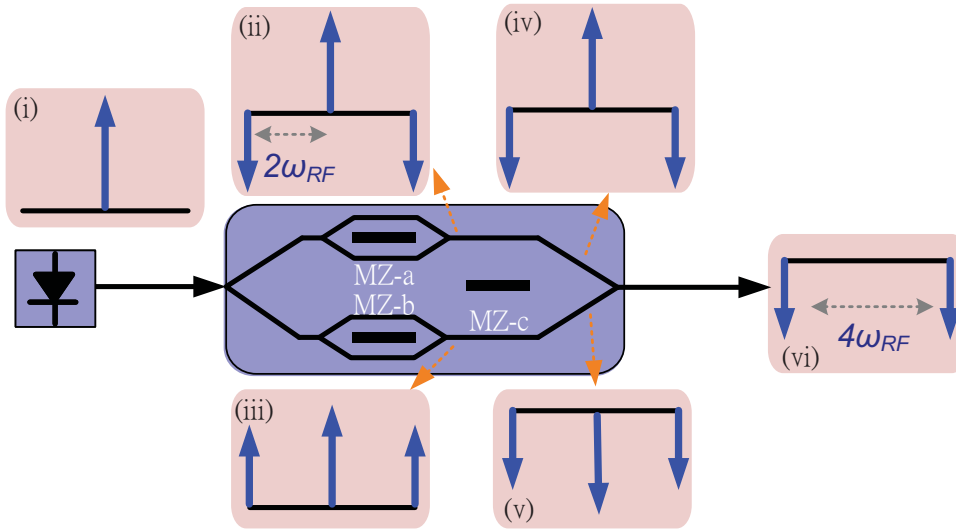


FIG. 3.4. Schematic principle of the optical millimeter-wave generation with frequency quadrupling

out of phase, but the second-order sidebands are in phase. Therefore, after MZ-c, the optical carrier is eliminated and only two second-order sidebands remain, which can be converted into an electrical quadruple-frequency millimeter-wave signal following square-law PD detection.

3.2 Impact of The PD-MZM Imbalance

Theoretical derivation of the frequency-quadrupled optical millimeter-wave generation using an ideal DP-MZM has been discussed in the last section. In the ideal case, only the optical sidebands with the order of $\pm(4n - 2)$ can be observed after the DP-MZM. However, the other optical sidebands can also be observed due to the limited extinction ratios (ERs) of the DP-MZM in a real case. The limited ERs come from the manufacturing defect of the Y-splitters in the DP-MZM which introduce imbalance of split ratio to the Y-splitters. Theoretical derivation of the impact of the MZM imbalances will be performed in this section.

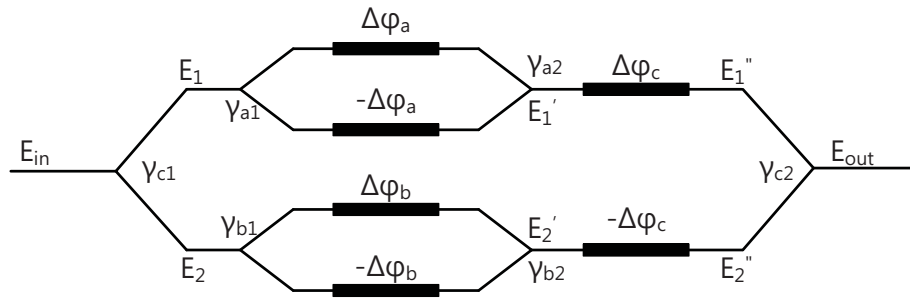


FIG. 3.5. DP-MZM with Y-splitter imbalance.

Figure 3.5 illustrates a conceptual diagram of a DP-MZM with Y-splitter imbalances, where γ denote the coupling factors at different Y-splitters of the sub-MZMs (ie. MZ-a and MZ-b) and main MZM (ie. MZ-c), and $\Delta\phi$ denotes the phase shifts introduced by the applied driving voltages. Assume that the electrical field of the laser source is $E_{in}(t) = E_o \cos(\omega_o t)$. After the input Y-splitter of MZ-c, the electrical fields become

$$\begin{aligned} E_1 &= \sqrt{1 - \gamma_{c1}} \cdot E_o \cdot \text{Exp}(j\omega_o t) \\ E_2 &= \sqrt{\gamma_{c1}} \cdot E_o \cdot \text{Exp}(j\omega_o t) \end{aligned} \quad (3.7)$$

Then, E_1 and E_2 are sent into MZ-a and MZ-b, respectively. MZ-a and MZ-b can be treated as two imbalanced MZM as shown in Appendix A. Therefore, the optical signal after the modulation of MZ-a and MZ-b can be expressed as

$$\begin{aligned} E_1' &= E_o \cdot \text{Exp}[j\omega_o t] \cdot \sqrt{1 - \gamma_{c1}} \cdot \{j \cdot \sqrt{1 - \gamma_{a1}} \sqrt{\gamma_{a2}} \cdot \text{Exp}(j\Delta\phi_a) \\ &\quad + j \cdot \sqrt{\gamma_{a1}} \sqrt{1 - \gamma_{a2}} \cdot \text{Exp}(-j\Delta\phi_a)\} \\ E_2' &= E_o \cdot \text{Exp}[j\omega_o t] \cdot \sqrt{\gamma_{c1}} \cdot \{j \cdot \sqrt{1 - \gamma_{b1}} \sqrt{\gamma_{b2}} \cdot \text{Exp}(j\Delta\phi_b) \\ &\quad + j \cdot \sqrt{\gamma_{b1}} \sqrt{1 - \gamma_{b2}} \cdot \text{Exp}(-j\Delta\phi_b)\} \end{aligned} \quad (3.8)$$

In the main MZM, a phase difference is introduced between the upper and lower arm signal. After the combination at the output Y-splitter, the generated optical signal can

be expressed as

$$\begin{aligned}
E_{out} &= j \cdot \sqrt{\gamma_{c2}} \cdot E'_1 \cdot \text{Exp}(j \cdot \Delta\phi_c) + \sqrt{1 - \gamma_{c2}} \cdot E'_2 \cdot \text{Exp}(-j \cdot \Delta\phi_c) \\
&= -E_o \cdot \sqrt{1 - \gamma_{c1}} \cdot \sqrt{\gamma_{c2}} \cdot \sqrt{1 - \gamma_{a1}} \cdot \sqrt{\gamma_{a2}} \cdot \text{Exp}[j \cdot (\omega_o t + \Delta\phi_a + \Delta\phi_c)] \\
&\quad - E_o \cdot \sqrt{1 - \gamma_{c1}} \cdot \sqrt{\gamma_{c2}} \cdot \sqrt{\gamma_{a1}} \cdot \sqrt{1 - \gamma_{a2}} \cdot \text{Exp}[j \cdot (\omega_o t - \Delta\phi_a + \Delta\phi_c)] \\
&\quad - E_o \cdot \sqrt{\gamma_{c1}} \cdot \sqrt{1 - \gamma_{c2}} \cdot \sqrt{1 - \gamma_{b1}} \cdot \sqrt{\gamma_{b2}} \cdot \text{Exp}[j \cdot (\omega_o t + \Delta\phi_b - \Delta\phi_c)] \\
&\quad - E_o \cdot \sqrt{\gamma_{c1}} \cdot \sqrt{1 - \gamma_{c2}} \cdot \sqrt{\gamma_{b1}} \cdot \sqrt{1 - \gamma_{b2}} \cdot \text{Exp}[j \cdot (\omega_o t - \Delta\phi_b - \Delta\phi_c)]
\end{aligned} \tag{3.9}$$

let

$$\begin{aligned}
W &= -E_o \cdot \sqrt{1 - \gamma_{c1}} \cdot \sqrt{\gamma_{c2}} \cdot \sqrt{1 - \gamma_{a1}} \cdot \sqrt{\gamma_{a2}} \\
X &= -E_o \cdot \sqrt{1 - \gamma_{c1}} \cdot \sqrt{\gamma_{c2}} \cdot \sqrt{\gamma_{a1}} \cdot \sqrt{1 - \gamma_{a2}} \\
Y &= -E_o \cdot \sqrt{\gamma_{c1}} \cdot \sqrt{1 - \gamma_{c2}} \cdot \sqrt{1 - \gamma_{b1}} \cdot \sqrt{\gamma_{b2}} \\
Z &= -E_o \cdot \sqrt{\gamma_{c1}} \cdot \sqrt{1 - \gamma_{c2}} \cdot \sqrt{\gamma_{b1}} \cdot \sqrt{1 - \gamma_{b2}}
\end{aligned} \tag{3.10}$$

Then, the real part of the optical output signal can be simplified as

$$\begin{aligned}
\text{Re}(E_{out}) &= W \cdot \cos(\omega_o t + \Delta\phi_a + \Delta\phi_c) + X \cdot \cos(\omega_o t - \Delta\phi_a + \Delta\phi_c) \\
&\quad + Y \cdot \cos(\omega_o t + \Delta\phi_b - \Delta\phi_c) + Z \cdot \cos(\omega_o t - \Delta\phi_b - \Delta\phi_c)
\end{aligned} \tag{3.11}$$

Equation (3.11) is the general form of an optical signal generated by an imbalanced DP-MZM. In the proposed optical millimeter-wave generation with frequency quadrupling system, MZ-a and MZ-b are biased at the full point and MZ-c is biased at the null point. Therefore,

$$\begin{aligned}
\Delta\phi_a &= m_a \cdot \cos(\omega_{RF} t) \\
\Delta\phi_b &= m_b \cdot \cos(\omega_{RF} t + \frac{\pi}{2}) = -m_b \cdot \sin(\omega_{RF} t) \\
\Delta\phi_c &= \frac{\pi}{2}
\end{aligned} \tag{3.12}$$

,where $m_a = (\pi \cdot V_{m_a})/(2V_\pi)$ and $m_b = (\pi \cdot V_{m_b})/(2V_\pi)$ are the modulation index of MZ-a and MZ-b, respectively. Then,

$$\begin{aligned}
Re(E_{out}) = & -W \cdot \sin(\omega_o t) \cdot \cos[m_a \cdot \cos(\omega_{RF} t)] - W \cdot \cos(\omega_o t) \cdot \sin[m_a \cdot \cos(\omega_{RF} t)] \\
& - X \cdot \sin(\omega_o t) \cdot \cos[m_a \cdot \cos(\omega_{RF} t)] + X \cdot \cos(\omega_o t) \cdot \sin[m_a \cdot \cos(\omega_{RF} t)] \\
& + Y \cdot \sin(\omega_o t) \cdot \cos[m_b \cdot \sin(\omega_{RF} t)] - Y \cdot \cos(\omega_o t) \cdot \sin[m_b \cdot \sin(\omega_{RF} t)] \\
& + Z \cdot \sin(\omega_o t) \cdot \cos[m_b \cdot \sin(\omega_{RF} t)] + Z \cdot \cos(\omega_o t) \cdot \sin[m_b \cdot \sin(\omega_{RF} t)]
\end{aligned} \tag{3.13}$$

Expanding equation (3.13) using Bessel function, the output signal becomes

$$\begin{aligned}
Re(E_{out}) = & -W \cdot \sin(\omega_o t) \cdot \left[J_0(m_a) + 2 \cdot \sum_{n=1}^{\infty} J_{2n}(m_a) \cdot (-1)^n \cdot \cos[2n\omega_{RF} t] \right] \\
& - W \cdot \cos(\omega_o t) \cdot \left[2 \cdot \sum_{n=1}^{\infty} J_{2n-1}(m_a) \cdot (-1)^{n-1} \cdot \cos[(2n-1)\omega_{RF} t] \right] \\
& - X \cdot \sin(\omega_o t) \cdot \left[J_0(m_a) + 2 \cdot \sum_{n=1}^{\infty} J_{2n}(m_a) \cdot (-1)^n \cdot \cos[2n\omega_{RF} t] \right] \\
& + X \cdot \cos(\omega_o t) \cdot \left[2 \cdot \sum_{n=1}^{\infty} J_{2n-1}(m_a) \cdot (-1)^{n-1} \cdot \cos[(2n-1)\omega_{RF} t] \right] \\
& + Y \cdot \sin(\omega_o t) \cdot \left[J_0(m_b) + 2 \cdot \sum_{n=1}^{\infty} J_{2n}(m_b) \cdot \cos[2n\omega_{RF} t] \right] \\
& - Y \cdot \cos(\omega_o t) \cdot \left[2 \cdot \sum_{n=1}^{\infty} J_{2n-1}(m_b) \cdot \sin[(2n-1)\omega_{RF} t] \right] \\
& + Z \cdot \sin(\omega_o t) \cdot \left[J_0(m_b) + 2 \cdot \sum_{n=1}^{\infty} J_{2n}(m_b) \cdot \cos[2n\omega_{RF} t] \right] \\
& + Z \cdot \cos(\omega_o t) \cdot \left[2 \cdot \sum_{n=1}^{\infty} J_{2n-1}(m_b) \cdot \sin[(2n-1)\omega_{RF} t] \right]
\end{aligned}$$

Due to the imbalanced splitting ratios of the Y-splitters, not only the optical sidebands with the order of $4n-2$, but also the other optical sidebands are obtained at the output of the DP-MZM. The electrical fields of the optical sidebands with the order

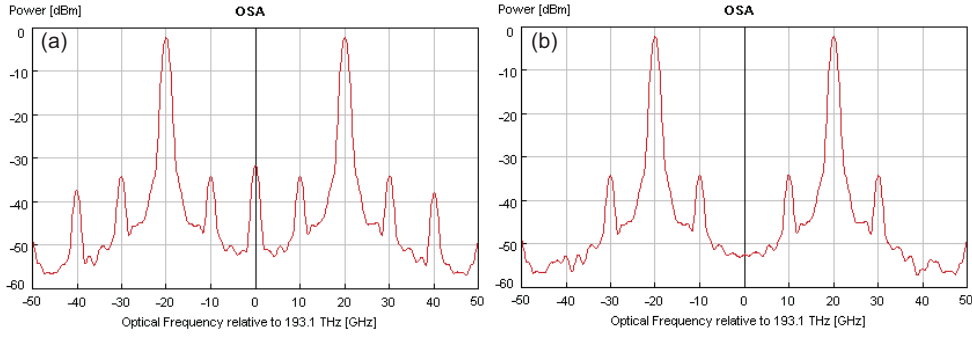


FIG. 3.6. Simulated optical spectra of 40-GHz optical millimeter-wave signals using the quadrupling system (a) with 25-dB extinction ratios; (b) with 25-dB extinction ratios and driving signal trimming.

up to 4th is shown as the following:

- Optical carrier (zero order sideband) :

$$\sin(\omega_o t) \cdot [-J_0(m_a) \cdot (W + X) + J_0(m_b) \cdot (Y + Z)].$$

- 1st sideband :

$$2 \cdot \cos(\omega_o t) \cdot [J_1(m_a) \cdot (-W + X) \cdot \cos(\omega_{RF} t) + J_1(m_b) \cdot (-Y + Z) \cdot \sin(\omega_{RF} t)]$$

- 2nd sideband :

$$2 \cdot \sin(\omega_o t) \cdot \cos(2\omega_{RF} t) \cdot [J_2(m_a) \cdot (W + X) + J_2(m_b) \cdot (Y + Z)]$$

- 3rd sideband :

$$2 \cdot \cos(\omega_o t) \cdot [J_3(m_a) \cdot (W - X) \cdot \cos(3\omega_{RF} t) + J_3(m_b) \cdot (-Y + Z) \cdot \sin(3\omega_{RF} t)]$$

- 4th sideband :

$$2 \cdot \sin(\omega_o t) \cdot \cos(4\omega_{RF} t) \cdot [-J_4(m_a) \cdot (W + X) + J_4(m_b) \cdot (Y + Z)]$$

In an ideal case, $\gamma_{a1} = \gamma_{a2} = \gamma_{b1} = \gamma_{b2} = \gamma_{c1} = \gamma_{c2} = 0.5$ when the DP-MZM has infinity extinction ratios. Therefore, $W = X = Y = Z$ and optical sidebands except for the $2 + 4n$ ones can be eliminated. However, the extinction ratios are always limited due to the imbalanced Y-splitter splitting ratio. Figure 3.6 (a) shows an simulated optical spectrum of a 40-GHz optical millimeter-wave signal which is generated

using the proposed quadrupling system with 25-dB MZM extinction ratios. The optical carrier can not be perfectly suppressed because of the limited MZM extinction ratios. In the proposed quadrupling system, the limited extinction ratio of the main MZM (MZ-c) can be compensated by trimming the driving powers of the sub-MZMs (MZ-a and MZ-b). From the equations in the last page, the optical carrier can be totally suppressed when $J_0(m_a) \cdot (W + X) = J_0(m_b) \cdot (Y + Z)$. Figure 3.6 (b) shows a simulated optical spectrum. The optical carrier and the 4th optical sideband are totally suppressed by trimming the driving powers. However, the 1st and the 3rd optical sidebands are also related to the limited extinction ratios of MZ-a and MZ-b which can not be compensated by the driving power trimming.

3.3 Experimental Results

To verify the proposed methods, optical millimeter-wave generation using the setup as shown in FIG. 3.2 has been demonstrated experimentally. The external integrated MZM is a commercially available LiNbO₃ modulator. A commercial distributed feedback (DFB) laser is employed as a light source and a polarization controller is adopted to adjust the polarization before the light is sent into the modulator. The frequency of the driving signal is set at 10 GHz and 18 GHz, respectively. The generated optical millimeter-wave signal is amplified using an erbium-doped fiber amplifier to compensate the loss of the integrated MZM and then transmitted with launch power of 0 dBm over 50-km single mode fiber. The optical power is normalized to 1 dBm before PD detection. Both optical and electrical spectra of the generated millimeter-wave signals are experimentally investigated.

Figure 3.7 shows the measured spectrum of the optical 40-GHz millimeter-wave signal using a 10-GHz driving signal before transmission. The optical carrier is effectively suppressed, and the power of the two second-order sidebands which can be

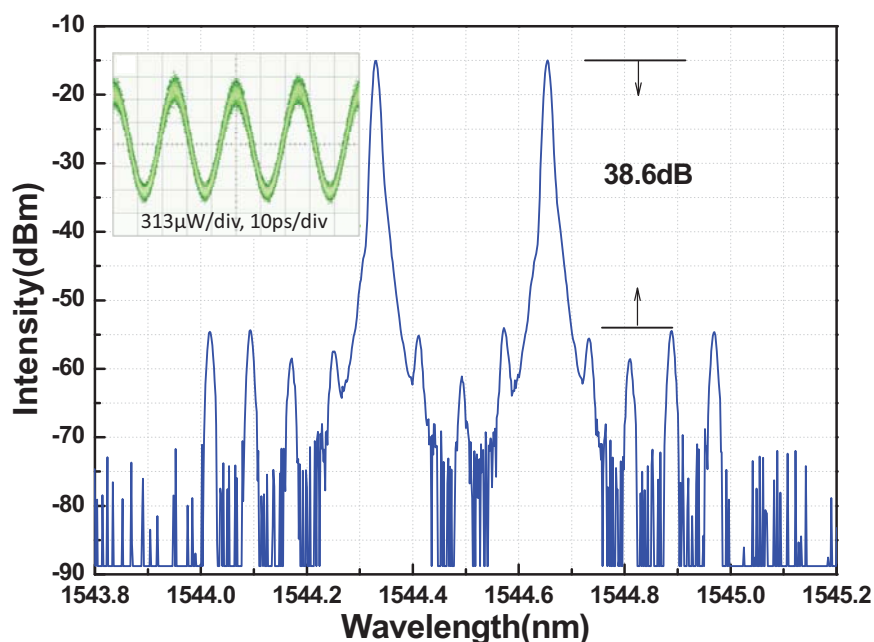


FIG. 3.7. Experimental results of 40-GHz optical millimeter-wave signal spectrum using maximum transmission operation mode. The resolution is 0.01 nm.

converted into a 40-GHz electrical millimeter-wave signal after PD detection is 38 dB higher than that of the other order sidebands. Sidebands other than the second- and sixth-order sidebands are observed due to the imbalance in the Y-junction splitting ratio of MZM. Due to the high suppression of the undesired harmonic sidebands, they negligibly affects the performance of the optical millimeter-wave signal. The inset of FIG 3.7 presents the waveform of the generated 40-GHz optical millimeter-wave signal with a 50% duty cycle.

Figure 3.8 presents the electrical spectrum of the generated millimeter-wave signal without fiber transmission with a 40-GHz span and 30-kHz resolution bandwidth. A strong electrical signal with the frequency four times of the driving signal is observed, and the first, second, and third terms of the electrical signal are totally suppressed below the noise floor. Since the suppression of the undesired harmonic sidebands is more than 38 dB, there is no observable change following 50-km single mode

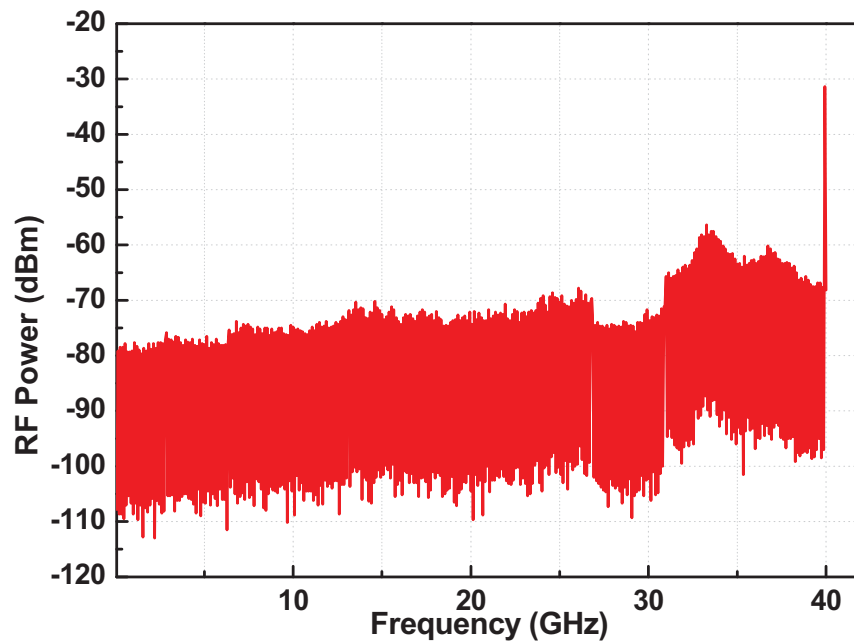
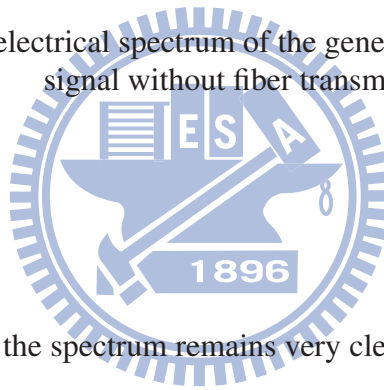


FIG. 3.8. Measured electrical spectrum of the generated 40-GHz millimeter-wave signal without fiber transmission.



fiber transmission and the spectrum remains very clear with the same suppression ratio as presented in FIG. 3.8. FIG. 3.9 (a) reveals that the linewidth of the generated 40-GHz signal is less than 5 Hz and almost equals to that of the 10-GHz driving signal. After transmission over 50-km single mode fiber, no linewidth broadening of the electrical 40-GHz signal due to fiber dispersion is observed, as shown in FIG. 3.9 (b). Due to available RF amplifier in the laboratory, only 72-GHz millimeter-wave signals can be demonstrated by using 18-GHz electrical driving signal. FIG. 3.10 shows the optical spectrum of the generated 72-GHz optical millimeter-wave signal. The optical powers of the two desired second-order sidebands of millimeter-wave signals are at least 36 dB higher than those of the other sidebands, which is sufficient for most practical applications.

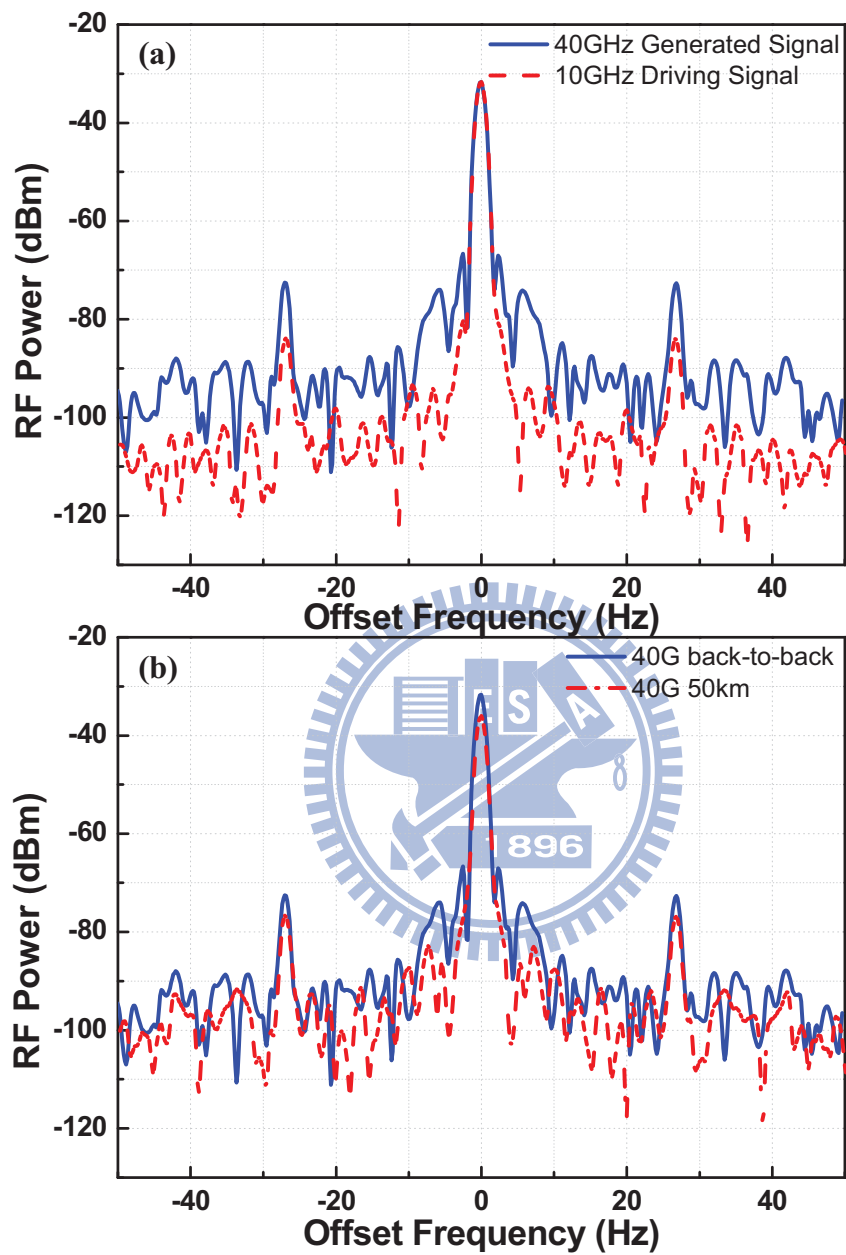


FIG. 3.9. Electrical spectra of the generated 40-GHz millimeter-wave signals with 100-Hz span. (a) Comparison of the generated 40-GHz signal and 10-GHz driving signal. (b) Comparison of generated 40-GHz signal at back-to-back and with 50-km single mode fiber transmission. The resolution bandwidth is 1 Hz.

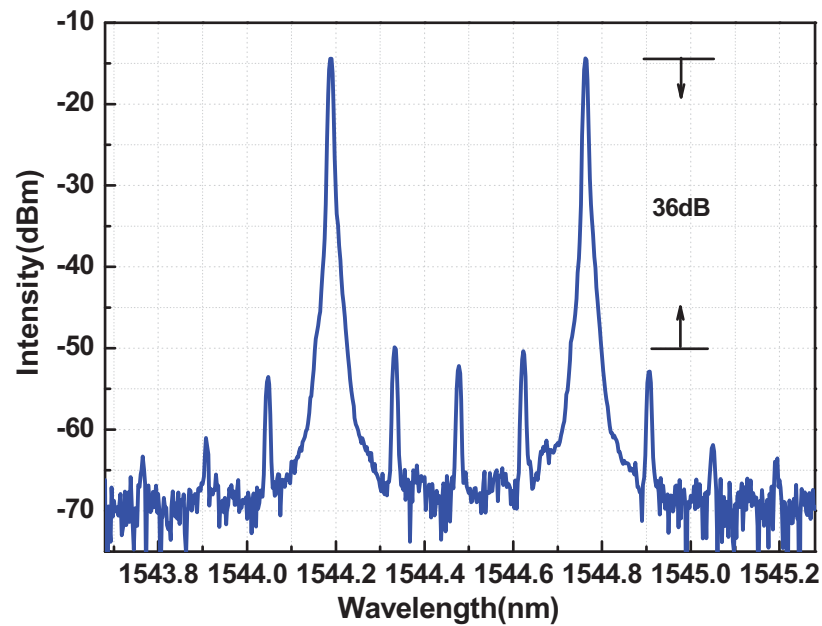


FIG. 3.10. Measured optical spectrum of the generated 72-GHz optical millimeter-wave signal.

3.4 WDM Up-Conversion Employing Frequency Quadrupling

3.4.1 Concept

Optical millimeter-wave generation and up-conversion are essential to Radio-over-Fiber (RoF) communication systems. In the proposed optical millimeter-wave generation system, frequency quadrupling can be achieved. Via the frequency quadrupling techniques, optical millimeter-wave signals can be generated using low-frequency RF components and equipment which markedly reduces the entire system costs. Moreover, no narrow band optical filter which hinders the implementation of optical up-conversion in wavelength-division-multiplexing (WDM) RoF systems is required in the proposed system.

In addition to RoF techniques, simultaneous transmission of wired baseband (BB) and wireless RF signals for low-cost quad-play services (wireless, telephone,

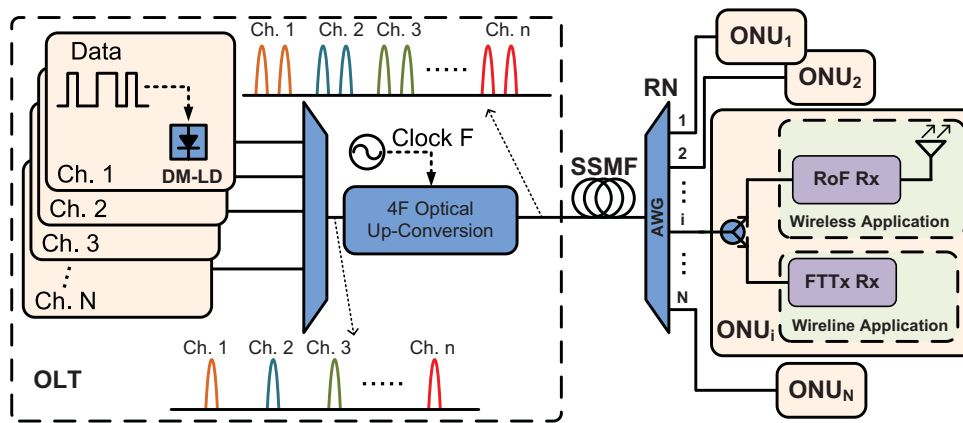


FIG. 3.11. Conceptual diagram of a WDM up-conversion system.

television and internet) over the constructed passive optical networks (PON) also attract much attention. In this section, an optical up-conversion system using a frequency quadrupling approach will be experimentally demonstrated. Four-channel BB 1.25-Gbits/s WDM millimeter-wave signals are simultaneously up-converted with optical carrier suppression using only one external modulator without narrowband optical filtering. Since no narrowband optical filter is needed, the proposed system can be implemented in WDM up-conversion systems. Based on the modified double sideband with carrier suppression (DS-CS) modulation scheme, the proposed architecture supports both wireless and wired services simultaneously. After transmission over 50-km standard single mode fiber (SSMF), the power penalties of 20-GHz wireless and wired signals are less than 1 dB, respectively. 40- and 60-GHz WDM up-conversion are also demonstrated experimentally in this work. The harmonic distortion suppression ratio of the generated 40- and 60-GHz millimeter-wave signals in each channel are also higher than 30 dB. Furthermore, the impact of the MZM bias drift on the performance of BB and RF signals is also investigated.

Figure 3.11 shows the conceptual diagram of the WDM up-conversion system. In the optical line terminal (OLT), direct modulation laser diodes are employed as optical

sources of WDM channels. After combining the channels, the BB WDM signals are sent into the optical up-conversion system and all WDM channels are up-converted simultaneously. After transmission over SSMF, WDM channels are separated using an array waveguide grating and sent to the optical network units (ONU). At the ONU, optical signals are separated by an optical coupler for wireless and wired applications.

3.4.2 Experimental Setup

Figure 3.12 shows the experimental setup of the WDM optical up-conversion system with frequency quadrupling. Four distributed feedback (DFB) lasers are utilized as the four-channel WDM signals with optical wavelengths from 1544.53 to 1546.92 nm with 100-GHz channel spacing. A 1.25-Gb/s on-off-keying (OOK) pseudo random bit sequences (PRBS) signal with a word length of $2^{31} - 1$ are simultaneously modulated on all of the WDM channels using a single electrode MZM. The WDM BB channels are then sent into the optical up-conversion system with frequency quadrupling, and all WDM channels are up-converted simultaneously. The up-converted millimeter-wave signals are then amplified by an erbium-doped fiber amplifier (EDFA) before being transmitted over 50-km SSMF. After the transmission, a tunable optical filter (TOF) is employed to select the desired channel. At the remote node (RN), an optical coupler is utilized to separate the optical power for wireless and wired applications. For wireless application, RF OOK signals are detected using a high-frequency photo receiver along with an electrical band pass filter to select the desired RF signal. The electrical RF OOK signals are then down-converted to BB and sent into a bit error rate tester (BERT). On the other hand, the BB OOK signals are received directly using a 1.25-GHz photo receiver, which is compatible with existing PON, and analyzed using the BERT.

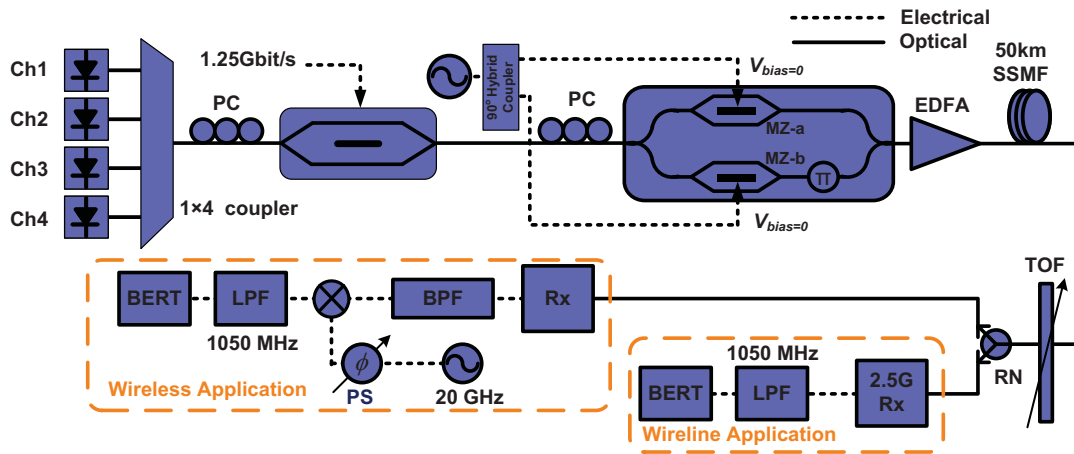


FIG. 3.12. Experimental setup of the WDM up-conversion system. (PC: polarization controller; TOF: tunable optical filter; RN: remote node; BPF: band pass filter; LPF: low pass filter; BERT: bit error rate tester.)

3.4.3 Results and Discussion

Although the MZM has been used for several decades, bias drift, which affects MZM performance, remains an important issue when the MZM is biased at the full or null point. In the proposed optical up-conversion system, both MZ-a and MZ-b are biased at the full point, and MZ-c is biased at the null point. Therefore, the single channel harmonic distortion suppression ratio and performance degrading due to bias drift are investigated.

Since MZ-a is biased at the full point, bias drift of MZ-a decreases the suppression of odd-order optical sidebands. FIG. 3.13 illustrates the 20-GHz optical millimeter-wave signal receiver sensitivities at BER of 10^{-9} and harmonic distortion suppression ratio versus different MZ-a bias voltage deviation ratios. Optical spectrum with optimized, -40%, and 40% bias deviation ratios are also shown in Fig. 3.13. The voltage deviation ratio is defined as $(\Delta V/V_\pi \times 100\%)$, where ΔV is voltage deviation and V_π is the half-wave voltage of the sub-MZ (i.e. 4.2 volts in this case). The harmonic distortion suppression ratio declines from 39 dB to 7.5 dB when bias

deviation ratio becomes 40%, and the receiver sensitivity penalty of the 20-GHz RF OOK signal is about 2 dB. However, no significant reductions in receiver sensitivities exist for the 1.25-Gb/s BB OOK signals. The behavior of MZ-b voltage deviation is similar to the results of that in MZ-a. FIG. 3.14 shows the 20-GHz optical millimeter-wave signal receiver sensitivities at BER of 10^{-9} and harmonic distortion suppression ratio versus different MZ-c bias voltage deviation ratios. Optical spectra with -50% and 50% bias deviation ratios are also shown in Fig. 3.14. Differing from the voltage drift effects of MZ-a and MZ-b, the harmonic distortion suppression ratio decreases from 39 dB to 17 dB when bias drift is almost 50%, which corresponds to a voltage deviation of roughly 2.1 volts and can be considered an extreme case. However, no significant sensitivity penalties of the 20-GHz RF OOK and BB OOK signals are observed. This work also investigates the declines of harmonic distortion suppression ratio and receiver sensitivities when all biases of the dual-parallel MZM drift from the optimal point. FIG. 3.15 shows the 20-GHz optical millimeter-wave signal receiver sensitivities at BER of 10^{-9} and harmonic distortion suppression ratio versus different bias voltage deviation ratios in all sub-MZM. Optical spectrum with -30% and 30% bias deviation ratios are also shown in FIG. 3.15. When the biases of all sub-MZM drift 30% from the optimal point, the harmonic distortion suppression ratio degrades from 39 dB to 5 dB, and the 20-GHz RF OOK signal has a penalty of about 3 dB. And there are still no significant power penalties of the BB OOK signal.

After the square-law detection, the RF OOK signal comes from the beating terms of the two second-order optical sidebands. However, the receiver sensitivity is defined as the total received optical power. If the harmonic distortion suppression ratio degrades due to bias drifts of the dual-parallel MZM, a portion of the total optical power is taken by the undesired optical sidebands; thus, the receiver sensitivity of the desired millimeter-wave signal is diminished. In the case of bias drifting in MZ-a and MZ-b, odd order optical sidebands steal a significant portion of the total optical power,

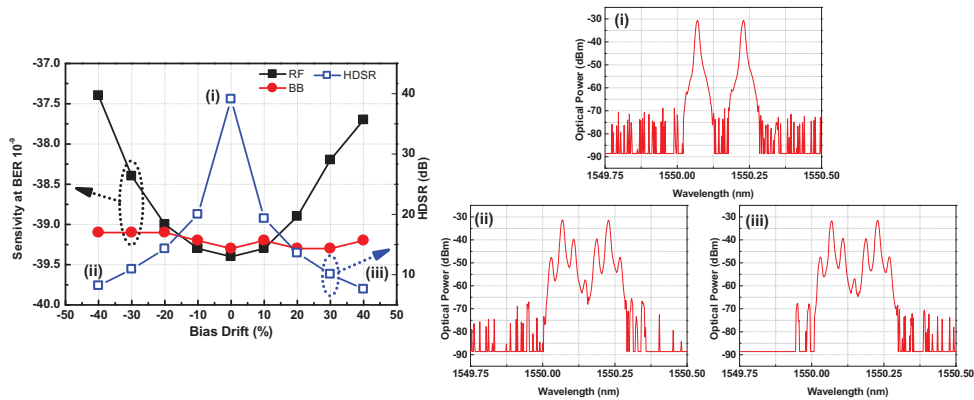


FIG. 3.13. Sensitivities and harmonic distortion suppression ratio versus MZ-a bias drifts, and optical spectrum with different bias drifts.

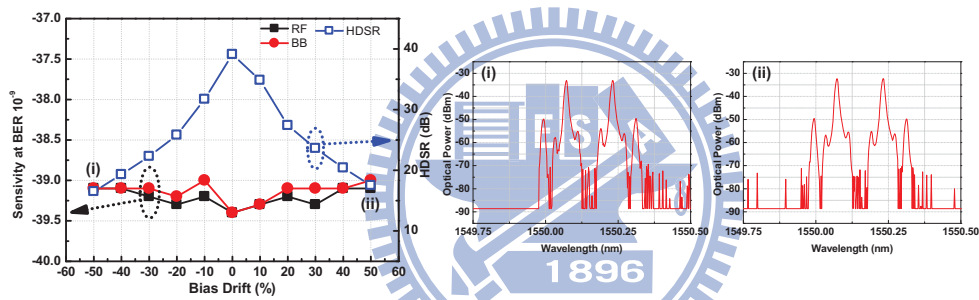


FIG. 3.14. Sensitivities and harmonic distortion suppression ratio versus MZ-c bias drifts, and optical spectrum with different bias drift.

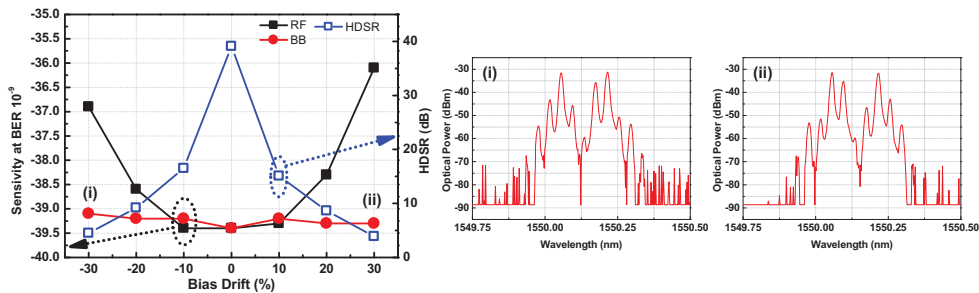


FIG. 3.15. Sensitivities and harmonic distortion suppression ratio versus all sub-MZ bias drifts, and optical spectrum with different bias drift.

resulting in receiver sensitivity penalties. Nevertheless, in the case of bias drifting in MZ-c, only the optical carrier and 4th order optical sidebands emerge with bias drifting. In the proposed system, the original optical carrier can be totally suppressed due to the advantage of the modulation depth trimming of the proposed frequency technique. The modulation depth trimming is done by adjusting the amplitudes of electrical signals for driving MZ-a and MZ-b. Therefore, only the 4th order optical sidebands contribute to the decline of RF receiver sensitivity when MZ-c bias drifts. Base on the properties of Bessel function, the optical power of 4th order optical sidebands are quite small compared with the desired 2nd optical sidebands. The harmonic distortion suppression ratio still exceed 20 dB when the MZ-c bias drifts about 50%. With such high harmonic distortion suppression ratio, no significant power penalty of RF signals exists when the MZ-c bias drifts. Receiver sensitivities of the proposed system can be less than 1 dB when bias drifts are controlled within 20% of the half-wave voltage using a bias feed-back control system. On the other hand, the BB OOK signal is related to the square terms of all optical sidebands; therefore, the BB OOK signal is insensitive to the biased drifts.

Figure 3.16 shows the optical spectrum of the 4×1.25 -Gb/s BB WDM signals and the up-converted 4×1.25 -Gb/s 20-GHz WDM signals. All WDM channels are up-

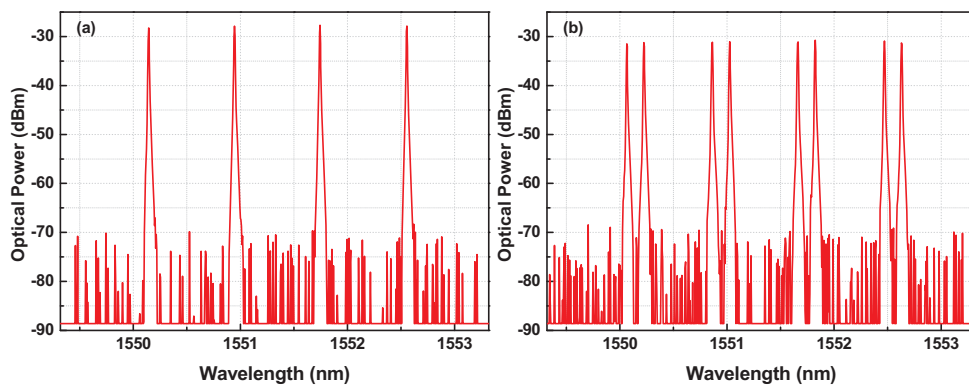


FIG. 3.16. Optical spectra of the (a) BB WDM signals; (b) 20-GHz WDM signals.

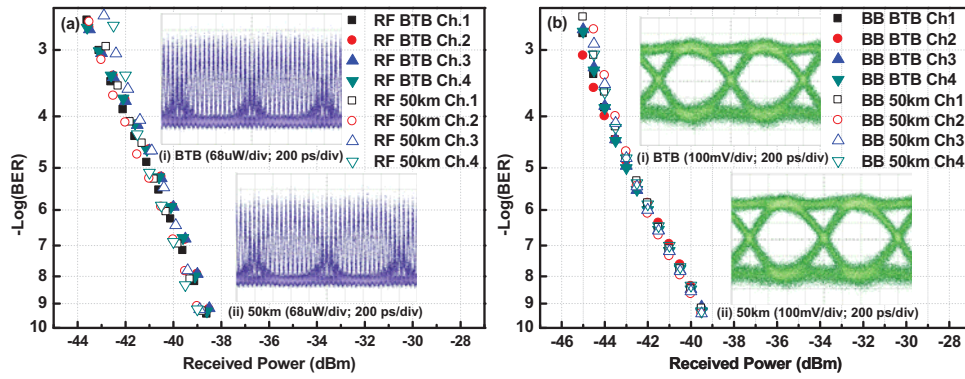


FIG. 3.17. BER curves of the 20-GHz WDM signals at (a) 20-GHz; (b) Baseband.

converted simultaneously using only one dual-parallel MZM. FIG. 3.17 (a) shows the BER curves and eye diagrams of the BTB and transmitted 20-GHz WDM RF OOK signals. After transmission over 50-km SSF, the receiver power penalty of each channel is less than 1 dB. FIG. 3.17 (b) shows the BER curves and eye diagrams of the BTB and transmitted WDM BB OOK signals. Receiver power penalties are negligible after transmission over the 50-km SSF. 40-GHz and 60-GHz WDM optical up-conversion systems are also demonstrated. Nevertheless, the receiver sensitivities and BER analysis are not shown here due to the unavailability of 40- and 60-GHz receiver systems in the laboratory. FIG. 3.18 (a) shows the optical spectra of the 40-GHz up-converted WDM signals. The harmonic distortion suppression ratio of the up-converted WDM signals are more than 35 dB. Figure 3.18 (b) shows the spectra of up-converted 60-GHz WDM signals. The harmonic distortion suppression ratio of the WDM channels are also more than 35 dB.

3.5 Conclusion

A frequency quadrupled optical millimeter-wave generation system was proposed in this chapter. Two tone optical millimeter-wave signal with frequency separation four times of the modulation frequency can be generated using only one external

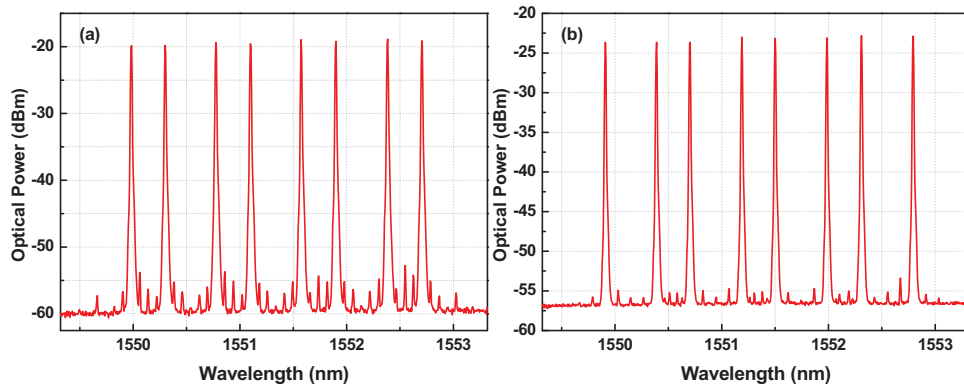


FIG. 3.18. Spectra of Up-converted WDM signals at (a) 40-GHz; (b) 60-GHz.

modulator without optical filtering. Theoretical derivations of ideal and imbalanced DP-MZM were demonstrated. 40- and 72-GHz optical millimeter-wave signals were experimentally demonstrated using the proposed system. The harmonic distortion suppression of the generated optical millimeter-wave signals are higher than 36 dB. Since no narrow-band optical filter is required, this system can be utilized in WDM up-conversion. 20-GHz dual-service hybrid access network which can simultaneously provides RF and BB transmissions were experimentally demonstrated. The harmonic distortion suppression of the generated 20-GHz signals are higher than 39 dB. Additionally, receiver sensitivity degraded due to MZM bias drifts is also investigated in this work for 20-GHz WDM signals. The receiver power penalty can be less than 1 dB when bias deviation ratios are less than 20% of the half-wave voltage, which can be achieved using a bias feedback control system. After transmission over a 50-km SSMF, the receiver power penalties of both the BB and 20-GHz RF OOK signals are less than 1 dB. The 40- and 60-GHz WDM up-conversion using 10- and 15-GHz RF driving signals are also demonstrated. The proposed system is compatible with existing WDM PON system. Since only low-frequency RF components and equipment are required, the proposed system is a potential solution for high frequency optical millimeter-wave signal generation and WDM up-conversion system.



Chapter 4

OPTICAL MILLIMETER-WAVE GENERATION SYSTEM WITH HIGHER ORDER MULTIPLICATION

The tremendous increase in the desired bandwidth of wireless data-transmission has attracted considerable attention on various methods to utilize the millimeter-wave bands with ultra high carrier frequency beyond 100 GHz [21, 57]. Not only the millimeter-wave band wireless communication, but many other applications, such as Large Scale Phase Array Antenna [36], millimeter-wave imaging [37], and Tera-hertz applications, require the ultra-high frequency up to several hundred GHz.

Although some CMOS technology can generate MMW signal beyond 60 GHz, the attenuation of millimeter-wave signal in copper wires is extremely high, which restricts the signal transmission distance. To transmit MMW signals over a long distance, optical millimeter-wave signal based on low transmission loss optical fiber network is a cost-effective and viable solution. Conventional optical millimeter-wave signal generation based on DSB, SSB and DSB-CS modulation schemes have been discussed in Chapter 2. Nevertheless, the generated optical millimeter-wave frequencies are still restricted by the bandwidth of LiNbO_3 modulators, which is typically less than 40 GHz. Moreover, radio-frequency (RF) components with frequency response

over 26 GHz are considerably more expensive than those below 26 GHz. In order to achieve optical MMW generation with frequency beyond 60 GHz cost-effectively, optical millimeter-wave signal generations with frequency multiplication are highly desirable. In Chapter 3, an frequency-quadrupled optical millimeter-wave generation system without any narrow-band optical filter was proposed. Optical millimeter-wave signals with frequency up to 72 GHz was experimentally demonstrated. However, to support higher frequency applications, optical millimeter-wave generation systems with higher order frequency multiplication are required. In this chapter, optical millimeter-wave generation system with frequency octupling and 12-tupling will be proposed. Theoretical derivation and experimental demonstration of the optical millimeter-wave generation systems will be performed. Optical millimeter-wave signals with frequency up to 210 GHz are generated. Utilizing the generated 100-GHz optical millimeter-wave signals, W-band wireless communication system is experimentally demonstrated with 3.75-Gb/s single carrier 8 Quadrature Amplitude Modulation (8-QAM) signals.

4.1 Optical Millimeter-Wave Generation with Frequency Octupling

4.1.1 Concept and Theoretical Model

Figure 4.1 shows the experimental setup of the optical millimeter-wave generation with frequency octupling. The frequency-octupled optical millimeter-wave generation system consists of two cascaded frequency-quadrupled optical millimeter-wave generation systems. Assume that the optical field at the input of the first DP-MZM is defined as $E_{in}(t) = E_o \cos(\omega_o t)$, where E_o is the amplitude of the optical field and ω_o is the angular frequency of the optical carrier. In the first stage, both of the sub-MZMs (MZ1-a and MZ1-b) are biased at the full point while the main MZM of the first DP-MZM is biased at the null point and introduces a 180° phase difference be-

tween the output of the two sub-MZMs. A 90° phase difference is introduced between the RF driving signals of MZ1-a and MZ1-b. Therefore, the electrical RF driving signal sent into MZ1-a and MZ1-b can be expressed as $V_{a1}(t) = V_{m1} \cdot \cos(\omega_{RF}t)$ and $V_{b1}(t) = V_{m1} \cdot \cos(\omega_{RF}t + \pi/2)$, respectively, where V_{m1} denotes the amplitude of the RF driving signal of the first dual-parallel MZM and ω_{RF} denotes the angular frequency of the RF driving signal. From equation (3.4), the optical field at the output of the first DP- MZM can be expressed as:

$$\begin{aligned} E_{out-1} &= \frac{1}{2} \cdot E_{in} \cdot \left\{ \cos[m_1 \cdot \cos(\omega_{RF}t)] - \cos[m_1 \cdot \cos(\omega_{RF}t + \frac{\pi}{2})] \right\} \\ &= -E_o \cdot \sum_{n=1}^{\infty} J_{4n-2}(m_1) \cdot \left\{ \cos[(\omega_o + (4n - 2)\omega_{RF})t] \right. \\ &\quad \left. + \cos[(\omega_o - (4n - 2)\omega_{RF})t] \right\} \end{aligned} \quad (4.1)$$

,where the phase modulation index m_1 is $\pi V_{m1}/2V_\pi$ and J_{4n-2} is the Bessel function of the first kind with order $4n-2$. Only optical sidebands with the order of $4n-2$ will be obtained. Due to the properties of Bessel function, without causing significant errors, it is reasonable to ignore the sidebands with orders higher than the second one.

Therefore, the optical field at the output of the first DP-MZM can be further

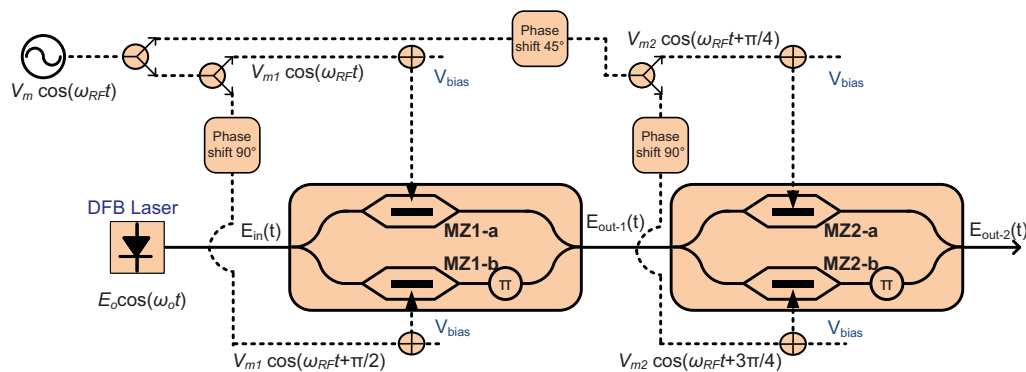


FIG. 4.1. Conceptual diagram and experimental setup of the frequency-occupied optical millimeter-wave signal generation system.

simplified as

$$E_{out-1}(t) = -E_o \cdot \{J_2(m_1) \cos[(\omega_o + 2\omega_{RF})t] + J_2(m_1) \cos[(\omega_o - 2\omega_{RF})t]\} \quad (4.2)$$

After the first stage, a frequency-quadrupled optical millimeter-wave signal is obtained. The generated optical millimeter-wave signal from the first DP-MZM is then sent into the second DP-MZM. Both of the sub-MZMs (MZ2-a and MZ2-b) are biased at the full point while the main MZM is biased at the null point. Note that a 45° phase delay is introduced between the driving signals of the first and second DP-MZMs. Therefore, the electrical RF driving signal sent into MZ2-a and MZ2-b can be expressed as $V_{a2}(t) = V_{m2} \cdot \cos(\omega_{RF}t + \pi/4)$ and $V_{b2}(t) = V_{m2} \cdot \cos(\omega_{RF}t + 3\pi/4)$, respectively. Then, the optical field at the output of the second DP-MZM can be expressed as

$$\begin{aligned} E_{out-2} &= \frac{1}{2} \cdot E_{out-1} \cdot \left\{ \cos\left[m_2 \cdot \cos\left(\omega_{RF}t + \frac{\pi}{4}\right)\right] - \cos\left[m_2 \cdot \cos\left(\omega_{RF}t + \frac{3\pi}{4}\right)\right] \right\} \\ &= \frac{1}{2} \cdot E_{out-1} \cdot \left\{ J_0(m_2) + 2 \cdot \sum_{n=1}^{\infty} J_{2n}(m_2) \cdot (-1)^n \cdot \cos\left[n \cdot (2\omega_{RF}t + \frac{\pi}{2})\right] \right. \\ &\quad \left. - J_0(m_2) - 2 \cdot \sum_{n=1}^{\infty} J_{2n}(m_2) \cdot (-1)^n \cdot \cos\left[n \cdot (2\omega_{RF}t + \frac{3\pi}{4})\right] \right\} \\ &= -E_o \cdot \left[\sum_{n=1}^{\infty} J_{4n-2}(m_1) \cdot \left\{ \cos[(\omega_o + (4n-2)\omega_{RF})t] \right. \right. \\ &\quad \left. \left. \cdot \left[2 \cdot \sum_{n=1}^{\infty} J_{4n-2}(m_2) \cdot (-1)^{n-1} \cdot \sin[(4n-2)\omega_{RF}t] \right] \right\} \right. \\ &\quad \left. \cdot \sum_{k=1}^{\infty} \left\{ \begin{aligned} &\sin[(\omega_o + 4k\omega_{RF})t] - \sin[(\omega_o - 4k\omega_{RF})t] \\ &\cdot \left[\sum_{-\infty}^{\infty} (-1)^n \cdot J_{2+4(k-1)+4n}(m_1) \cdot J_{2-4n}(m_2) \right] \end{aligned} \right\} \right] \quad (4.3) \end{aligned}$$

,where the phase modulation index m_2 is $\pi V_{m2}/2V_\pi$. After the frequency-octupled optical millimeter-wave signal generation system, only the optical sidebands with the order of $4n$ will be obtained. Based on the characteristic of Bessel function, the higher

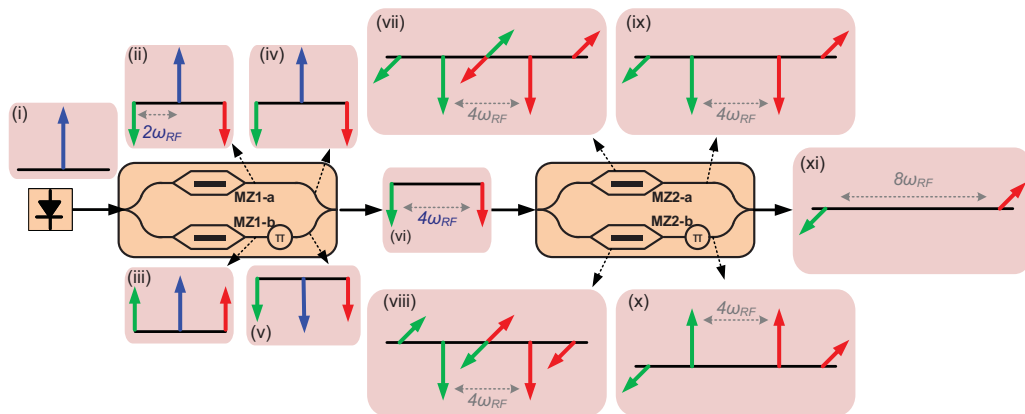


FIG. 4.2. Principle of the frequency-octupled optical millimeter-wave signal generation system.

order terms can be ignored without causing significant effect. The generated optical millimeter-wave signals can be simplified as

$$E_{out-2} = E_o \cdot [J_2(m_1)J_2(m_2) - J_2(m_1)J_6(m_2) - J_6(m_1)J_2(m_2)] \cdot \{-\sin[(\omega_o + 4\omega_{RF})t] + \sin[(\omega_o - 4\omega_{RF})t]\} \quad (4.4)$$

Notably, no optical filter is required to remove undesired optical sidebands. After square-law detection using a photo diode, the electrical signal with frequency eight times that of the RF driving signal is obtained.

Figure 4.2 schematically depicts the principle of the proposed millimeter-wave generation system. Since MZ1-a and MZ1-b are biased at the full point, optical spectra with two second-order sidebands are performed after MZ1-a and MZ1-b as shown in insets (ii) and (iii) of FIG. 4.2. The 90° phase delay between the driving signal of MZ1-a and MZ1-b causes the 180° phase difference of the two second order sidebands at the output of MZ1-a and MZ1-b. Since the main MZM is biased at the null point, an additional 180° phase delay is introduced between the output signals of MZ1-a and MZ1-b. After the combination at the output of the first DP-MZM, the original optical

carrier is inherently suppressed. Optical millimeter-wave signal with frequency quadrupling is obtained at the output of the first DP-MZM as shown in the inset (vi) of FIG. 4.2. The generated second order sidebands from the first DP-MZM are treated as two new optical carriers and send into the second DP-MZM. Due to the 45° phase delay of the second DP-MZM driving signals, optical spectra as shown in insets (vii) and (viii) of FIG. 4.2 are generated from MZ2-a and MZ2-b, respectively. Optical sidebands with the same frequency as the original optical carrier are suppressed. The second main MZM, which is biased at null-point, introduces a 180° phase difference between the output signals of MZ2-a and MZ2-b as shown in insets (ix) and (x) of FIG. 4.2. After combination at the output of the second DP-MZM, an optical millimeter-wave signal with frequency eight times that of the driving signal is obtained as shown in inset (xi) of FIG. 4.2.

4.1.2 Experimental Setup and Results

Following the setup shown in FIG. 4.1, a CW laser with 4-dBm optical power is used as the optical source. To generate 60-GHz optical millimeter-wave signal, a 7.5-GHz sinusoid driving signal is utilized. The modulation indices of both DP-MZMs are about $1.6 \times (V_\pi/2)$. As shown in FIG. 4.3 (a), a 30-GHz optical millimeter-wave signal with 29-dB harmonic distortion suppression ratio and -6.8-dBm optical power is obtained after the first DP-MZM. The generated optical millimeter-wave signal is sent into the second DP-MZM. At the output of the second DP-MZM, a 60-GHz optical millimeter-wave signal with 30-dB undesired sideband suppression ratio and -19-dBm optical power is obtained. The optical spectrum is shown in Fig. 4.3 (b). After the frequency octupling system, an EDFA is utilized to boost the optical power. Because of the slight different V_π of the PD-MZMs, tunable attenuators are employed after the first electrical splitter to control the driving power of two DP-MZMs.

The 45° phase difference between the driving signal of the first and second DP-

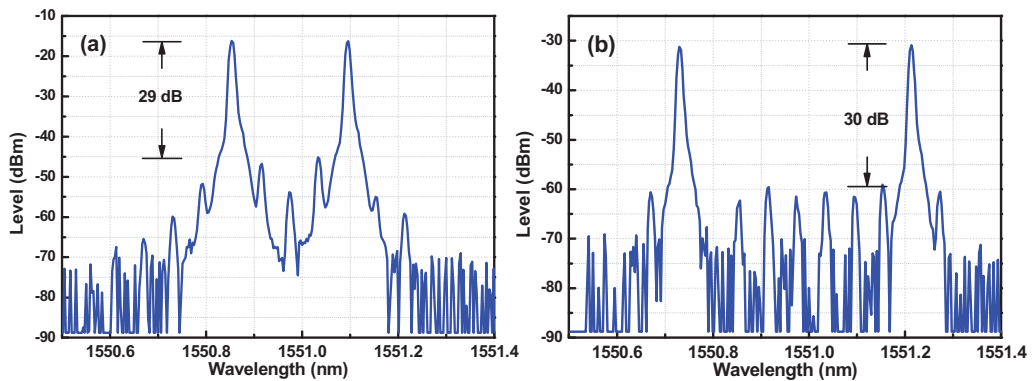


FIG. 4.3. Optical spectra of (a) the 30-GHz millimeter-wave signal generated from the first stage of the frequency octupling system; (b) the generated 60-GHz millimeter-wave signal from the frequency octupling system.

MZM is a key factor which affects the suppression of the original optical carrier. The optical carrier suppression ratio of the original carrier will degrade if the phase difference is not equal to 45° . Fig. 4.4 (a) shows the degradation of the optical carrier suppression ratio due to imperfect phase delay between two DP-MZM driving signals with varying phase delay from 30° to 60° . The best carrier suppression ratio is obtained with 45° phase delay. The optical spectra with 30° and 60° are also shown in insets (b) and (c) of Fig. 4.4. Fig. 4.5 (a) and (b) shows the waveform of the generated 60-GHz millimeter-wave signal using a V-band photo-diode at back-to-back (BTB) and after transmission of 25-km standard single mode fiber (SSMF), respectively. Because of the high undesired sideband suppression ratio, a 60-GHz millimeter-wave signal with a 50% duty cycle is observed. Moreover, no significant signal distortion is observed after fiber transmission. The electrical spectrum of the generated 60-GHz millimeter-wave signal is shown in FIG. 4.6.

To demonstrate W-band millimeter-wave signal generation, 80-GHz millimeter-wave signal is generated using 10-GHz driving signal. FIG. 4.7 shows the optical spectrum of the generated 80-GHz optical millimeter-wave signal. The undesired sideband suppression ratio of the 80-GHz optical millimeter-wave signal is about 30

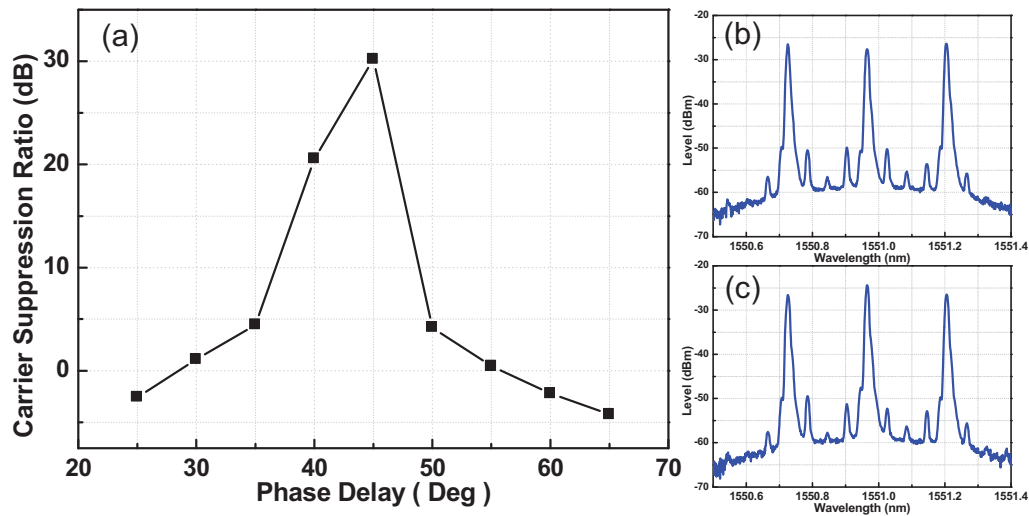


FIG. 4.4. (a) Optical carrier suppression ratio versus phase delay of two DP-MZMs and optical spectra of (b) 30 deg (c) 60 deg phase delay.

dB.

To evaluate the performance of the proposed system, undesired sideband suppression ratio degradation with DP-MZM bias drifts are also investigated. FIG. 4.8 depicts the undesired sideband suppression ratio degradations with bias drifts of the first-stage DP-MZM. The undesired sideband suppression ratios degrade from 30 dB to 3 dB with 25% bias voltage deviation ratio. The bias voltage deviation ratio is

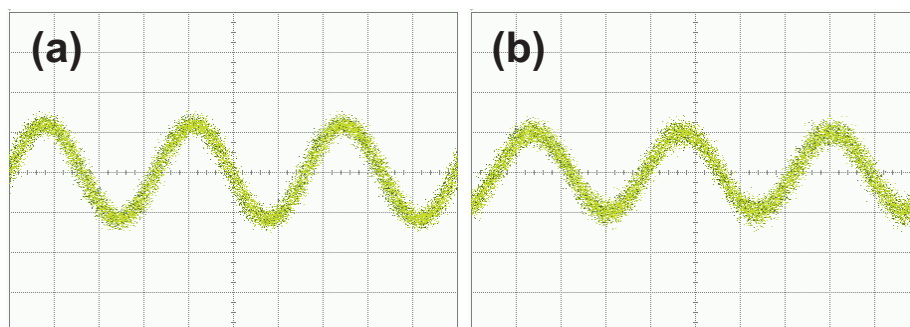


FIG. 4.5. Time domain waveform of the generated 60-GHz millimeter-wave signal (a) BTB (b) 25-km SMF Transmission. (100 mV/div; 5 ps/div)

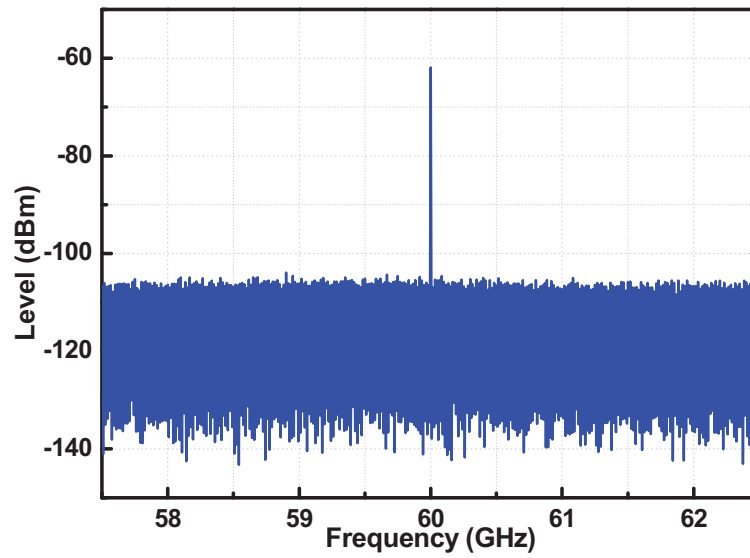


FIG. 4.6. Electrical spectrum of the generated 60-GHz millimeter-wave signal.

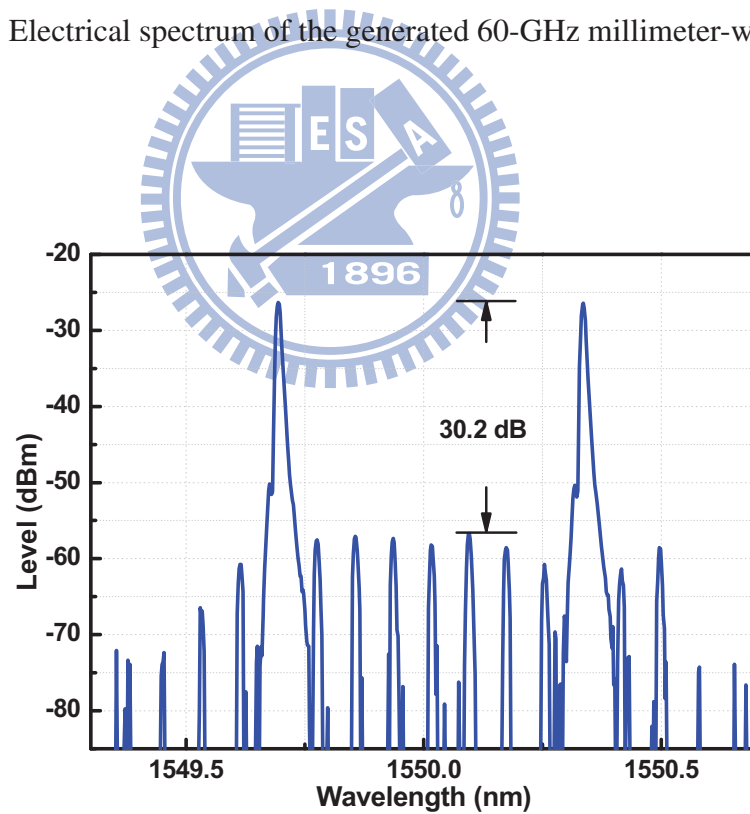


FIG. 4.7. Optical spectrum of the generated 80-GHz optical millimeter-wave signal.

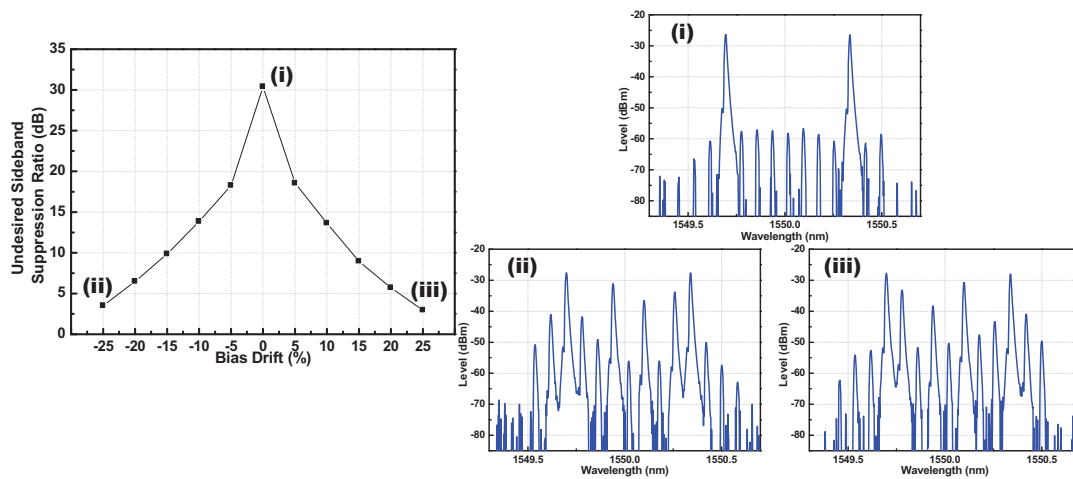


FIG. 4.8. Undesired sideband suppression ratio versus first DP-MZM bias deviation ratio, and optical spectra.

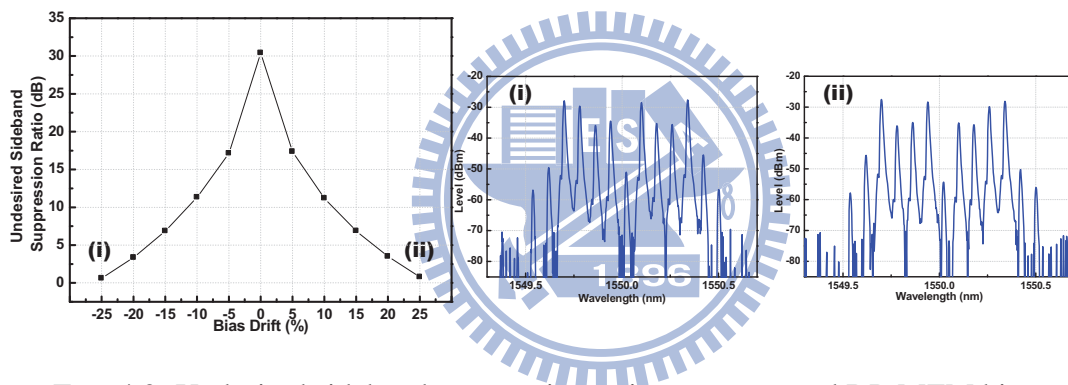


FIG. 4.9. Undesired sideband suppression ratio versus second DP-MZM bias deviation ratio, and optical spectra.

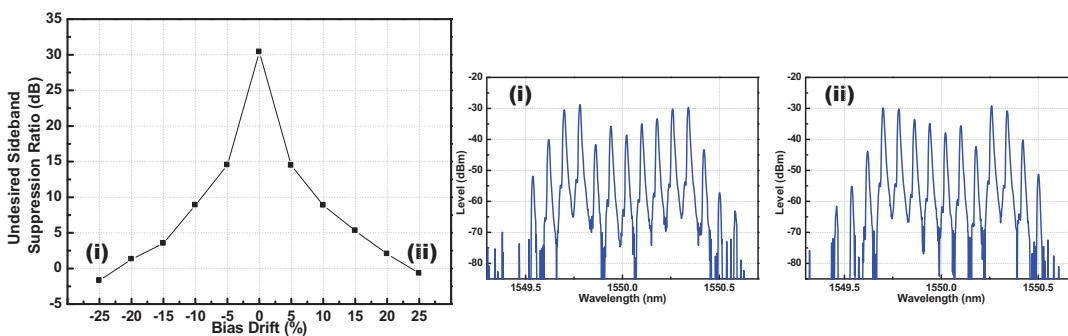



FIG. 4.10. Undesired sideband suppression ratio versus all DP-MZM bias deviation ratio, and optical spectra.

defined as $(\Delta V/V_\pi) \times 100\%$, where ΔV is bias voltage deviation and V_π is the half-wave voltage of the sub-MZs. Optical spectra with the optimal and 25% bias drift conditions are shown in insets of FIG. 4.8. The undesired sideband suppression ratio degradations and optical spectra with second-stage DP-MZM bias drifts are also shown in FIG. 4.9. 30-dB degradation is observed with 25% bias voltage deviation ratio. FIG. 4.10 shows the undesired sideband suppression ratio degradation with all the DP-MZM bias drafts. About 30-dB undesired sideband suppression ratio degradation is observed with 25% bias voltage deviation ratio. The undesired sideband suppression ratio will be higher than 15 dB, which is sufficient for most millimeter-wave application when the bias voltage deviation ratios are controlled within $\pm 5\%$ using bias feedback control circuits.

4.1.3 Summary



A filterless frequency-octupled optical millimeter-wave generation system is proposed in this section. Two commercially available DP-MZMs are keys to the proposed system. V-band 60-GHz and W-band 80-GHz optical millimeter-wave signal are experimentally generated from 7.5- and 10-GHz driving signals with 30-dB undesired sideband suppression ratios. Time domain waveform with a 50% duty cycle is observed. After transmission of 25-km SSMF, no significant signal distortion is observed. The undesired sideband suppression ratio is higher than 15 dB when the bias deviation ratios are less than $\pm 5\%$ of the half-wave voltages. Optical millimeter-wave signal with frequency up to 320-GHz can be generated using the state-of-the-art 40-GHz DP-MZMs. The proposed frequency octupling optical millimeter-wave generation is a potential solution for the future ultra-high frequency millimeter-wave applications.

4.2 W-Band Wireless Communication

The tremendous increase in the necessary bandwidth of wireless data-transmission has attracted attention on ways to use the millimeter wave bands at 60 GHz (V-band) or above 100 GHz (W-band) as the carrier frequency for the realization of systems with very high transmission data rates over many gigabits-per-second [21, 57]. Lately, the research group at NTT reported excellent results for a 10 Gb/s line-of-sight wireless linking at 120 GHz, achieved by using a uni-traveling-carrier photodiode (UTC-PD) based photonic transmitter [57] with on-off keying (OOK) data format and direct modulation on 120-GHz optical carrier wave. However, in such a system, the serious fading and time-shifting effects induced by fiber chromatic dispersion of the data signal with the high-frequency optical local-oscillator (LO) signal at the V or W bands may seriously limit range of data transmission in optical fiber [58]. To obtain a transmission range, two different optical wavelengths are usually adopted for the data and LO signals [59, 60] in ROF systems. An additional high-frequency millimeter-wave mixer or electro-optic (E-O) modulator is usually necessary at the base station to up-convert the data signal and then radiate the up-converted signal to the user-end [58].

The idea of utilizing the nonlinearity of high-speed PDs [60–64] to serve as the optoelectronic (OE) mixer, such as UTC-PDs [61, 62], and realize this up-conversion process is very attractive, because this could eliminate the necessity of the high-frequency electronic mixer or E-O modulator. In this work, a near-ballistic uni-traveling carrier photodiode (NBUTC-PD) [65, 66] which can provide low up-conversion loss and wide modulation bandwidth is utilized to demonstrate wireless QPSK and 8-QAM data transmission at W-band (100-GHz) under bias modulation without using the forward bias operation to enhance the nonlinearity as for the case of UTC-PD [63, 64]. The NBUTC-PD is composed of a quasi-yagi radiator for feeding the photo-generated millimeter-wave power into WR-10 waveguide based horn

antenna. Compared to the p-i-n PD based OE mixer [60], the UTC-PD based OE mixer has much lower up-conversion loss and higher up-converted RF power due to its superior high-speed and high-power performance to p-i-n PDs [67].

4.2.1 Device Structure And Measurement Setup

Figure 4.11 (a) shows a top view of the demonstrated device, which is consisted of a diced NBUTC-PD chip with a $64\text{-}\mu\text{m}^2$ active area, which exhibits a optical-to-electrical (OE) bandwidth of more than 110-GHz under a $25\text{-}\Omega$ load resistance with a responsivity of 0.15A/W [66], a quasi-Yagi antenna, and a RF choke. The entire module is formed on an AlN substrate, which gives it sufficient thermal conductivity for high-power operation. The structure of the epi-layer and the fabrication process were described in our earlier work [66]. FIG. 4.11 (b) shows the measured optical-to-electrical (OE) frequency response of the NBUTC-PD chip under -3-V bias, which is flat from DC to 110 GHz. In contrast with a taper-slot antenna, which is typically used for rectangular waveguide feeding and has an electrical length as long as 3 to 5 times that of the operating wavelengths, the size of the proposed radiator is much more compact and electrical length is as short as half of the wavelength. The fan-shaped broadband transition between the co-planar waveguide (CPW) and the slot-line acts as an impedance matching circuit. During operation, the electrical- data signal is fed at the IF input port, as shown in FIG. 4.11 (a), and the RF choke can effectively block the electrical leakage of photo-generated LO signal and up-converted RF signal both at around 100GHz to IF input port.

FIG. 4.11 (c) and (d) shows a conceptual diagram and a photograph of our device used for WR-10 waveguide feeding. As can be seen, during operation, only the quasi-yagi radiator was inserted into the WR-10 rectangular waveguide-based standard horn antenna at the W-band (with a 24 dBi gain) for feeding photo-generated millimeter-wave signal. The optical LO signal, which is generated by the octupling optical fre-

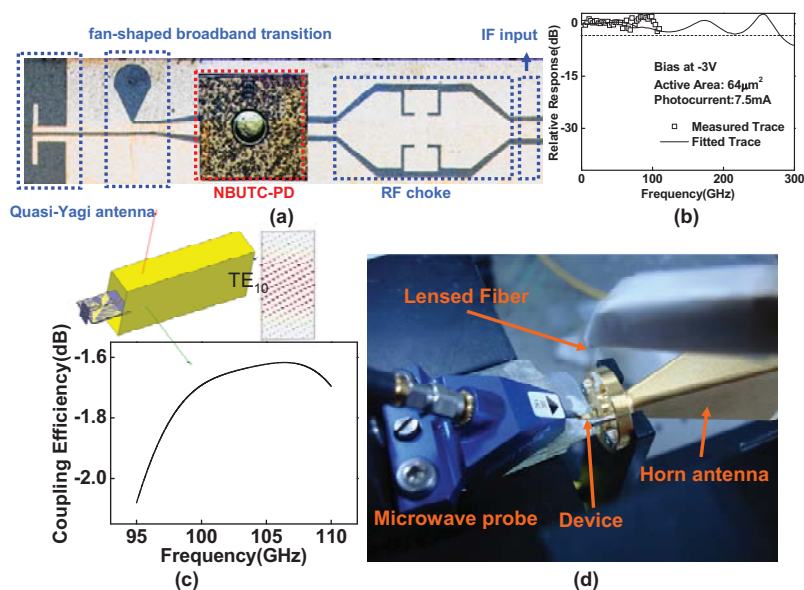


FIG. 4.11. (a) The top-view of the demonstrated device; (b) the measured and fitted OE frequency response of the used NBUTC-PD chip under -3V bias; (c) the conceptual diagram and (d) picture of our device for feeding WR-10 waveguide.

quency technology with the central optical wavelength fixed at around 1550nm and 12.5-GHz driving signals, runs through the EDFA and tunable optical attenuator. Lens fiber is then used to focus the signal onto the substrate microlens of NBUTC-PD. Thus, all electrical photo-generated LO signals and up-converted data signals are radiated into free space by using the aforementioned horn antenna feeding technique.

A spectrum analyzer (Agilent E444BA) with a W-band mixer (Agilent 11970W) was used to detect the millimeter-wave power output from our device. FIG. 4.12 (a) shows the transfer curve of measured millimeter-wave power (at 102.5-GHz operating frequency) in log scale and photocurrent vs. reverse DC bias of the device without optical LO power injection. This figure reveals that, the measured millimeter-wave power varies substantially when the reverse bias ranges from -1.5 V to -2.5 V (33.67dB/Volt). In addition, the variation of measured DC photocurrent in such range of bias voltage (-3 V to -1 V bias) is slight. FIG. 4.12 (b) shows the same trace of de-

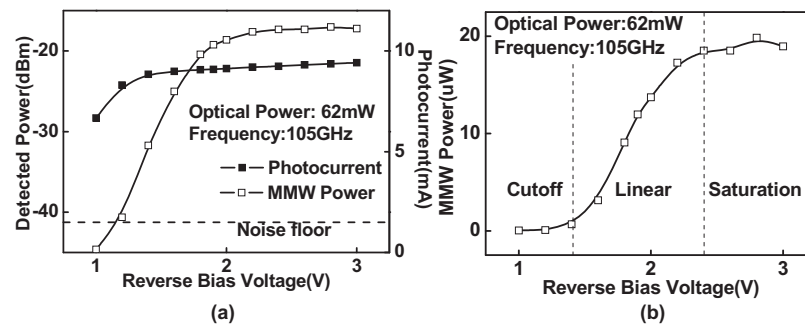


FIG. 4.12. (a) the transfer curve of measured millimeter-wave power with corresponded photocurrent vs. reverse DC bias; (b) the same power trace plot in linear scale.

tected millimeter-wave power vs. bias voltage in linear scale. As shown in FIG. 4.12 (b), this trace can be divided into three regions: cutoff, linear, and saturation. Thus, the optimum pre-bias point for highest modulation efficiency in our device is expected to approximate -2 V in the middle of linear region.

Figure 4.13 shows the system setup for W-band wireless QPSK or 8-QAM data transmission. The QPSK/8QAM IF signal is generated by an arbitrary waveform generator (AWG) and then fed into the IF port of the device to modulate the bias point of the device. The inset shows the optical spectrum of the high-performance optical MMW source with 18-dB harmonic distortion suppression ratio. The receiver end consists of a W-band horn antenna, a W-band low-noise-amplifier (LNA) (QuinStar: QLW-90a06030-P1, gain: 30dB, NF: 60dB), and a fast W-band power detector (Militech: DXP-10-RPFW0) to detect the envelope and data signal phase at 2.5-GHz IF. The signal detected by the power detector is boosted by an IF amplifier (MITEQ: AMF-3D-00101200-24-10p, gain: 27 dB, NF: 2 dB) and then fed into a high-speed real-time scope before performing off-line signal processing. After the NBUTC-PD, the W-band 1.25-Gsymbol/sec QPSK/8QAM signals were generated with the center wavelength at 102.5 GHz, which occupies from 101.25 GHz to 103.75 GHz as transmission band, equivalently.

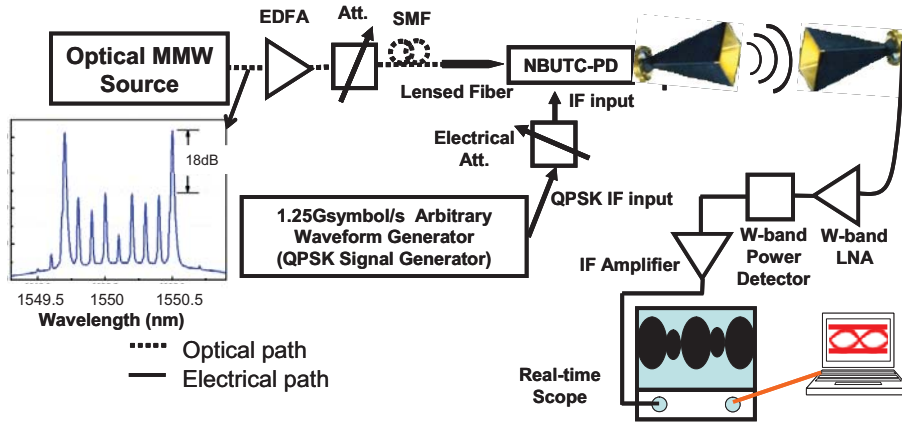


FIG. 4.13. The system setup for W-band wireless QPSK or 8-QAM data transmission.

4.2.2 Experimental Results

Figure 4.14 (a) shows transmission distance vs. $-\log(\text{BER})$ of 2.5-Gbit/s QPSK wireless data transmission under different photocurrent and bias condition. The traces under optimized condition (close symbols) have a lower bit error rate (BER) than the non-optimized one (open symbols) does under the same transmission distance and photocurrent. FIG. 4.14 (b) and (c) show the constellations under 15-cm and 180-cm transmission distance with 9-mA photocurrent and optimized pre-bias condition, respectively. The corresponded in-phase (I) and quadrature-phase (Q) eye-patterns of these constellations are shown in the inset. The eye-height of both decrease as transmission distance increases. This phenomenon results from diffraction loss during wireless link, which depends on the gain and directivity of the antenna. A clear 2.5-Gbit/s QPSK signal with 180cm transmission distance can be achieved successfully.

Figure 4.15 (a) shows the transmission distance vs. Error Vector Magnitude (EVM) of 3.75-Gb/s 8QAM wireless data transmission with different photocurrent and bias condition. The EVM was defined as $\text{EVM}[\%] = 100 \times \left[\frac{\sum_{i=1}^N |\bar{d}_r - d_i|^2}{N} \right]^{1/2} / |d_{max}|$, where \bar{d}_r and d_i are the received and ideal sym-

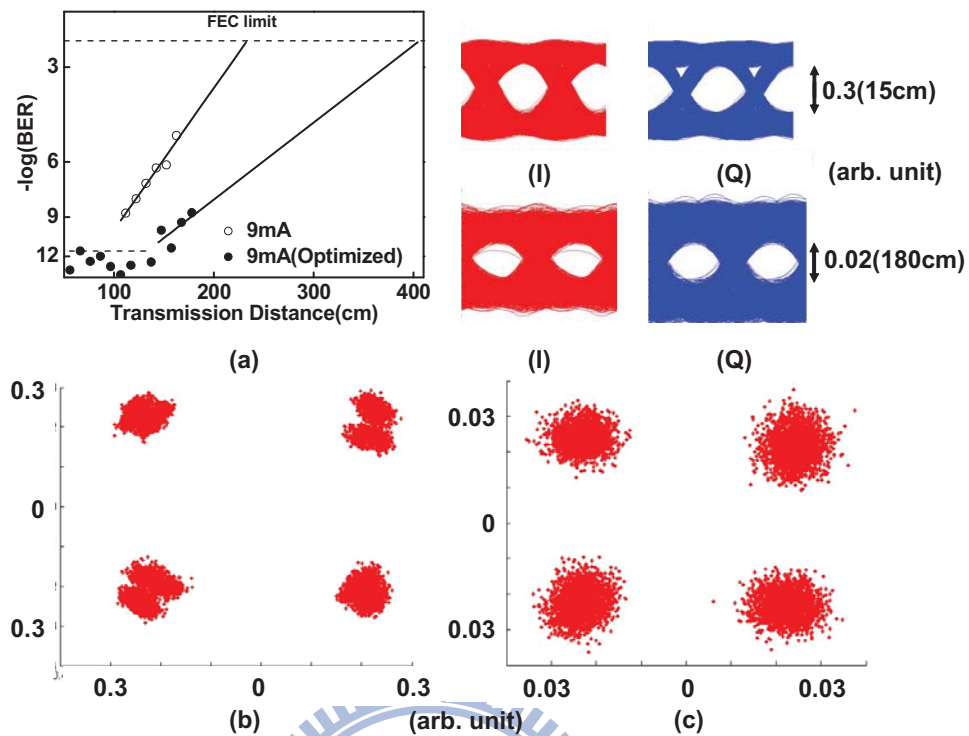


FIG. 4.14. (a) transmission distance vs. $-\log(\text{BER})$ of 2.5Gbit/s QPSK wireless data transmission under different photocurrent and bias condition. And the constellations under (b) 15cm and (c) 180cm transmission distance with 9mA photocurrent. The inset shows the corresponded in-phase (I) and quadrature-phase (Q) eye-patterns of these constellations.

bols, respectively, and d_{max} is the maximum symbol vector in the constellation. An optimized condition with 9-mA photocurrent can be obtained. An 18% EVM can be achieved after 170-cm wireless transmission with 9-mA photocurrent and bias condition. FIG. 4.15 (b) and (c) also show constellations under 25- and 170-cm wireless transmission distance with optimized condition. A clear 3.75-Gb/s constellation diagram can be achieved after 170-cm wireless transmission.

Optical fiber transmissions of the generated optical millimeter-wave signals are also experimentally demonstrated. FIG. 4.16 (a) and (b) show the constellation diagrams of demodulated 8QAM signals with transmissions of 50- and 100-km standard single mode fiber (SSMF), respectively, and 25-cm wireless transmission. The EVMS

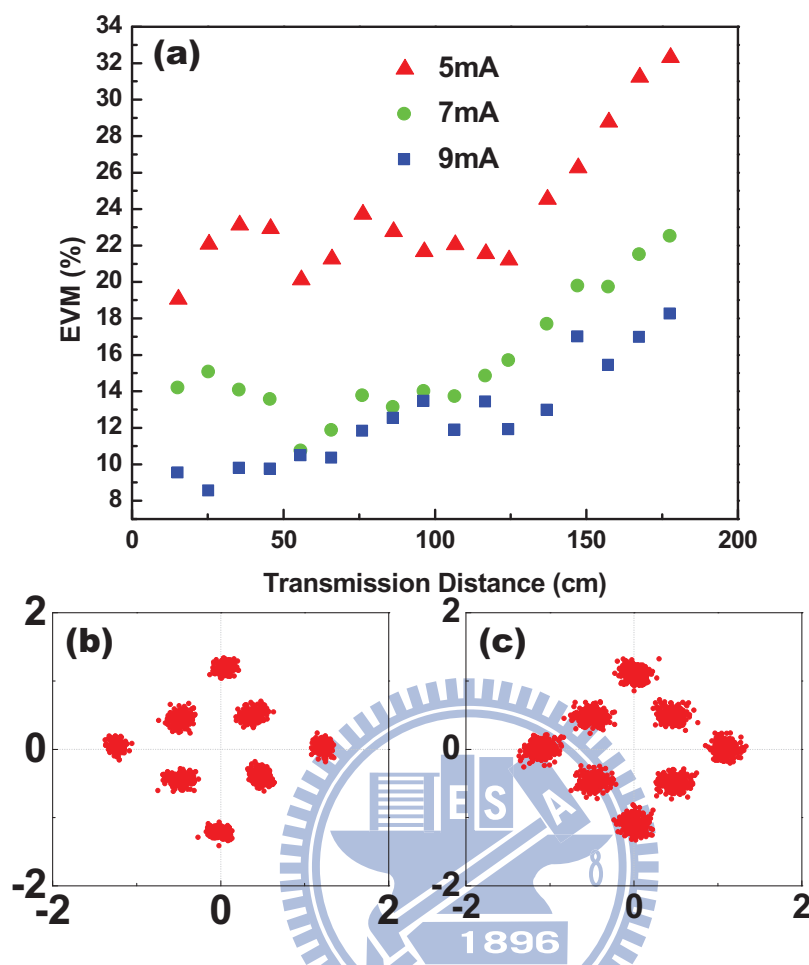


FIG. 4.15. (a) transmission distance vs. EVM of 3.75-Gbit/s 8QAM wireless data transmission with different photocurrent and bias condition. And the constellations under (b) 25 cm and (c) 170 cm transmission distance with 9mA optimized photocurrent and optimized condition.

of FIG. 4.16 (a) and (b) are 9.28% and 9.35%, respectively. Constellations of 8QAM signals with 50- and 100-km SSMF transmission, and 170-cm wireless transmission are also shown in FIG. 4.16 (c) and (d). The EVMs of FIG. 4.16 (c) and (d) are 16.09% and 16.57% respectively. Based on the measurement results, as shown in FIG. 4.16, we can thus conclude that by use of the bias modulation technique, which means that the photonic transmitter-mixer directly be modulated by the remote-regenerated data signal [58] at different optical wavelength with optical LO signals, the base station

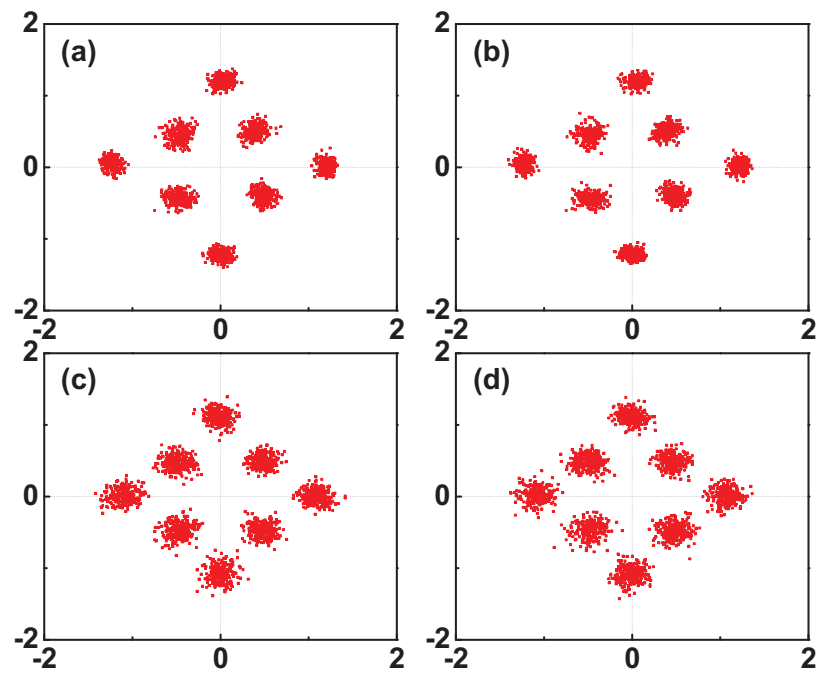


FIG. 4.16. Constellation diagrams of 8QAM signals with (a) 50-km fiber transmission and 25-cm wireless transmission; (b) 100-km fiber transmission and 25-cm wireless transmission; (c) 50-km fiber transmission and 170-cm wireless transmission; (d) 100-km fiber transmission and 170-cm wireless transmission.

can be extended to more than 100km far from central office through SSMF without sacrificing the signal quality in the proposed 100-GHz ROF systems.

4.2.3 Summary

In this section, a W-band wireless vector signal generation using a NBUTC-PD with bias modulation was experimentally demonstrated. 1.25-GSymbol/sec QPSK and 8QAM wireless data transmission at 102.5-GHz were achieved with 170-cm wireless distance and 100-km fiber transmission. Such measurement result clearly indicates the nonlinear photodetection scheme (bias modulation technique) can definitely be utilized in W-band ROF network.

4.3 Optical Millimeter-Wave Generation with Frequency 12-tupling

To meet the requirements of ultra-high frequency millimeter-wave applications, an optical frequency 12-tupling approach to generate high-purity optical two-tone signal for millimeter-wave generation with frequency up to 210 GHz is proposed in this section, as the conceptual diagram shown in FIG. 4.17.

The proposed approach consists of two main steps. The first step is the proposed frequency-quadrupled optical millimeter-wave signal generation system. High purity two-tone optical signal with 36-dB optical carrier and harmonic distortion suppression ratio can be obtained. In the second step, a semiconductor optical amplifier (SOA) is utilized to perform four-wave mixing effect and thereby generating two new sixth-order optical sidebands. Due to the high optical carrier and harmonic distortion suppression ratios of the four-wave-mixing pump signal, the suppression ratios of the undesired optical sidebands are more than 16 dB relative to the sixth-order sidebands after four-wave mixing. Following, optical interleavers are employed to simultaneously suppress two undesired second-order sidebands, the optical carrier and undesired harmonic distortion suppression ratios of the generated optical two-tone signals with 120-GHz and 210-GHz separation can exceed 30 and 20 dB, respectively. Because high frequency optical millimeter-wave signals can be generated using low frequency components and transmitted over low-loss optical fiber networks, the proposed system can be a potential candidate for next generation ultra-high frequency millimeter-wave applications.

4.3.1 Concept and Theoretical Model

Figure 4.18 shows the experimental setup of the proposed system. A commercial distributed feedback (DFB) laser is employed as the optical source. As shown in equation (3.5), the electrical field of the optical signal at the output of the DP-MZM

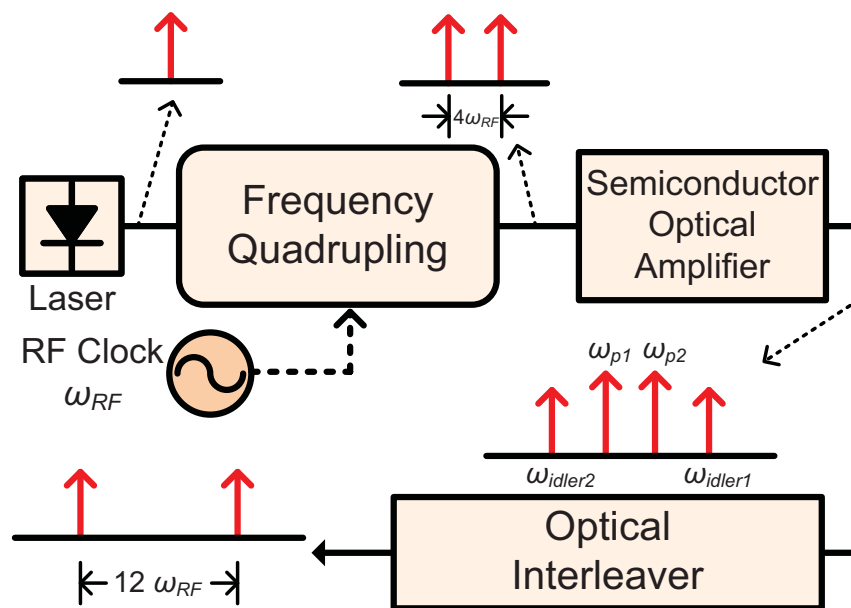


FIG. 4.17. Conceptual diagram of the optical millimeter-wave signal generation with frequency 12-tupling.

can be expressed as the following with the high order terms ignored.

$$E_{out} = -E_o \cdot \{J_2(m) \cos[(\omega_o + 2\omega_{RF})t] + J_2(m) \cos[(\omega_o - 2\omega_{RF})t]\} \quad (4.5)$$

Then, the generated two-tone optical signal is sent into an SOA to perform the Four-Wave-Mixing (FWM). FWM is an optical nonlinear Kerr effect which relates to the third-order electric susceptibility. To demonstrate the concept and feasibility of the proposed method, we use an SOA whose potential to integrate with other photonic devices makes SOAs a reasonable choice [68]. After the frequency-quadrupled optical millimeter-wave signal generation system, the optical FWM effect is created using an SOA. Two new optical sixth-order sidebands are emerged with a frequency separation of $12\omega_{RF}$ when two optical second-order sidebands with a frequency separation of $4\omega_{RF}$ are incident into the SOA (Uniphase CQF872). The bias current is set at 300mA, with optical power gain of 20 dB, gain bandwidth of 60 nm and noise figure of 9 dB.

Consider that an optical signal composed of three different frequencies incidents into a nonlinear medium. The frequency of the newly emerging signal is a combination of the incident optical signal frequencies:

$$\omega_{idler} = \omega_{p1} + \omega_{p2} - \omega_{probe} \quad (4.6)$$

where ω_{idler} is the optical angular frequency of the newly emerging signal which is commonly called an “idler”. ω_{p1} and ω_{p2} denotes the pump signal angular frequencies, and ω_{probe} is the probe signal angular frequency.

If an optical signal with only two different optical frequencies incident into the nonlinear medium, a special case that has been known as partially degenerate four-wave mixing arises. Each tone of the input optical signal can be the pump signal or the probe signal when they are sent into the nonlinear material. The optical frequency of the new emerged idler can be expressed as

$$\omega_{idler} = 2\omega_p - \omega_{probe} \quad (4.7)$$

,where ω_p denotes the angular frequency of the pump signal. While the high-purity two-tone optical millimeter-wave signal is generated by frequency quadrupling and incident into the SOA, the second-order optical sidebands with angular frequencies of $\omega_o - 2\omega_{RF}$ and $\omega_o + 2\omega_{RF}$ lead to the partially degenerate four-wave mixing and the emergence of two new idlers. The idler frequencies can be expressed as

$$\begin{aligned} \omega_{idler1} &= 2\omega_{p1} - \omega_{probe1} \\ &= 2(\omega_o - 2\omega_{RF}) - (\omega_o + 2\omega_{RF}) \\ &= \omega_o - 6\omega_{RF} \end{aligned} \quad (4.8)$$

and

$$\begin{aligned}
 \omega_{idler2} &= 2\omega_{p2} - \omega_{probe2} \\
 &= 2(\omega_o + 2\omega_{RF}) - (\omega_o - 2\omega_{RF}) \\
 &= \omega_o + 6\omega_{RF}
 \end{aligned} \tag{4.9}$$

Two optical idler sidebands (ie. ω_{idler1} and ω_{idler2}) are obtained with frequency spacing of 12 times that of the RF driving signal through optical FWM.

After the four-wave-mixing, the sixth-order sidebands are emerged. However, the original two-tone pump lightwaves are also amplified by the SOA. In order to yield a high-purity optical millimeter-wave signal, these two optical pump signals (ie. ω_{p1} and ω_{p2}) must be eliminated and optical interleavers are utilized to suppress those. The advantage of using optical interleavers is that two optical pump lightwaves can be simultaneously suppressed [38, 43, 69]. Furthermore, this architecture can be implemented for wavelength divisions multiplexing (WDM) up-conversion in radio-over-fiber (RoF) systems [69].

Figure 4.18 presents the conceptual diagrams of high-purity 120- and 210-GHz two-tone signal generations. For the 120-GHz optical two-tone signal generation, two second order sidebands with 40-GHz frequency spacing along with two sixth-order sidebands with 120-GHz frequency spacing are obtained after the four-wave-mixing, as shown in inset (i) of FIG. 4.18 (a). To suppress undesired optical sidebands, the optical signal generated from SOA are sent into the first optical interleaver with a channel spacing of 25 GHz, as shown in inset (ii) of FIG. 4.18 (a). At the odd channel output of the first optical interleaver, the original pump signal are partially suppressed. However, the suppression is insufficient. Therefore, the second optical interleaver with a channel spacing of 50 GHz is employed, as shown in inset (iii) of FIG. 4.18 (a). Two-tone optical signal separated by 120 GHz with high optical carrier and harmonic distortion suppression ratio is obtained at the even output of the second

optical interleaver, as displayed in inset (iv) of FIG. 4.18 (a). On the other hand, 210-GHz optical two-tone signal can be obtained by using the same concept as shown in FIG. 4.18 (b). Nevertheless, the 210-GHz optical two-tone signal is obtained at the odd output of the second optical interleaver, as shown in inset (iv) of FIG. 4.18 (b).

4.3.2 Experimental setup and results

To generate optical millimeter-wave signal using four-wave-mixing by high non-linear materials, a high-purity pump signal is required. If the optical carrier and harmonic distortion suppression ratio is low, four-wave-mixing efficiency will be degraded and undesired optical sidebands will also be obtained. The proposed optical millimeter-wave signal generation technique with frequency quadrupling provides a high-purity pump signal for four-wave mixing. The MZM extinction ratio is an important factor in carrier suppressed optical millimeter-wave signal generation schemes. The optical carrier should be totally suppressed under ideal condition with infinite MZM extinction ratio. However, the extinction ratios of the commercially available MZMs are finite due to amplitude imbalance in MZM arms. The typical extinction ratios of commercially available MZMs are 20-30 dB which come from the fabrication errors. In the proposed frequency quadrupling technique, the amplitude imbalance can be compensated by trimming the modulation depth between MZ-a and MZ-b, and the extinction ratio of the MZ-c are improved.

Figure 4.19 shows the optical spectrum of the generated optical tones separated by 40 GHz without modulation depth trimming. The resolution bandwidth of the optical spectrum analyzer (OSA) in this work is 0.01 nm. The optical carrier suppression ratio is about 19 dB which is restricted by intrinsic MZM extinction ratio. After the FWM in an SOA, not only the expected second and sixth order optical sidebands are obtained but the optical carrier and fourth order terms are obtained, as shown in FIG. 4.20. Low optical carrier suppression ratio pump signals degrades the efficiency of

FWM, and signals with unwanted sidebands could be obtained.

Figure 4.21 shows the optical spectrum of the optical tones separated by 40 GHz that are generated from the 10-GHz RF driving signal using frequency quadrupling with modulation depth trimming. After employing modulation depth trimming, the optical carrier is suppressed and the undesired harmonic distortion suppression ratios exceed 36 dB. The generated high-purity two-tone signals are sent into the SOA as the pump signal to perform the four-wave-mixing effect. FIG. 4.22 shows the optical spectrum after the FWM in the SOA. Two new optical sixth order sidebands with a frequency spacing of 120 GHz are obtained along with the original 40-GHz optical tones. Compared with the optical spectrum which is shown in FIG. 4.20, the undesired optical sidebands are much lower than that in FIG. 4.22. After filtering using two optical interleavers, high-purity two-tone optical signal separated by 120 GHz is obtained with -9-dBm average optical power. The optical spectrum is shown in FIG. 4.23. The optical carrier and harmonic distortion suppression ratios exceed 30 dB, which is excellent in millimeter-wave applications.

Optical spectrum of optical tones separated by 210 GHz generated from a 17.5-GHz RF driving signal is also demonstrated experimentally in this work. FIG. 4.24 presents the optical tones separated by 70 GHz which is generated by frequency quadrupling with modulation depth trimming. By using the modulation depth trimming, the optical carrier is suppressed perfectly. The optical carrier and undesired harmonic distortion suppression ratios of the optical tones separated by 70 GHz are higher than 36 dB. The high-purity two-tone signal was also sent into the SOA to perform fFWM. FIG. 4.25 shows the optical spectrum at the output of the SOA. Two sixth order sidebands with 210-GHz frequency spacing are emerged along with the original second order sidebands with 70-GHz frequency spacing. After the filtering of optical interleavers, high purity two-tone signal separated by 210 GHz are obtained as shown in FIG. 4.26. The optical power of the generated optical two-tone signal is about

-11 dBm. The optical carrier and undesired harmonic distortion suppression ratios exceed 20 dB, which is good enough for most millimeter-wave application.

4.3.3 Summary

In this section, an optical millimeter-wave signal generation with a frequency of 12 times that of the RF driving signal was proposed. The key to the proposed system is the optical high-purity frequency-quadrupled millimeter-wave signal generation using a DP-MZM. 40- and 70-GHz high purity two-tone optical signals were experimentally demonstrated from 10- and 17.5-GHz RF driving signals. Modulation depth trimming between MZ-a and MZ-b are employed to compensate the amplitude imbalance between the MZM arms and improve the optical carrier suppression ratio. The optical carrier and harmonic distortion suppression ratios of the generated optical two-tone signals separated by 40 and 70 GHz using frequency quadrupling technique were more than 36 dB. Following optical frequency quadrupling, optical FWM was promoted utilizing an SOA. Since the excellent optical carrier and harmonic distortion suppression ratio of the FWM pump signals, only the second and sixth order sidebands were obtained at the output of the SOA. After filtering out the undesired sidebands using optical interleavers, high-purity optical two-tone signals separated by 120 and 210 GHz were obtained. The optical carrier and harmonic distortion ratios of the generated 210- and 120-GHz optical two-tone signals were 20 and 30 dB, respectively.

The frequency of the generated optical millimeter-wave signal is 12 times that of the RF driving signal. Millimeter-wave signals with frequency beyond 100 GHz can be easily achieved using low frequency RF equipments and components. Since the frequency response of the state-of-the-art MZM is up to 40 GHz, the proposed system provides a reliable and cost-effective solution for optical millimeter-wave generation with frequencies of up to 480 GHz and is a promising candidate for ultra-high

frequency millimeter-wave applications.

4.4 Conclusion

Optical millimeter-wave generation system with frequency octupling and 12-tupling for ultra-high frequency millimeter-wave applications were proposed in this chapter. With the high order multiplication factors, high frequency millimeter-wave signals can be generated using low-frequency RF components and modulators. In addition, the signal coverages of the generated millimeter-wave signals can be increased using low-loss optical fiber.

W-band wireless communication system with single carrier vector signals were also demonstrated in this chapter. The 100-GHz LO signal was generated from the frequency-octupled optical millimeter-wave generation system. A NBUTC-PD with bias modulation was utilized for the W-band wireless vector signal generation. 1.25-GSymbol/sec QPSK and 8QAM wireless data transmission at 102.5-GHz were achieved with 170-cm wireless distance and 100-km fiber transmission.

In summary, the feasibility of ultra-high frequency optical millimeter-wave generation with high order multiplication was demonstrated. The proposed optical millimeter-wave generation systems can be potential candidates for the future high frequency millimeter-wave applications.

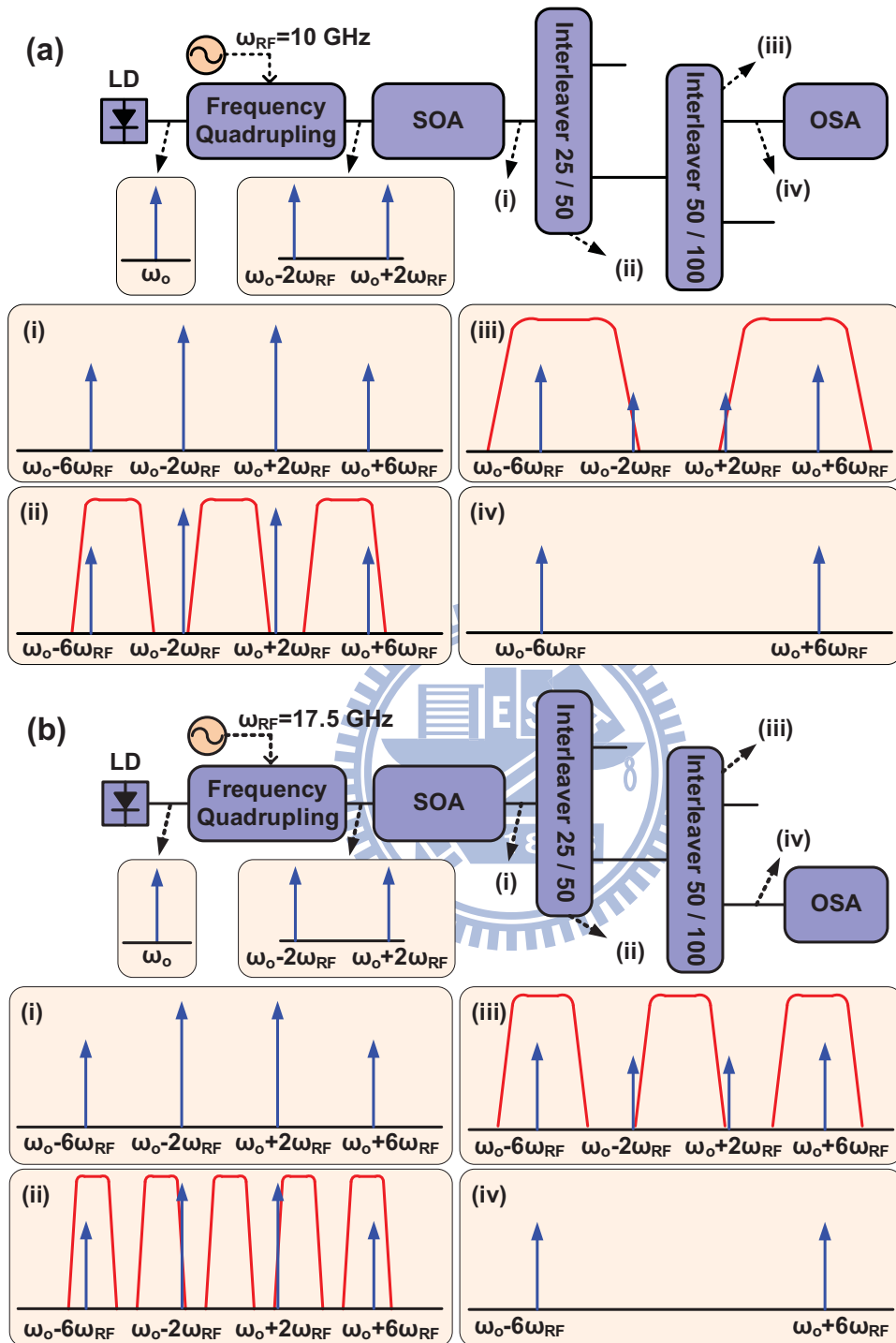


FIG. 4.18. Conceptual diagram of (a) 120-GHz and (b) 210-GHz optical millimeter-wave generations.

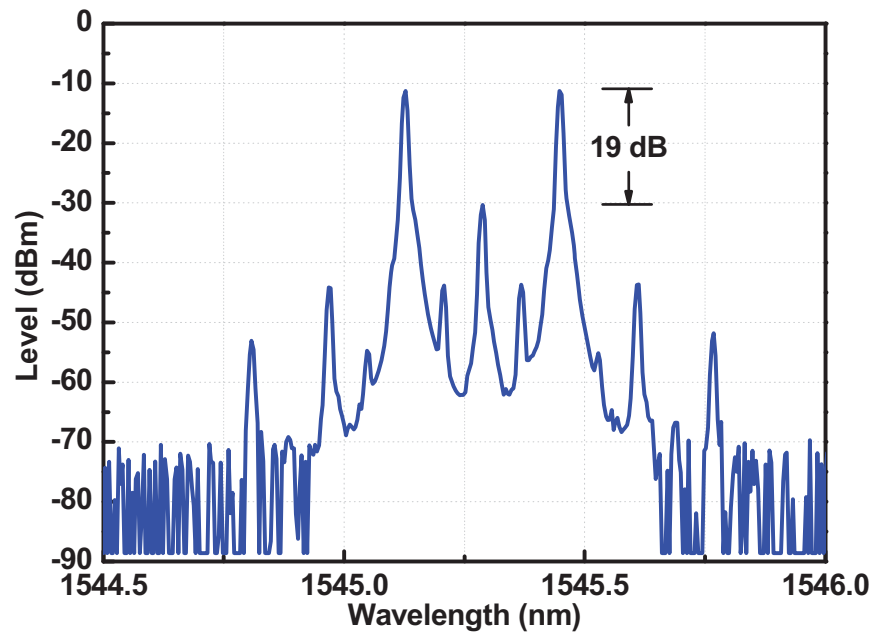


FIG. 4.19. Optical spectrum of the generated optical tones separated by 40 GHz without modulation-depth trimming.

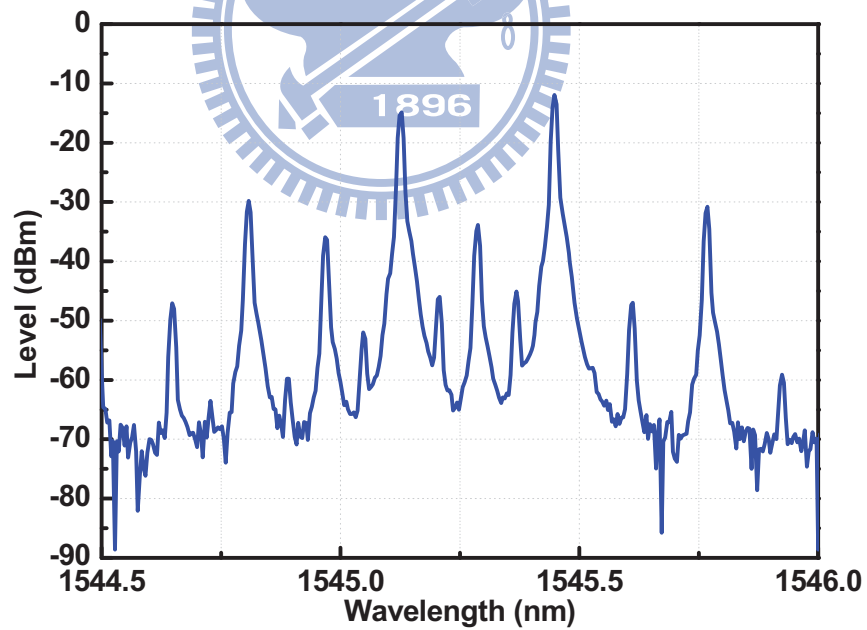


FIG. 4.20. Optical spectrum of the generated optical tones after the FWM for 120-GHz optical millimeter-wave signal generation without modulation-depth trimming.

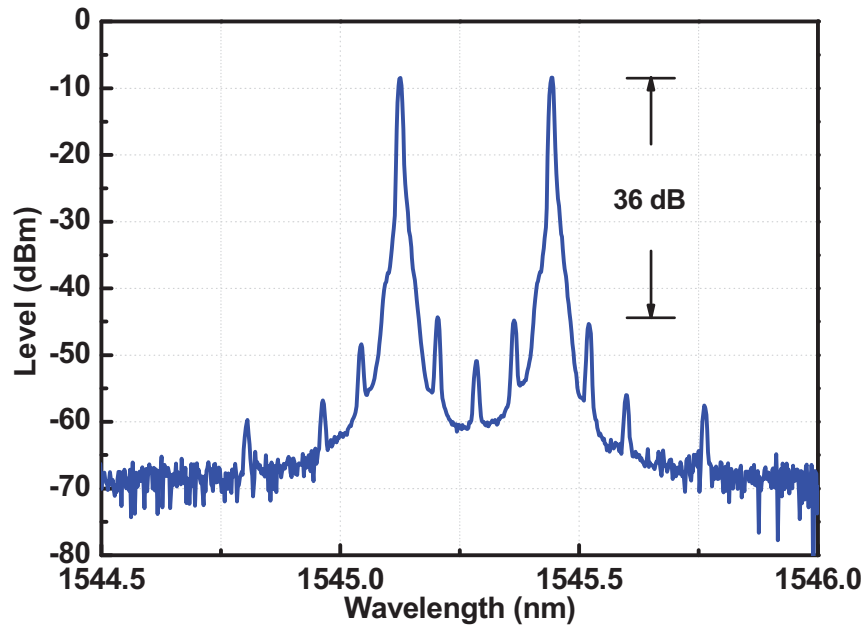


FIG. 4.21. Optical spectrum of the generated optical tones separated by 40 GHz.

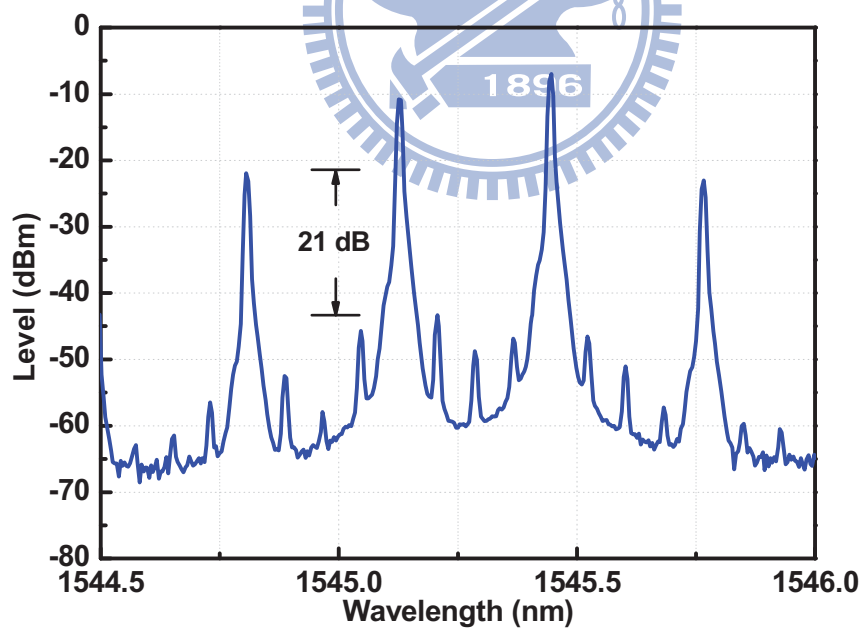


FIG. 4.22. Optical spectrum of the generated optical tones after the FWM for 120-GHz optical millimeter-wave signal generation.

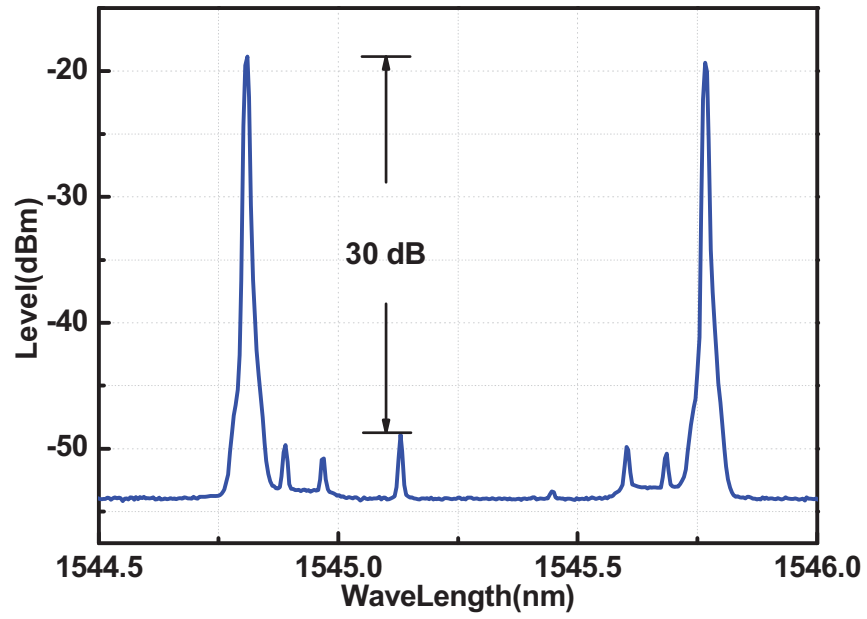


FIG. 4.23. Optical spectrum of the generated optical tones separated by 120 GHz.

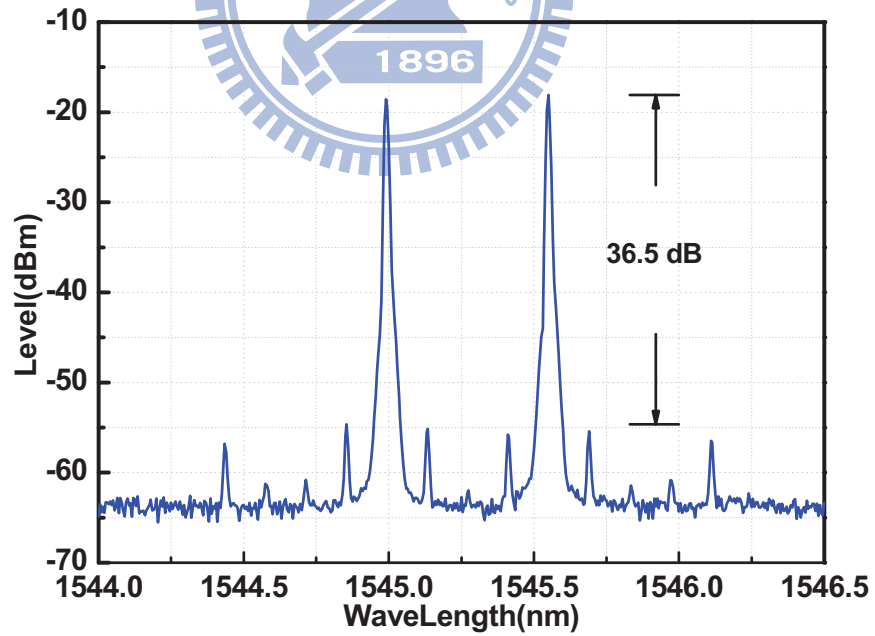


FIG. 4.24. Optical spectrum of the generated optical tones separated by 70 GHz.

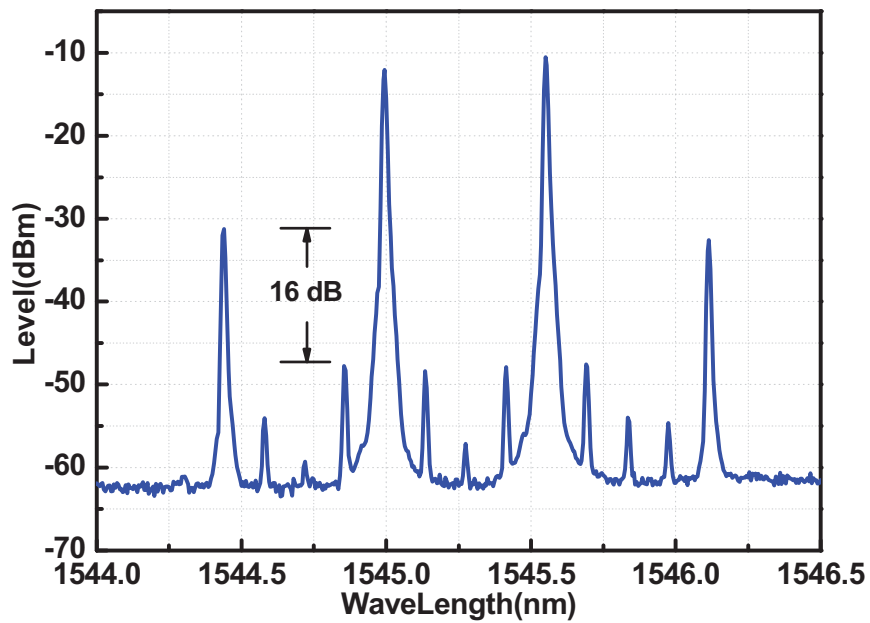


FIG. 4.25. Optical spectrum of the generated optical tones after the FWM for 210-GHz optical millimeter-wave signal generation.

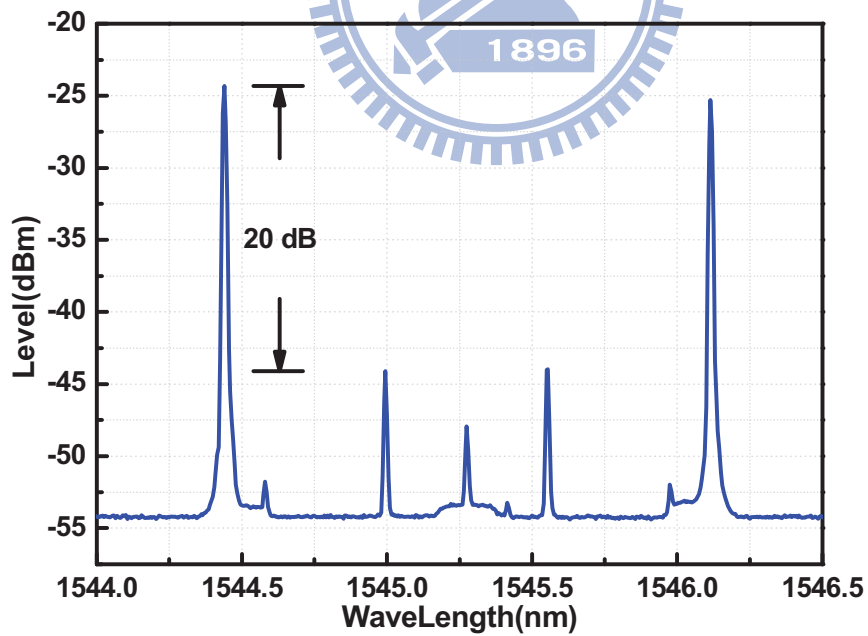


FIG. 4.26. Optical spectrum of the generated optical tones separated by 210 GHz.

Chapter 5

60-GHZ RADIO-OVER-FIBER COMMUNICATION SYSTEM

With the rapidly growing demand for bandwidth, millimeter-wave frequencies along with spectrally efficient modulation formats have become potential candidates for next generation multi-Gbps wireless communication systems. Thanks to the recently released 7-GHz licensed-free band, 60-GHz wireless communication has attracted a lot of attention to support wireless High-Definition TV (WirelessHD TV) or uncompressed video transmission. However, the transmission distance of the 60-GHz wireless signals is strongly restricted by the high path losses and for longer wireless transmission distances, the oxygen absorption [21]. To extend the 60-GHz wireless signal coverage, RoF technologies provide the most promising choice [21–34]. However, the use of RoF systems to generate and transmit 60 GHz signals modulated with spectrally efficient modulation formats still remain a challenge.

There are many techniques for 60-GHz RoF signal generation including one-step electrical signal up-conversion and optical up-conversion with optical multiplication. In this chapter, several modulation systems for 60-GHz RoF signal generation will be proposed. The Tandem-Single-Sideband (TSSB) modulation system and the frequency-sextupled modulation system are electrical along with optical up-conversion system with frequency doubling. The TSSB system can provide frequency

doubling, while the frequency-sextupled system generated the RoF signals with frequency six times that of the driving signals. The Intensity Modulation Direction Detection (IMDD) systems using high speed modulators are with the one-step electrical up-conversion. The systems with optical up-conversion can provide better system performance and longer fiber transmission distance, however, these optical up-conversion are much more complex compared with the IMDD systems. The IMDD systems provide very simple system architectures, but the the fiber transmission distance is limited due to the chromatic dispersion induced performance fading. Beside the modulation systems, the Orthogonal-Frequency-Division-Multiplexing (OFDM) modulation format which utilized in the 60-GHz RoF systems will also be introduced.

5.1 Orthogonal-Frequency-Division-Multiplexing Modulation Format

5.1.1 Introduction

OFDM has become a popular modulation format which is widely adopted in broadband digital communication systems. It has been utilized not only in the wireline communication systems, such as Asymmetric Digital Subscriber Line (ADSL), and cable TV, but also the wireless communication systems, such as Wireless Local Area Network (WLAN, IEEE 802.11 a, g, n), Digital Video Broadcasting (DVB), HD digital radio and wireless HDTV.

Different from the conventional single-carrier modulation formats, such as BPSK, QPSK, 16QAM, and 32QAM, the OFDM is a multi-carrier modulation format provides many advantages. Due to the multi-carrier characteristic, the bandwidth of each sub-carrier is very small compared with the conventional single-carrier modulation format. In single-carrier modulation formats, complex non-linear equalizers are usually required for the compensation for uneven channel response. However, only a simple one-tap equalizer is usually required for the uneven channel response com-

pensation. Moreover, the OFDM modulation can provide higher spectral efficiency compared with the conventional DSB single carrier modulation formats, because of the orthogonality among the sub-carriers.

Another benefit of using OFDM is the low symbol rate. Since multi-channels of signals are transmitted simultaneously in an OFDM symbol, the symbol rate is much lower than the single-carrier modulation format with the same data rate. The low symbol makes the use of a guard interval or a cyclic prefix (CP) between the OFDM symbols affordable, making it possible to handle the time-spreading. Therefore, the OFDM modulation is robust to the inter-symbol interference (ISI) due to the wireless multi-path effect and the fiber chromatic dispersion. Based on these advantages, OFDM has been adopted in long-haul coherent communications (ie. CO-OFDM). To compensate for the uneven channel response and generate wideband signal within the 7-GHz licensed-free band, OFDM is also extensively utilized in 60-GHz wireless communication systems, recently.

However, there are still disadvantages in OFDM which remain great challenges in system design and optimization. The main challenge in OFDM format is the high Peak-to-Average-Power Ratio (PAPR) due to the multi-carrier characteristic. The high PAPR of an OFDM signal easily drives the RF components into saturation and distorts the signal. Another challenge of using OFDM signal is that the OFDM signal is sensitive to the frequency synchronization problems. Therefore, Carrier Frequency Offset (CFO) and Sampling Frequency Offset compensators which increase the requirement of computing power might be required in the OFDM demodulator.

5.1.2 OFDM signal generation

To demonstrate the OFDM signal transmission within the 7-GHz wide license-free band at 60-GHz, OFDM signal generation and demodulation programs using Matlab along with the Arbitrary Waveform Generator (AWG) and Realtime Digital Os-

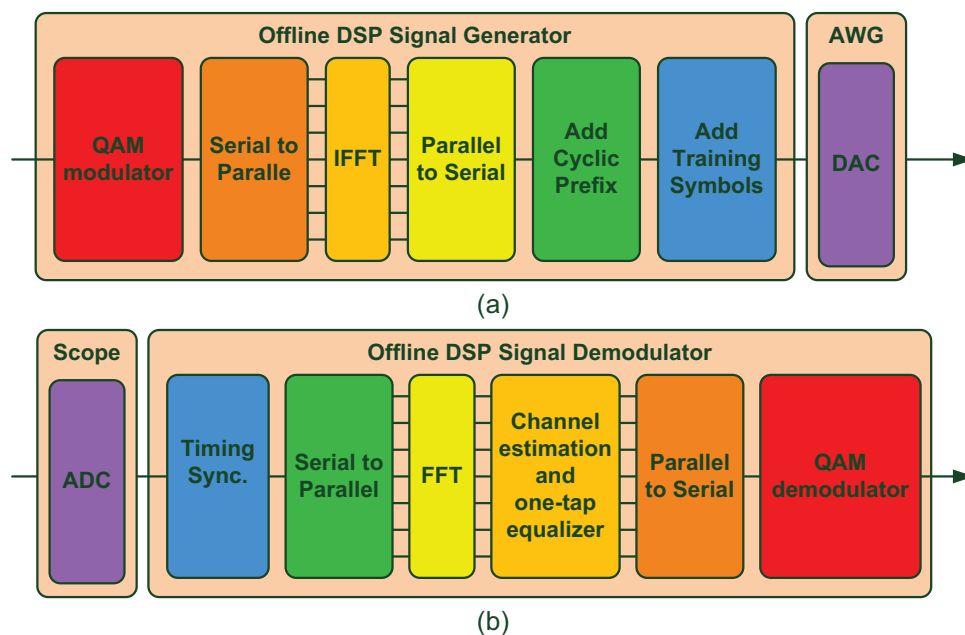


FIG. 5.1. Conceptual diagrams of the OFDM signal generator and demodulator.

cilloscope were developed. FIG. 5.1 (a) shows the conceptual diagram of the OFDM signal generator. In the signal generator, the original binary data stream is sent into a QAM modulator to map the original data on to a QAM constellation. Then, a serial to parallel converter converts the QAM symbol stream in to a parallel symbol stream and mapped the parallel symbol stream to different carrier frequencies which are orthogonal to each other. Then, an Inverse Fast Fourier Transformer (IFFT) and a parallel to serial converter convert the frequency domain signal into a time domain signal and generate the OFDM time domain waveform. Before sending the signal into the AWG for Digital to Analog Conversion (DAC), cyclic prefix and training symbols for timing synchronization and channel estimation are added. After the AWG, the electrical OFDM waveform are sent into the modulation system, transmitted over the system and received using the real-time scope for Analog to Digital Conversion (ADC). FIG. 5.1(b) shows the conceptual diagram of the OFDM signal demodulator. In the demodulator program, timing synchronization using the training symbols is performed

first to find the beginning of the OFDM signal. Then, a serial to parallel converter and Fast Fourier Transformer (FFT) are used to converted the time-domain OFDM waveform into the frequency domain and extract frequency-domain signals. However, all of the OFDM channels experience different amplitude and phase responses from the transmission channels. To compensate the channel responses, channel estimation and one-tap equalization are executed. After the equalization, the received QAM constellation is obtained. Then, a QAM demodulator is utilized for system performance estimation, including the Signal-to-Noise Ratio (SNR) and EVM.

5.2 Tandem-Single-Sideband Modulation System

5.2.1 Concept

Figure 5.2 shows the conceptual diagram of the proposed frequency doubling modulation system using TSSB modulation. TSSB modulation scheme is achieved using a dual-electrode MZM biased at the quadrature point. An OFDM-modulated upper optical sideband and an un-modulated lower optical sideband are performed by adding additional 90° phase shifts to the upper path of the OFDM signal and the lower path of the sinusoidal signal, respectively. The OFDM signal and sinusoidal signal are then combined, as shown in insets (iii) and (iv) of FIG. 5.2 and sent into the dual-electrode MZM. At MZM output, a TSSB optical spectrum that consists of the original optical carrier (ω_c), OFDM-modulated optical sideband ($\omega_c + \omega_{rf1}$), and un-modulated optical sideband ($\omega_c - \omega_{rf2}$) are obtained, as shown in inset (v) of FIG. 5.2. At the remote node, following the transmission of a SSMF, the original optical carrier (ω_c) is separated from the other two optical sidebands by using a fiber Bragg grating (FBG) and an optical circulator, as shown in insets (vi) and (vii) of FIG. 5.2. The original optical carrier can be utilized for an uplink application. The un-modulated and OFDM-modulated optical sidebands are received for wireless ap-

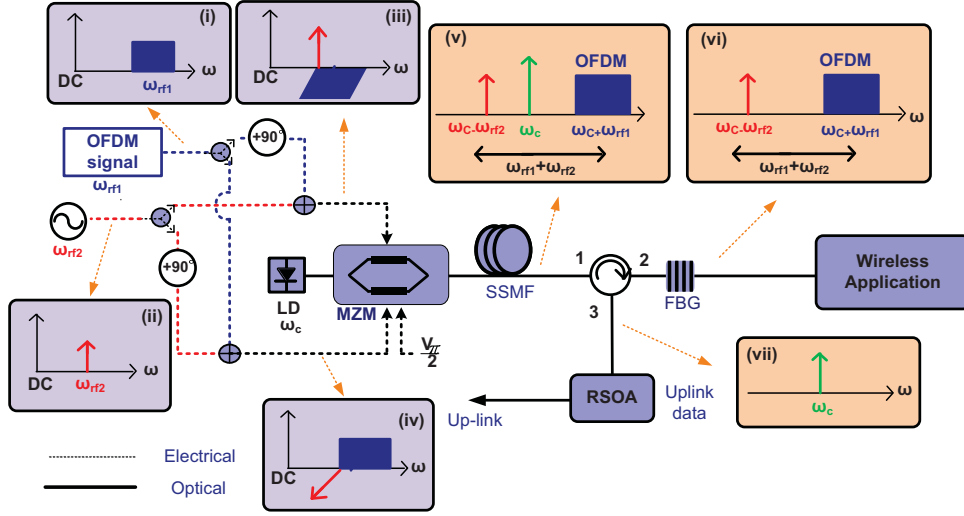


FIG. 5.2. Conceptual diagram of the frequency doubling system using TSSB modulation.

applications. Notably, frequency doubling can be achieved when ω_{rf1} equals ω_{rf2} . The optical power ratio between the un-modulated and OFDM-modulated optical sidebands ($OPR = P_{un-modulated}/P_{data-modulated}$) is an important factor for optimizing the receiver performance [70]. Since the un-modulated and OFDM-modulated optical sidebands are generated from two driving signals, the OPR can be freely adjusted to optimize the receiver performance. Based on the proposed TSSB modulation scheme, high spectral efficiency vector signals can be utilized, and the proposed system does not incur dispersion induced performance fading.

5.2.2 Experimental Setup

Figure 5.3 illustrates the experimental setup of the TSSB system. A tunable laser is utilized as the optical source. The QPSK (quadrature phase-shift keying)-OFDM signal is generated at baseband (BB) from the AWG (Tektronix®AWG7102) with the following parameters: sampling rate of 20 GSa/s for the DAC; IFFT size of 256; subcarrier frequency separation of 78.125 MHz, and 44 subcarriers generated at the

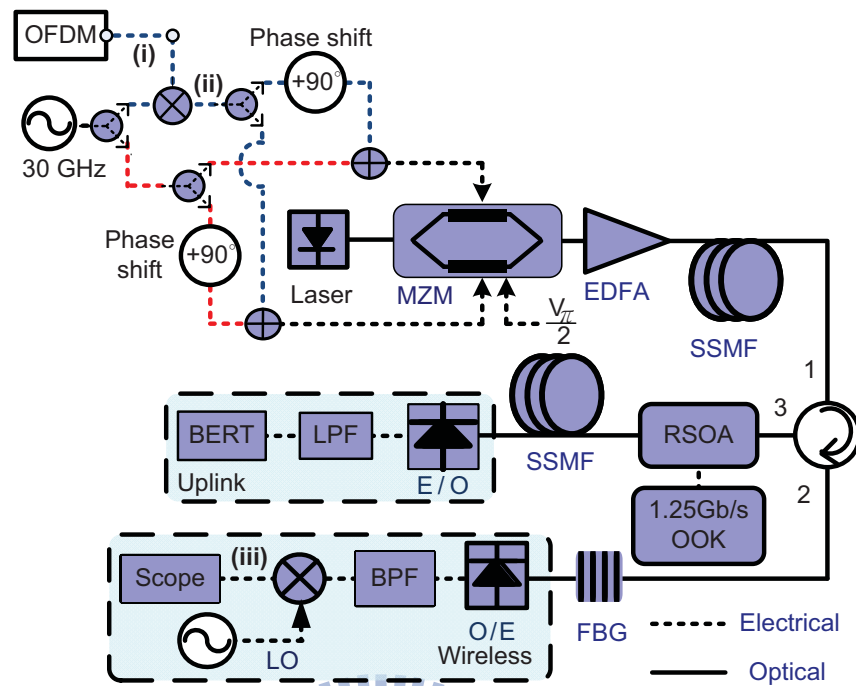


FIG. 5.3. Experimental setup of the frequency doubling system using TSSB modulation.

baseband, as shown in FIG. 5.4 (i). After up-conversion using an electrical mixer with a 30-GHz sinusoidal signal, a 30-GHz QPSK-OFDM driving signal with 88 subcarriers is obtained, as shown in inset FIG. 5.4 (ii). This produces two OFDM sidebands centered at 30 GHz, with a combined bandwidth of 7 GHz. Both sidebands are transmitted over the RoF system. Since the subcarriers are transmitted independently, and demodulated independently at the receiver, the total bit-rate of the emulated 7 GHz-wide OFDM signal is double that of the original OFDM signal generated by the AWG. Hence, the total data rate of the 30-GHz QPSK-OFDM signal is 13.75 Gb/s.

Subsequently, both 30-GHz OFDM-QPSK and sinusoidal signals are divided into two paths using two 90° hybrid couplers. The combined signals are amplified to drive the dual-electrode MZM which is biased at the quadrature point. At MZM output, the optical power before fiber transmission is boosted using an EDFA. The generated

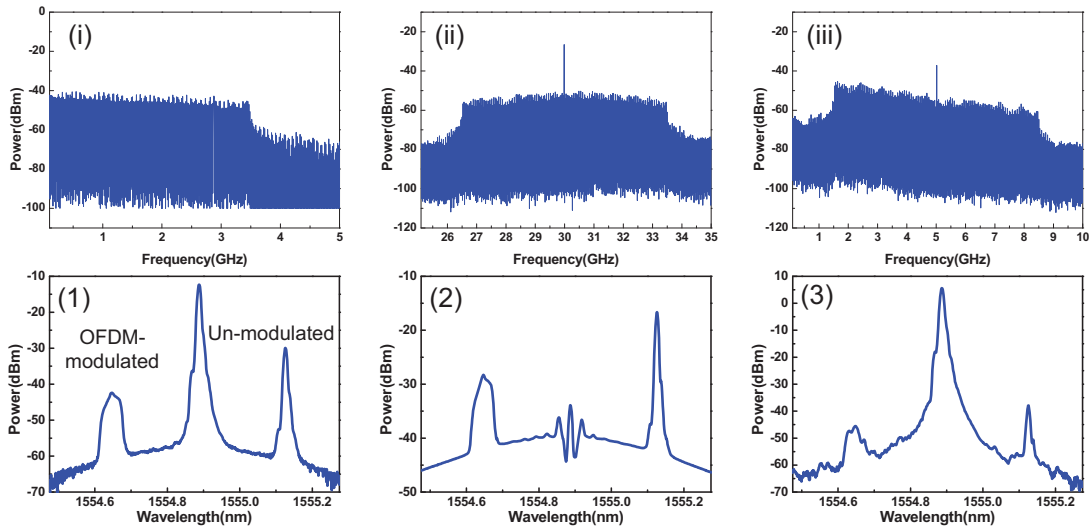


FIG. 5.4. Electrical and optical spectra of the TSSB system.

optical TSSB OFDM signal is transmitted over 50-km SSMF, and the original optical carrier and two optical sidebands are separated for up-link and wireless applications, respectively, by using an optical fiber Bragg grating. The two optical sidebands are received using a V-band photo-diode (PD) for optical-electrical conversion. FIG. 5.4 (1)-(3) show the generated optical spectrum of TSSB OFDM signal and the optical spectra of the signals after filtering. The generated electrical 60-GHz OFDM signals are down-converted using an electrical mixer with a 55-GHz local oscillator (LO) signal and then sent into a digital signal oscilloscope to capture the time domain waveform for off-line demodulation. Based on the multi-carrier characteristic of the OFDM signal, one-tap equalizer can compensate for the uneven frequency response of the 60-GHz components efficiently. Bit error rate (BER) is estimated from the constellation diagrams to evaluate the signal performance.

5.2.3 Experimental Results and Discussion

OPR of the optical un-modulated sideband to OFDM-modulated sideband significantly affects the receiver performance. In the conventional SSB modulation

scheme, OPR cannot be easily adjusted. An additional narrow band optical filter is normally required to suppress the original optical carrier and enhance the receiver performance [70]. The proposed TSSB system generates the un-modulated and OFDM-modulated optical sidebands from two driving signals. Therefore, OPR can be adjusted by controlling the amplitude of driving signals. FIG. 5.5 illustrates the QPSK-OFDM BER versus OPR curves. The best receiver performance is obtained with 6-dB OPR, where the power of the un-modulated sideband is 6 dB higher than that of the OFDM-modulated sideband. The insets of FIG. 5.5 show the constellation diagrams with OPRs of -1dB, 6dB and 11 dB. Notably, OPR in OFDM systems are higher than a conventional single carrier system, which has 0-dB optimal OPR [70]. Due to the high PAPR property, OFDM signals are sensitive to the nonlinearity of the transmission systems, while the signal performance can be easily degraded. Therefore, increasing the optical power of the un-modulated optical sideband can effectively enhance the OFDM signal performance.

Figure 5.6 shows the BER curves and constellation diagrams of the 13.75-Gb/s QPSK-OFDM down-link signals. Without using the one-tap equalizer, the OFDM signal cannot be recovered due to an uneven amplitude and phase frequency response of the 60 GHz system, inset (a) of FIG. 5.6. Notably, the QPSK-OFDM signal can be recovered after using the one-tap equalizer. No significant signal distortion of the constellation diagram is observed after a transmission of 50-km SSMF. The receiver power penalty after the SSMF transmission can be ignored. The constellation of the demodulated QPSK signal at BTB and after fiber transmission are also shown in insets (b) and (c) of FIG. 5.6.

Figure 5.7 shows the BER curves of the up-link 1.25-Gb/s OOK signal signals using a bias modulated RSOA. No significant receiver power penalty is observed after 50-km SSMF transmission. The eye diagrams of the OOK signals are also shown in the inset of FIG. 5.7. The eye diagram is also very clear after 50-km SSMF transmis-

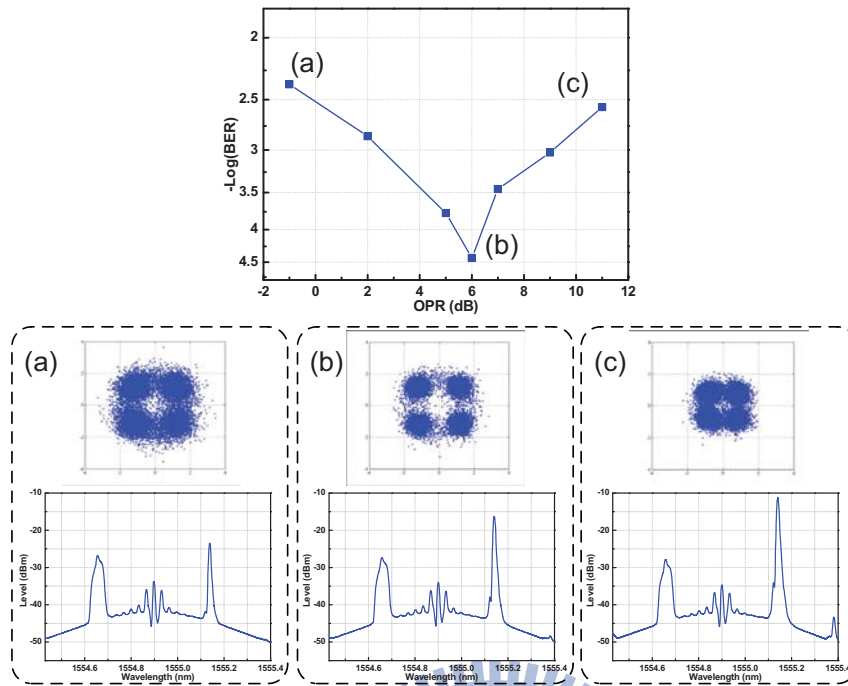


FIG. 5.5. OPR versus $-\log(\text{BER})$ of the QPSK-OFDM signal.

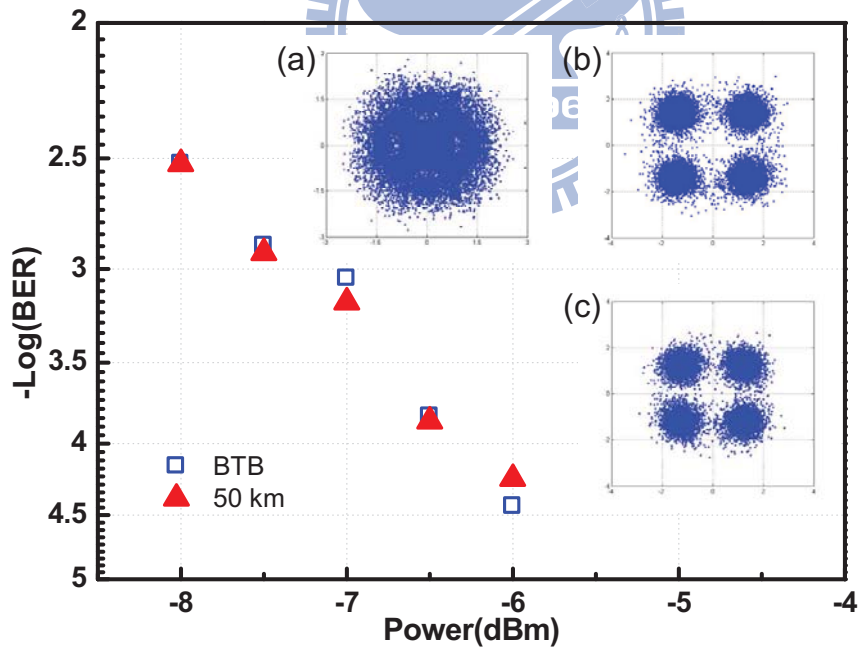


FIG. 5.6. BER curves and constellation diagrams of the down-link transmission. (a) Back-to-back without one-tap equalizer; (b) back-to-back with one-tap equalizer; (c) 50-km SSMF.

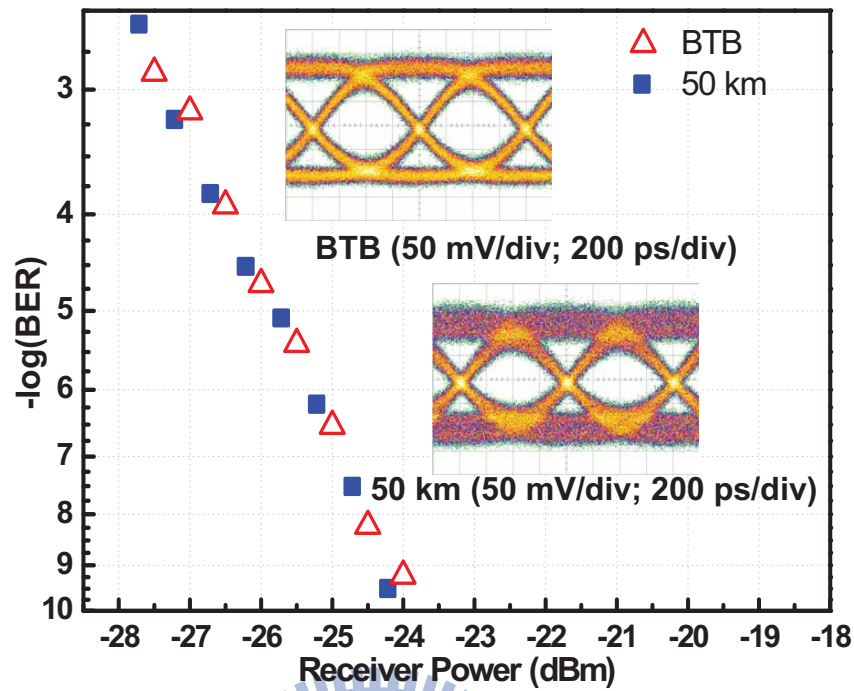


FIG. 5.7. BER curves of the OFDM system uplink 1.25-Gb/s OOK signals.

sion.

5.2.4 Summary

A full duplex modulation technique utilizing TSSB scheme for 60-GHz RoF links is proposed in this section. Frequency doubling, high spectral efficiency vector signal, and full-duplex systems are achieved. Furthermore, the proposed system does not suffer from dispersion induced performance fading issue. 13.75-Gb/s QPSK-OFDM signals is experimentally demonstrated. To compensate for the uneven frequency response of the 60-GHz RF components, one-tap equalizers are utilized. After transmission of 50-km SSMF, no significant receiver power penalties is observed. Wavelength reuse using RSOAs for uplink transmissions is also experimentally demonstrated. 1.25-Gb/s OOK signals are modulated on the original optical carrier and transmitted over 50-km SSMF. No significant receiver power penalty of the uplink signal is

observed on the uplink signal.

5.3 Modulation System with Frequency Sextupling

There are three main drawbacks of the frequency doubling method discussed earlier. Firstly, the electrical mixer will significantly degrade the signal quality. Secondly the modulator is not operated at linear E-field region. For an OFDM signal which is sensitive to PAPR, this considerably limits the modulation index. Thirdly, at transmitter, expensive components with frequency up to 35 GHz are needed. To overcome these issues, a new modulation scheme with frequency sextupling is proposed in this section.

5.3.1 Concept

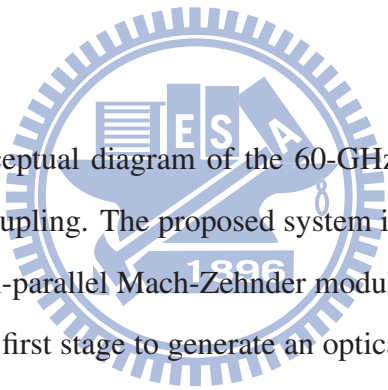


Figure 5.8 shows the conceptual diagram of the 60-GHz vector signal generation system with frequency sextupling. The proposed system is composed of two up-conversion stages with two dual-parallel Mach-Zehnder modulators (DP-MZM). The first DP-MZM is utilized in the first stage to generate an optical single sideband with carrier suppression (SSB-CS) signal [71]. A local oscillator (LO) and an intermediate frequency (IF) vector data signal are combined to form a composite driving signal. After the first DP-MZM, an LO optical carrier is generated at the lower sideband and a data-modulated OFDM signal is generated at the upper sideband, as shown in the inset (i) of FIG. 5.8. Notably, frequency doubling is achieved after the first stage.

The second stage is an optical up-conversion system which is composed of the wavelength-independent optical millimeter-wave generation system with frequency quadrupling along with an optical interleaver. After the optical up-conversion, both the LO and data-modulated optical sidebands are up-converted with frequency four times that of the up-conversion system driving signal, as shown in inset (ii) of FIG.

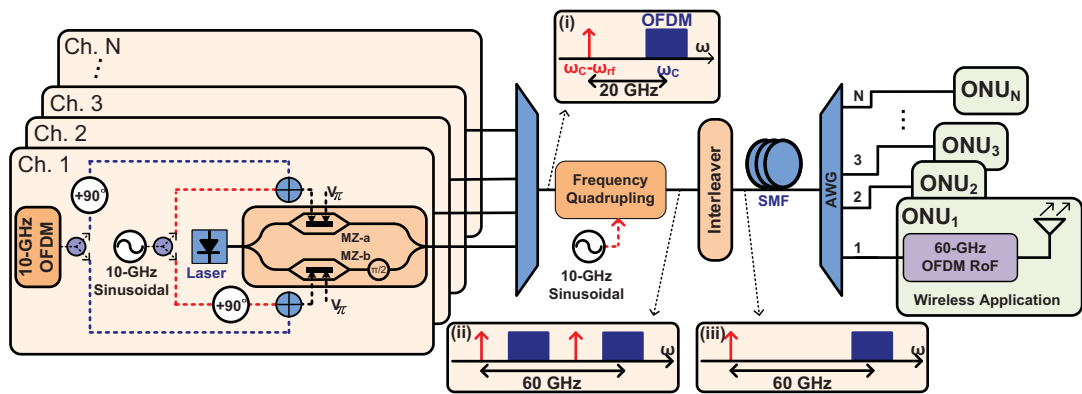


FIG. 5.8. Conceptual diagram of the 60-GHz vector signal generation system with frequency sextupling.

5.8. Then, the optical interleaver is employed to select the desired optical sideband and a modified SSB signal with frequency sextupling is obtained, as shown in inset (iii) of FIG. 5.8. Based on the modified SSB modulation scheme, high spectral efficiency vector signals, such as M-PSK, QAM and OFDM can be transmitted without dispersion-induced fading performance degradation. Since the LO and data-modulated optical sidebands are generated from two individual driving signals, the receiver performance can be optimized by controlling the OPR between two optical sidebands. Because of the frequency sextupling using optical up-conversion system, signal processing can be handled using 10-GHz components with higher reliability and lower costs. Moreover, wavelength-division-multiplexed (WDM) up-conversion can be realized based on the wavelength independent optical up-conversion system.

Figure 5.9 schematically depicts the principle of the RoF system. Since the sub-MZMs in the first stage (ie. MZ1-a, and MZ1-b) are biased at null point, DSB-CS modulation schemes will be generated. The driving signals in the first stage are the combination of LO and OFDM signals, and 90° phase delays are added on the lower-arm LO signal and upper-arm OFDM signal. Optical spectra after the modulation of MZ1-a and MZ1-b will be obtained as shown in inset (ii) and (iii) of FIG. 5.9. The

main MZM of the first stage is biased at quadrature point, and a 90° phase difference is introduced between the output of MZ1-a and MZ1-b. At the output of the first DP-MZM, a modified SSB signal will be obtained as shown in inset (v) of FIG. 5.9. Then, the 20-GHz modified SSB signal is sent into the second stage. Since the sub-MZMs in the second DP-MZM (ie. MZ2-a and MZ2-b) are biased at the full point, DSB modulation scheme will be obtained. Because of a 90° phase delay which is added on the lower-arm of the second-stage driving signal, optical spectra as shown in inset (vi) and (vii) will be obtained. Since the main MZM of the second DP-MZM is biased at the null point, a 180° phase difference is introduced between the output of MZ2-a and MZ2-b. The combined output signal of the second DP-MZM will have the optical spectrum shown in inset (ix) of FIG. 5.9. Then, an optical interleaver is utilized to select the desired optical sidebands. A 60-GHz modified SSB signal as shown in inset (x) of FIG. 5.9 will be obtained at the output of the optical interleaver.

5.3.2 Experimental Setup

Figure 5.10 shows the experimental setup of the proposed 60-GHz RoF system with frequency sextupling. A distributed-feedback (DFB) laser is utilized as the opti-

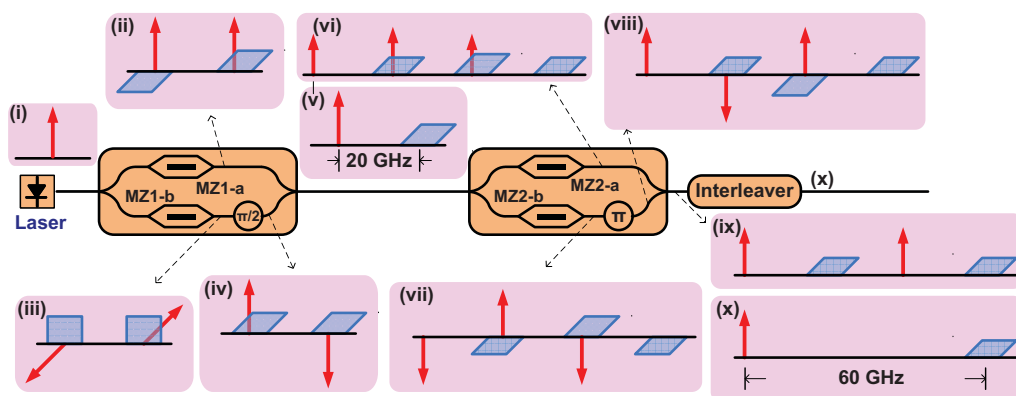


FIG. 5.9. The principle of the proposed RoF system with frequency sextupling.

cal source. In the first stage, the sub-MZMs (MZ1-a and MZ1-b) of the first DP-MZM are biased at the null point, while the main MZM is biased at the quadrature point. The OFDM signals are generated at base band (BB) using an arbitrary waveform generator (AWG, Tektronix®AWG7102) with the following parameters: the digital to analog converter (DAC) sampling rate is 20 GHz; inverse-fast-Fourier transform (IFFT) size is 256; subcarrier frequency separation is 78.125 MHz; 44 subcarriers are generated at BB and the bandwidth is 3.4375 GHz. The BB OFDM signal is then up-converted using an electrical mixer driven with a 10-GHz LO signal, resulting in a 6.875-GHz-wide OFDM signal with 88 sub-carriers centered at 10-GHz. Restricted by the bandwidth of the AWG, the 7-GHz OFDM signals are emulated using a DSB OFDM signal. Although both sidebands of the OFDM signals are related after electrical up-conversion, the OFDM sub-carriers are transmitted independently (un-correlated) and they are demodulated independently at the receiver. Each sub-carrier experiences different amplitude and phase response from the transmission. Therefore, there was no correlation between sub-carriers in two sidebands of the recovered OFDM signal.

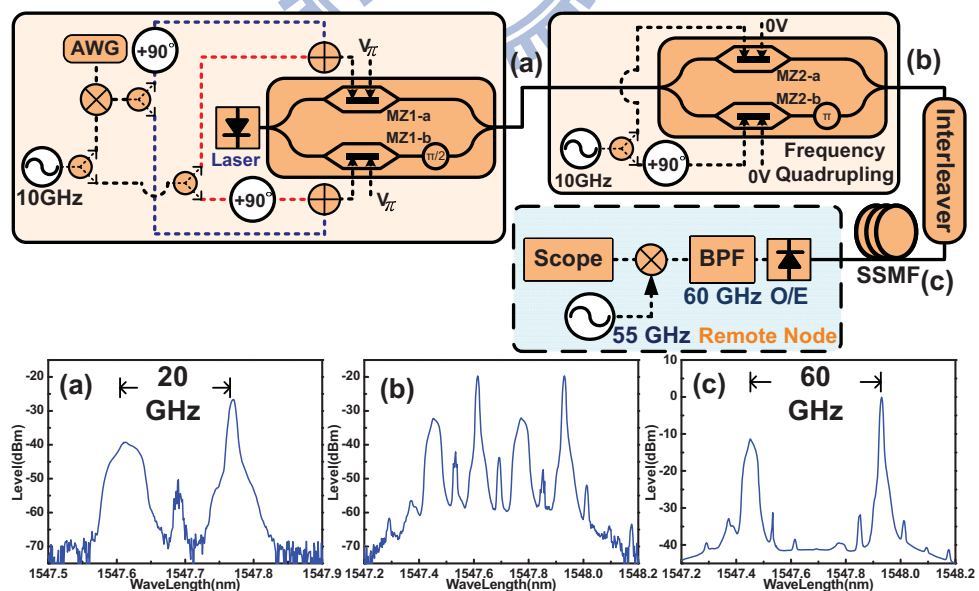


FIG. 5.10. Experimental setup of the frequency sextupling system.

As a result the 88 sub-carriers occupying the 6.875-GHz band all together represent the total throughput of the system, which was 13.75 and 20.625 Gb/s for QPSK-OFDM and 8QAM-OFDM, respectively. The 10-GHz LO signal was generated by an RF signal generator. Both the 10-GHz OFDM signal and the 10-GHz LO signal are divided into two paths (upper path and lower path). To generate the modified SSB signal using the SSB-CS modulation scheme, a 90-deg phase delay is added on the upper path of the OFDM signal and the lower path of the 10-GHz sinusoid. The upper path and lower path signals are combined and fed into the DP-MZM as the driving signals. At the output of the first stage, a 20-GHz modified SSB signal is obtained as shown in inset (a) of FIG. 5.10.

Then, the 20-GHz modified SSB signal is fed into the second stage for optical up-conversion. After the second DP-MZM, both the LO and data-modulated optical sidebands of the 20-GHz modified SSB signal are up-converted as shown in the optical spectrum in inset (b) of FIG. 5.10. To generate the 60-GHz modified SSB OFDM signal, an optical interleaver is utilized to select the desired sidebands, as shown in inset (c) of FIG. 5.10. After transmission over 25-km SSMF, the optical signal is received using a V-band photo diode. The received 60-GHz OFDM signal is down-converted to 5-GHz using an electrical mixer driven by a 55-GHz local LO signal. The down-converted IF frequency of the signal was chosen to fit the bandwidth of IF amplifier, the bandwidth of the real-time digital oscilloscope and the IFFT size of the OFDM signal. The down-converted signal waveforms are captured by a real-time digital oscilloscope for off-line demodulation and analysis using the Matlab program.

5.3.3 Experimental Results and Discussion

By controlling the intensity of the driving signals, the OPR can be freely adjusted in the proposed modified SSB system. FIG. 5.11 shows the bit error rate (BER) versus OPR curve and related constellation diagrams of the QPSK-OFDM signal. The OPR

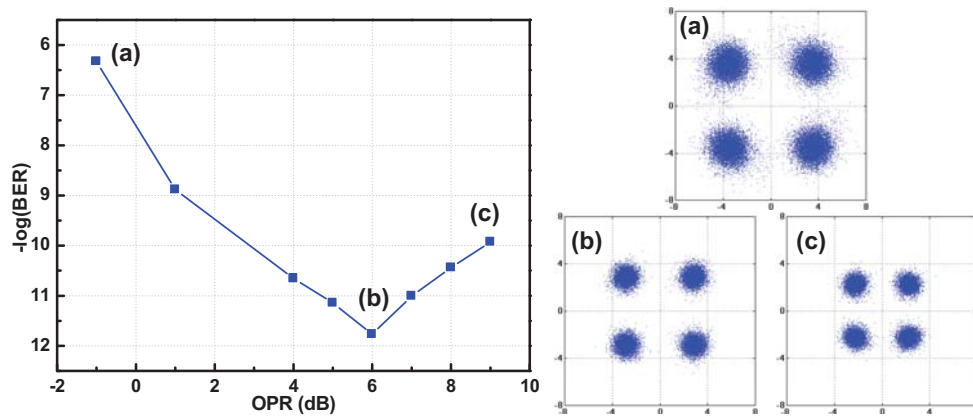


FIG. 5.11. Bit error rate versus optical power ratio curve and constellation diagrams of the QPSK-OFDM signal, and constellations with (a) -1-dB , (b) 6-dB , and (c) 9-dB OPR.

here is defined as the LO optical sideband power to data-modulated optical sideband power ratio. The OPR was measured using an optical spectrum analyzer with 0.01-nm resolution.

For QPSK-OFDM modulated signals the best receiver performance was obtained when the OPR was equal to +6 dB shown in FIG. 5.11. FIG. 5.12 shows the EVM versus OPR curve and related constellation diagrams of the 8QAM-OFDM signal. The optimal OPR for 8-QAM-OFDM modulated signals was found to be +5-dB as shown in FIG. 5.12. Compared with the conventional single carrier system which has 0-dB optimal OPR [70], the optimal OPR in the proposed OFDM systems was found to be higher.

Figure 5.13 shows the BER curves of the transmission result of the QPSK-OFDM signal. After transmission over 25-km SSMF, the received power penalty was negligible. The constellation diagrams at back to back (BTB) and after fiber transmission are also shown in insets of FIG. 5.13. After fiber transmission, no significant distortion is observed in the constellation diagrams. FIG. 5.14 shows the EVM curves of the transmission result of the 8QAM-OFDM signal. Similar to the QPSK-OFDM sys-

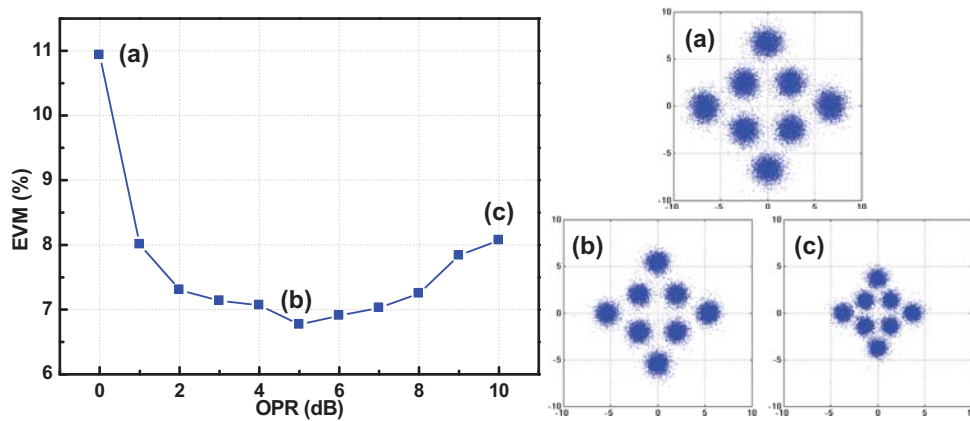


FIG. 5.12. Error vector magnitude versus optical power ratio curve and constellation diagrams of the 8QAM-OFDM signal, and constellations with (a) 0-dB , (b) 5-dB , and 10-dB OPR.

tem, negligible receiver penalty is observed after transmission over 25-km of standard single-mode fiber. In addition there is no significant distortion of the constellation diagrams observed, as shown in insets of FIG. 5.14.

5.3.4 Summary

A signal up-conversion and transmission system for 60-GHz RoF links was proposed in this section. Based on the modified SSB modulation scheme, high spectral efficiency OFDM modulation format can be transmitted with no performance degradation due to dispersion-induced fading. Since frequency sextupling was employed, only highly reliable 10-GHz components were utilized in the transmitter. Frequency-quadrupling WDM optical up-conversion can also be realized using the proposed system. The generation and transmission of 13.75-Gb/s QPSK-OFDM and 20.625-Gb/s 8QAM-OFDM signals occupying the full 7-GHz license-free band at 60 GHz was experimentally demonstrated. After transmission over 25-km of standard single-mode fiber, no significant received power penalty was observed with both OFDM signal formats.

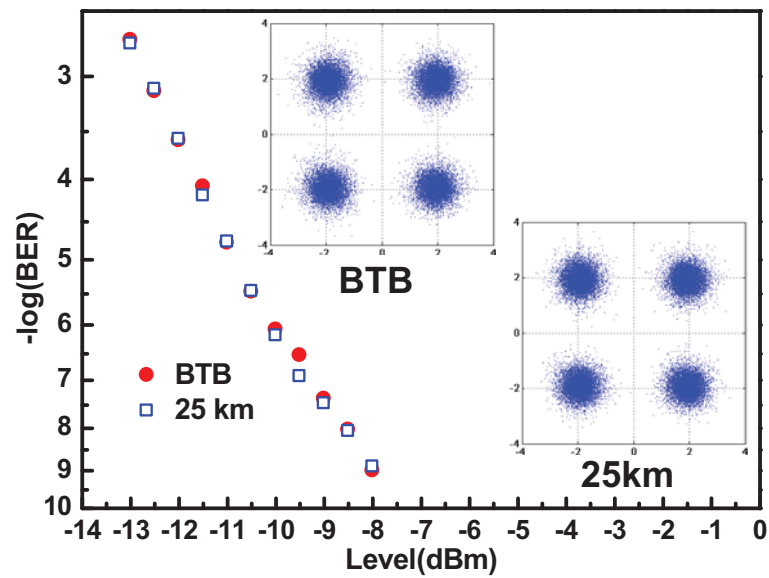


FIG. 5.13. Bit error rate curves of the QPSK-OFDM signal fiber transmission results.

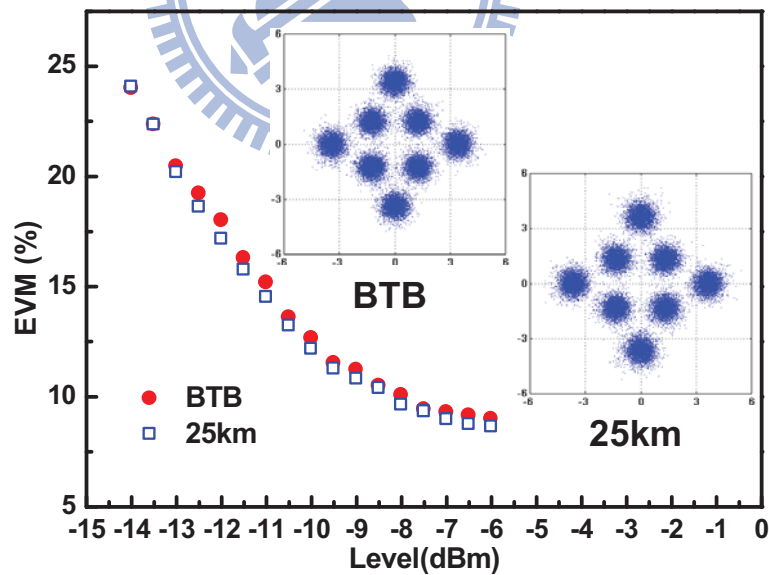


FIG. 5.14. Error vector magnitude curves of the 8QAM-OFDM signal fiber transmission results.

5.4 Intensity Modulation Direction Detection Systems Using a Mach-Zehnder Modulator

Although the optical up-conversion system for 60-GHz RoF can provide better performance and longer fiber transmission distances, most of them are very complex and impractical for real applications. Intensity Modulation Direction Detection (IMDD) RoF systems have the advantage that they are extremely simple and can offer seamless multi-standard system operation. In this section, a wideband OFDM-modulated IMDD RoF system using a high speed single-electrode MZM is proposed. A simple DSB IMDD RoF system to directly transport a 7 GHz-wide OFDM signal at 60 GHz is experimentally demonstrated. Ultra-high data-rate of 21 Gbps with transmission over standard single-mode optical fiber and 10m wireless distance can be achieved. The impact of chromatic dispersion is also investigated. 500m SSMF transmission which is sufficient for most in-building applications can be achieved in this 60-GHz RoF architecture.

5.4.1 Experimental Setup

The schematic of the experimental set-up is shown in FIG. 5.15. A one-step electrical up-converter was used to generate a 7-GHz-wide OFDM signal centered at 60.5 GHz, by retaining both OFDM signal sidebands following up-conversion, as shown. The OFDM signal at baseband was 3.5 GHz wide and it was generated by an AWG. The resolution of the DAC and the sampling rate of the AWG were set to 8 bits and 24 GSa/s, respectively. The IFFT length was 256, resulting in a subcarrier symbol rate of 93.75 MSym/s. The 3.5-GHz-wide OFDM signal consisted of 37 sub-carriers, which were modulated with the 8QAM data format. Therefore, the 7 GHz-wide OFDM signal at the output of the electrical up-converter consisted of a total of 74 sub-carriers with a combined data-rate of 20.8125 Gbps.

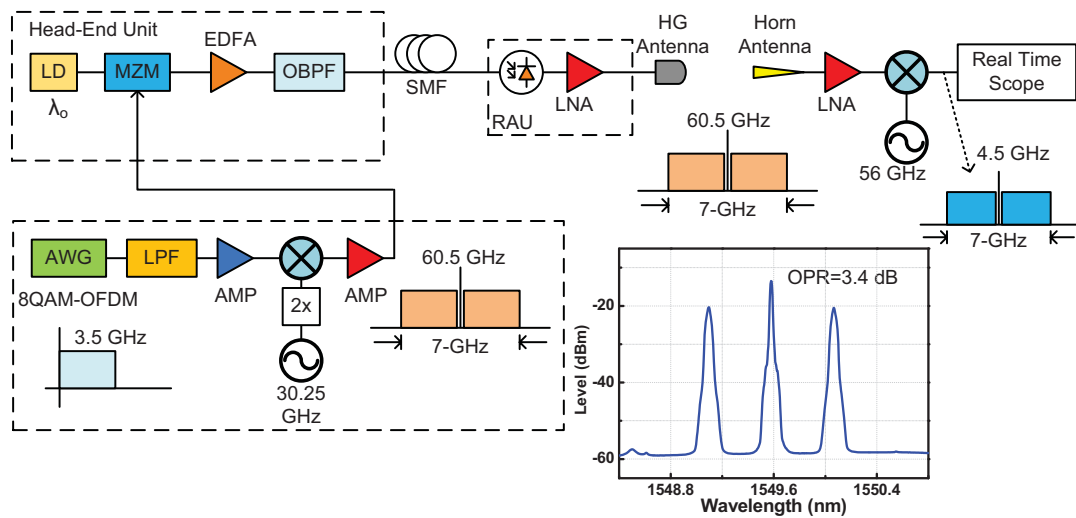


FIG. 5.15. Experimental setup of the simple IMDD 60-GHz RoF system using a MZM.

The high-speed MZM used to modulate the optical signal was specified for 40 Gbps but had reasonable performance around 60 GHz. The modulator was biased around the quadrature point resulting in a DSB optical signal (with carrier) as shown in insert (i) of FIG. 5.15. The optical signal source was a CW DFB laser emitting +10.5 dBm of optical power around 1550 nm.

After amplification using an EDFA and filtering for ASE noise, the intensity-modulated optical signal was transmitted to the Remote Antenna Unit (RAU) via standard single-mode fibers of various lengths. At the RAU, the transmitted 60 GHz signal was generated by direct detection in the 67 GHz photodiode, amplified by a LNA with 38-dB gain, and transmitted wirelessly over a distance of 10m. In order to realize 10m wireless transmission distance a Gaussian Optics antenna (37 dBi) was used as the transmit antenna and a standard horn antenna (23 dBi) was used at the wireless terminal. No power amplifier was used at the RAU.

The 60-GHz signal received after 10-m wireless transmission was amplified by another LNA with 22-dB gain, and filtered by a band pass filter before it was down-

converted to an intermediate frequency (IF) centered at 4.5 GHz. This IF frequency was chosen so as to maintain the spectrum of the down-converted OFDM signal at 7 GHz. The down-converted signal waveforms were captured by a real-time digital oscilloscope with 50-GSa/s sampling rate for offline processing and analysis. Before capturing the results, the whole RoF system was optimized stage by stage to reduce the impact of the high PAPR of OFDM signals for the highest received SNR.

5.4.2 Results and Discussion

Figure 5.16 shows the spectrum of the 21-Gbps OFDM signal down-converted from the 60-GHz signal after optical fiber and 10m wireless transmission. The detected optical power was -8 dBm. It can be seen from the spectrum that the signal bandwidth is 7-GHz-wide and it is centered at 4.5 GHz. A strong peak at 4.5 GHz is observed. This is the residual LO signal from the one-step electrical up-conversion back at the Head-End Unit (HEU). The spectrum also shows that the RoF link had an amplitude flatness of about 10 dB over the entire 60 GHz band (57 GHz to 64 GHz). This flatness would have an adverse impact on system performance if single carrier modulation was used. However, this uneven response can be compensated for due to the multi-carrier characteristic of the OFDM signals. FIG. 5.17 (a) shows the clean constellation diagram of the received 8QAM OFDM signal for the detected optical power of -8 dBm with only 60-m fiber transmission. The SNR and Error Vector Magnitude (EVM) corresponding to this constellation diagram were 16 dB and 12.6 %, respectively.

Since both sidebands of the optical signal were transmitted, fiber chromatic dispersion-induced fading of the generated 60-GHz carrier after fiber transmission was expected. In order to investigate the nature of the fading and its impact on the performance of the OFDM IMDD RoF system, the intensity-modulated optical signal was transmitted over various fiber lengths and the average SNR of the received

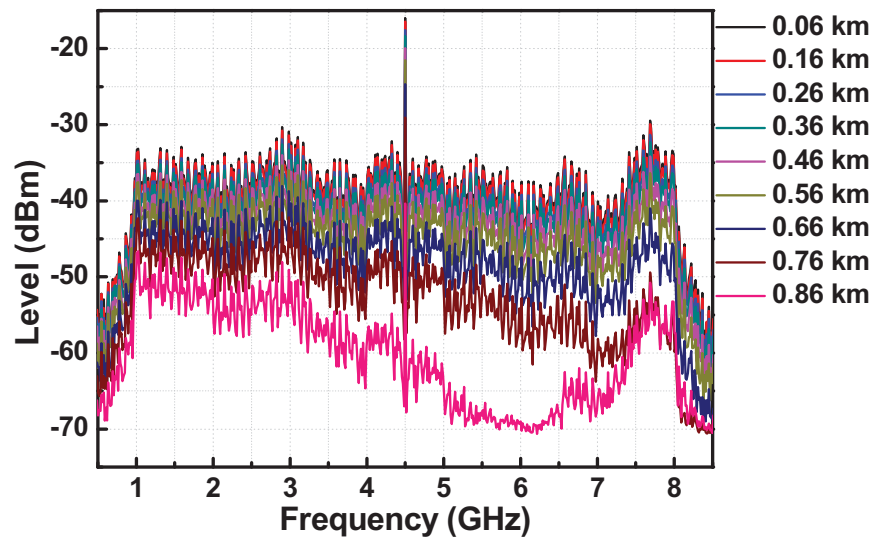


FIG. 5.16. Electrical spectrum of the down-converted OFDM signal.

signal analyzed. 10-m wireless transmission distance was included in all cases. FIG. 5.18 shows the impact of chromatic dispersion on the sensitivity of the IMDD RoF system. No penalty was observed for transmission over 160 m standard single-mode fiber. A small 1-dB optical power penalty measured at the SNR equal to 14 dB was observed after transmission over 360-m fiber. The dispersion penalty grew to 3.5 dB after 560-m fiber transmission. The constellation diagram corresponding to 560-m fiber transmission with -8 dBm detected optical power is shown in FIG. 5.17 (b). In this case, the measured SNR and EVM were 11.1 dB and 22.6 %, respectively. The progressive deterioration of the system performance at longer fiber spans was caused by progressive increase in the signal fading suffered by sub-carriers inside the 7-GHz-wide OFDM signal as shown in FIG. 5.16. The signal after 860-m fiber transmission could not be recovered.

A detailed study of the impact of chromatic dispersion on the wide-band OFDM signal was conducted by transmitting the RoF signal over fiber spans ranging from 60 m to 3.56 km, with a length resolution of 100m. FIG. 5.19 shows the measured

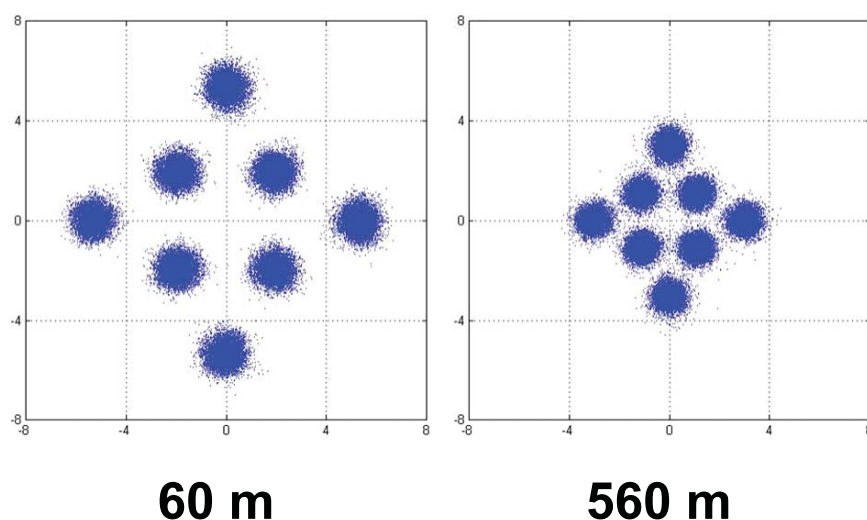


FIG. 5.17. Constellation diagrams of the recovered 21-Gbps 8QAM OFDM signals with (a) 60 m and (b) 560 m fiber transmission distances.

system performance in terms of the average SNR. An apparent “fading cycle” of 2 km was observed. The “fading cycle” of the OFDM signal was similar to that of an unmodulated CW signal at 60.5 GHz. However, as shown in FIG. 5.19, the OFDM signal faded earlier and recovered later ($>200\text{m}$) than the CW signal due to the former’s wide spectrum of 7-GHz. The detail of the chromatic dispersion induced fading of the DSB signal will be discussed in Appendix B.

5.4.3 Summary

A simple DSB IMDD RoF system was experimentally demonstrated to directly transport a high data-rate (21 Gbps) OFDM signal at 60 GHz over 500 m of standard single-mode fiber and 10 m wireless distance. Experimental results confirm that using OFDM modulation format rather than single-carrier modulation formats significantly reduces the impact of serious uneven frequency response found in ultra-wideband IMDD RoF systems. Considering the average system SNR, a “fading cycle” of 2km was observed, which was similar to the fading cycle of a un-modulated CW signal at

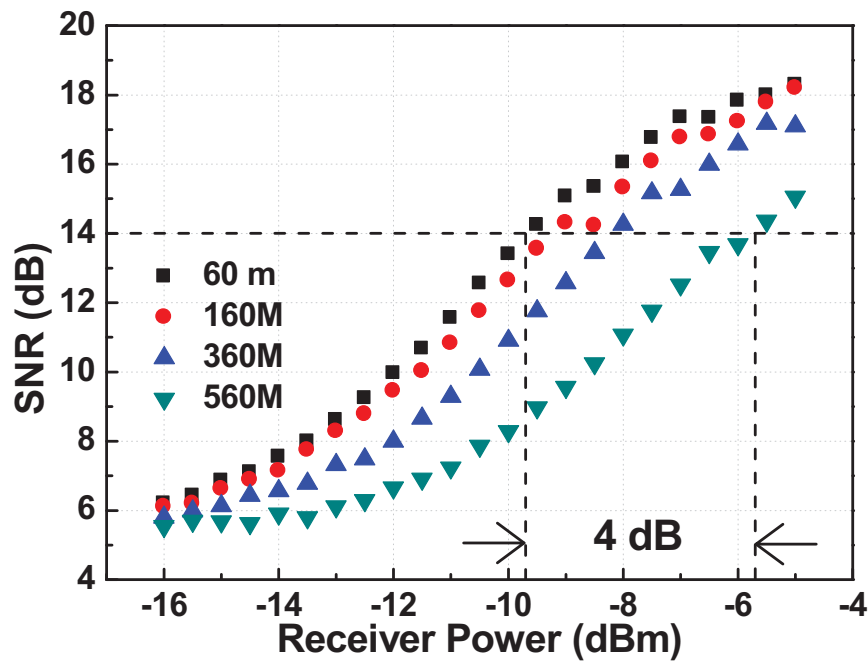


FIG. 5.18. SNR vs. Received Optical Power with different fiber distances and 10-m wireless transmission distance.

60.5 GHz. The dispersion-induced fading issue can be avoided by using SSB modulation schemes with more complexity or dispersion compensation techniques, but the 500m fiber transmission distance achieved without any dispersion compensation is sufficient for most in-building applications.

5.5 Intensity Modulation Direction Detection System Using an Electro-absorption Modulator

An 60-GHz IMDD RoF system using a high speed MZM was proposed in last section. The advantage of using IMDD RoF systems are the extremely simple architecture and the possibility of seamless multi-standard system operation. However, there are still some disadvantages of using MZM for the IMDD systems. First of all, the size of a MZM is usually large compared with the other electrical and optical com-

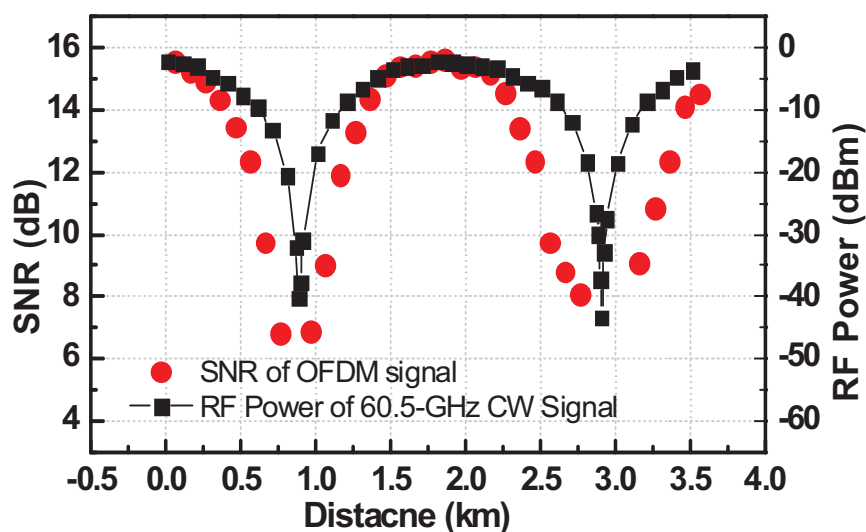


FIG. 5.19. Impact of fiber chromatic dispersion on the SNR performance of the 60 GHz IMDD RoF and 60.5-GHz sinusoidal signal.

ponents due to the inherent characteristic of MZM. Second, the MZM is a polarization sensitive device. An accurate polarization controller is usually required. Finally, the MZM is also sensitive to the bias drifting. Therefore, a feed-backed bias controller is usually needed to compensate for the bias drifting.

In this section, a 60-GHz IMDD system using an electro-absorption modulator (EAM) will be proposed. Compared with the MZM, the size of an EAM is much smaller. In addition, the EAM has the potential to be integrated with the other photonic components and reduce the size of the entire devices. Although the EAM is still a polarization dependent component, it is insensitive to the polarization drifting compared with the MZM. Finally, the EAM is insensitive to the bias drifting compared with the MZM. Therefore, the EAM is a potential choice for an IMDD RoF system.

Ultra-high data-rate of 21 Gbps is also achieved in the IMDD RoF system using an EAM. Fiber transmission distance of 900m with 3 m wireless transmission distance is experimentally demonstrated.

5.5.1 Experimental Setup

Figure 5.20 schematically depicts the experimental setup of the 60-GHz IMDD system using an EAM. The one-step electrical up-conversion which is same as up-converter in the IMDD MZM system is utilized to generate the 60-GHz OFDM driving signal. 8QAM constellations is also utilized. The total bandwidth and data-rate are 6.9375 GHz and 20.8125 Gbps, respectively. The 60-GHz OFDM signal was used to drive the high speed Reflective Electro-Absorption Modulator (R-EAM). After the amplification of an EDFA and filtering for the ASE noise, The generated DSB OFDM signal was transmitted over the SSMF to the RAU. At the RAU, the electrical 60 GHz signal was generated by direct detection in the 67 GHz photodiode, amplified by a LNA with 38-dB gain, and transmitted wirelessly over a distance of 3m. A Gaussian Optics antenna (37 dBi) was used as the transmit antenna and a standard horn antenna (23 dBi) was used at the wireless terminal. No power amplifier was used at the RAU. At the Wireless Terminal Unit (WTU), the received 60-GHz OFDM signal was amplified by another LNA with 22-dB gain, and filtered by a band pass filter before it was down-converted to an intermediate frequency (IF) centered at 4.5 GHz. The down-converted signal waveforms were captured by a real-time digital oscilloscope with 50-GSa/s sampling rate for offline processing and analysis.

The entire system was optimized stage by stage to have the highest received signal SNR. The inset of FIG. 5.20 shows the optical spectrum of the generated DSB optical signal. The carrier to optical sideband OPR of the EAM generated signal is much higher than the MZM generated signal. To keep the system simplicity, no narrow band optical filter is utilized to reduce the OPR and increase the received signal SNR. A limited portion of the optical carrier power can be suppressed by increasing the reversed bias of the EAM. However, the increasing of the reversed bias reduces the linearity of the EAM. Therefore, the reversed bias of the EAM was optimized be-

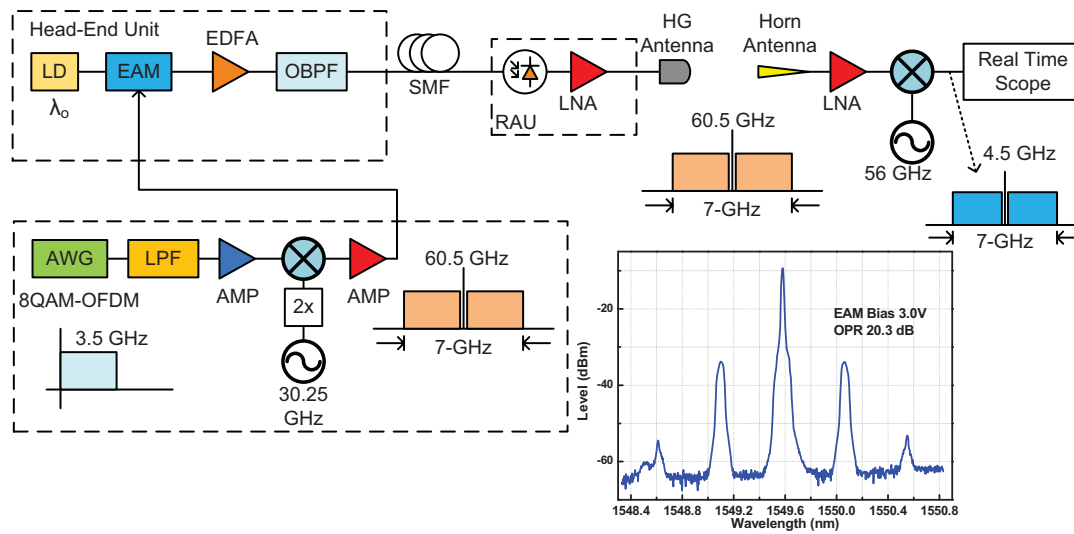


FIG. 5.20. Experimental setup of the simple IMDD 60-GHz RoF system using a R-EAM.

tween the OPR of the generated signal and the modulator linearity to have the highest received signal SNR. The optimized bias voltage is about -3V.

5.5.2 Results and Discussion

Figure 5.21 shows the electrical spectra of down-converted OFDM signal with 3-m wireless transmission distance and different fiber transmission distances. The center frequency of the down-converted signals are also 4.5 GHz, and the bandwidth of the OFDM signals is about 7 GHz. No significant spectrum distortion with the increasing of the fiber transmission distance up to 800 m. However, spectrum distortion due to the chromatic dispersion can be observed when the transmission fiber distance is longer than 900 m. FIG. 5.22 shows the impact of chromatic dispersion on the sensitivity of the IMDD RoF system using the EAM. No significant receiver optical penalty is observed with 3-m wireless and 500-m fiber transmission distances. 2.8-dB receiver power penalty at 14-dB SNR is observed with 900-m fiber transmission distance which is longer than the results of MZM system.

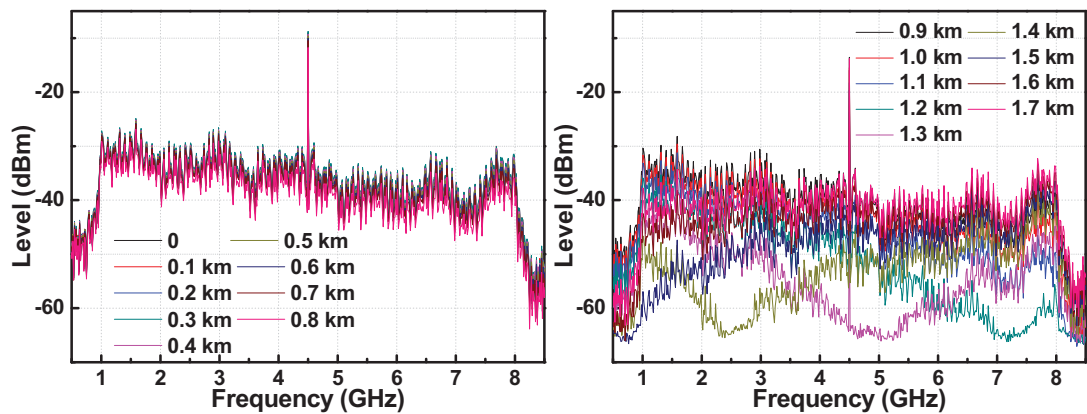


FIG. 5.21. Electrical spectra of the down-converted OFDM system in the EAM IMDD system.

Although the EAM system can provide longer fiber transmission distance, the receiver sensitivity of the EAM system is lower than that in the MZM system. FIG. 5.23 shows the SNR versus the receiver optical of the MZM and EAM systems at BTB. 4.3 dB difference of the receiver sensitivities at 14 dB SNR is observed. Because the high optical carrier to sideband OPR of the EAM, the receiver sensitivity is much lower in the EAM system compared with the MZM system. The insets of FIG. 5.23 show the optical spectra of the generated DSB signals from MZM and EAM.

5.5.3 Summary

An IMDD system using a high-speed R-EAM for the 60-GHz RoF system was proposed in this section. 8QAM OFDM signal with 21-Gbps data-rate was transmitted over 900 m of SSMF and 3 m of wireless distance at 60-GHz. Although the receiver sensitivity is lower in the EAM system compared with the IMDD system using a high speed MZM, the EAM can be integrated with the other photonic components. Furthermore, the device size of the EAM is much smaller than a MZM. Therefore, the EAM has the potential to be utilized in the future millimeter-wave RoF system for broadband wireless applications.

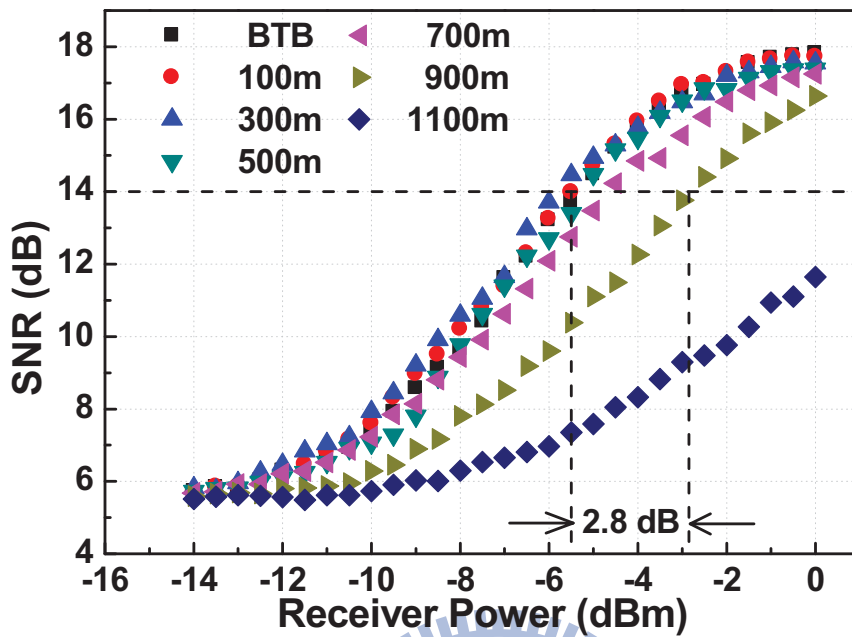


FIG. 5.22. SNR vs. Received Optical Power with different fiber distances and 3-m wireless transmission distance.

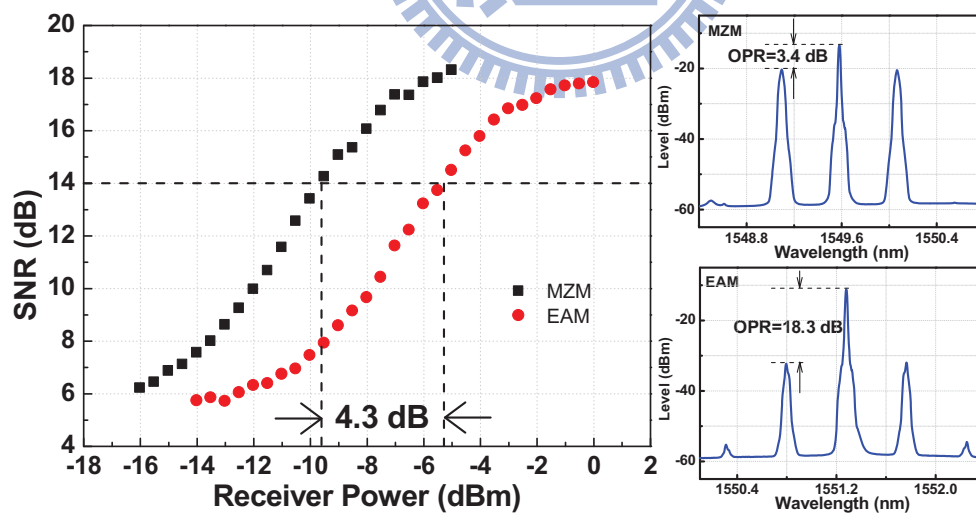


FIG. 5.23. Receiver sensitivities comparison between the IMDD systems using a MZM and an EAM.

5.6 Full-Duplex Bidirectional Transmission

The RoF technology is an ideal technology for high-density wireless networks because it enables the significant simplification of antenna units. However, most of the proposed RoF systems for millimeter-wave wireless communication employ very complex optical up-conversion techniques in order to utilize low frequency RF and optical components with uniform wideband performance for the generation and transmission of wide-band mm-wave signals [72, 73]. However, these systems cannot be utilized at the RAU where the up-link signal requiring transmission is at millimeter-wave frequencies rather than at baseband or IF frequency.

In last section, an IMDD system for 60-GHz RoF technology using a R-EAM was proposed. Based on the advantages of EAM, a bidirectional full-duplex 60-GHz RoF system for multi-Gbps wireless applications will be proposed. A high speed MZM is utilized in the down-link transmission, while a high speed R-EAM is utilized in the RAU for the up-link transmission. Symmetrical 2×20.8125 Gbps full-duplex data transmission over 500-m standard single mode fiber and 2.5-m wireless distance is successfully achieved. The interferences between the down-link and up-link channels are investigated and prevented by using polarization multiplexing between the two channels. The impact of fiber chromatic dispersion on the performance of the full-duplex DSB RoF system was also investigated and the receiver sensitivity penalty found to be 2dB for the downlink, and no penalty for the uplink for 500m fiber transmission. The proposed bidirectional RoF system is simple and fully transparent, making it ideal for in-building high data-rate wireless applications, which are characterized by short fiber spans.

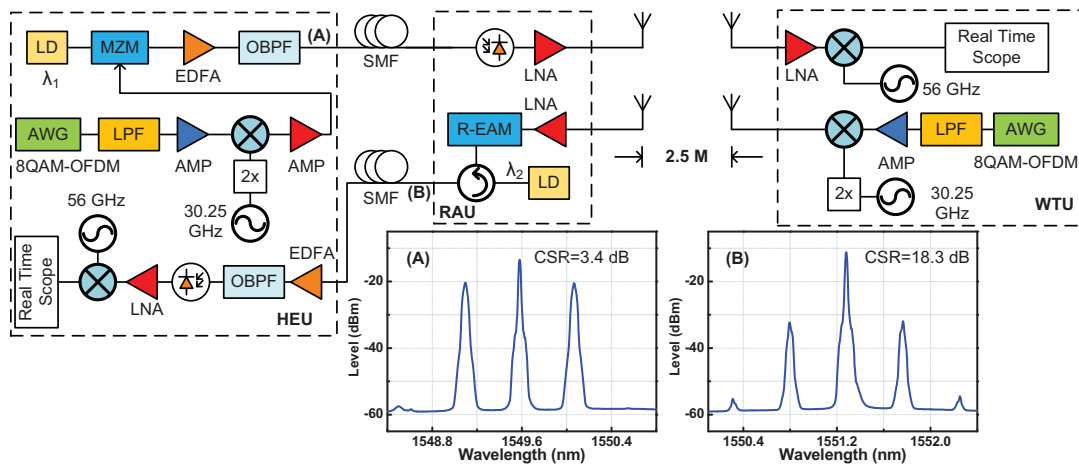


FIG. 5.24. Experimental setup of the symmetrical full-duplex bidirectional 60-GHz RoF system.

5.6.1 Experimental Setup

Figure 5.24 shows the schematic of the experimental setup. The down-link signal was a 7-GHz-wide OFDM signal centered at 60.5 GHz, which was generated by an AWG and a one-step electrical up-converter. The sampling rate and DAC resolution for the OFDM signal were 12 GS/s and 8 bits, respectively. The IFFT size was 128 resulting in an OFDM symbol rate of 93.75 MSym/s. With 74 subcarriers obtained after the one-step electrical up-conversion and the 8QAM modulation format on each sub-carrier, the total data rate of the OFDM signal was 20.8125 Gbps. A high-speed MZM was utilized to modulate the down-link optical signal. The CW laser source was a DFB laser emitting 10.5-dBm optical power at 1550 nm. After amplification by an EDFA and filtering for ASE noise, the down-link optical signal was transmitted to the RAU using standard single mode fiber.

The optical spectrum of the down-link optical signal is shown in inset (A) of FIG. 5.24. At the RAU, the down-link 60 GHz signal was detected using a 67-GHz photodiode. The generated 60-GHz signal was amplified by a LNA with 38-dB gain, fed into a standard gain horn antenna (23 dBi), and transmitted wirelessly over a distance of

2.5 m to the WTU, as shown in FIG. 5.24. At the WTU, the 60-GHz signal was amplified by a LNA with 22-dB gain and then down-converted to an Intermediate Frequency (IF) of 4.5 GHz using a 56-GHz LO signal. The down-converted signal was captured using a real-time digital oscilloscope for offline signal processing and analysis.

For the up-link, the AWG and a second one-step up-converter were used to generate a 7 GHz-wide OFDM signal at 60 GHz (also 21 Gbps) similar to the downlink signal. The up-link 60 GHz signal was first transmitted from the WTU over the same wireless distance of 2.5 m to the RAU using a separate pair of standard gain horn antennas. At the RAU the up-link signal was amplified by a LNA with 38-dB gain and used to drive a 60-GHz R-EAM as shown in FIG. 5.24. The CW optical source was another DFB laser emitting 10.5-dBm optical power at 1551.7 nm. Therefore, the modulated up-link optical signal was also a DSB-C signal as shown in insert (B) of FIG. 5.24. From the R-EAM the signal was transmitted over a separate 500 m length of standard single-mode fiber to the HEU. At the HEU an EDFA was used to pre-amplify the uplink optical signal prior to direct detection by a 67-GHz photodiode. The detected 60-GHz OFDM signal was down-converted to an IF frequency of 4.5 GHz, and captured by a real-time digital oscilloscope for offline signal processing and analysis. The uplink EDFA was deliberately placed at the HEU instead of the RAU in order to keep the RAU simple.

5.6.2 Results and Discussion

The performances of the down-link and the up-link subsystems were optimized separately prior to fiber transmission. Given that single-electrode optical modulators were used without any linearization and considering the large number of sub-carriers in the transmitted OFDM signals, the RF powers of the drive signals and the biases of the modulators were carefully tuned to reduce the impact of modulator non-linearity

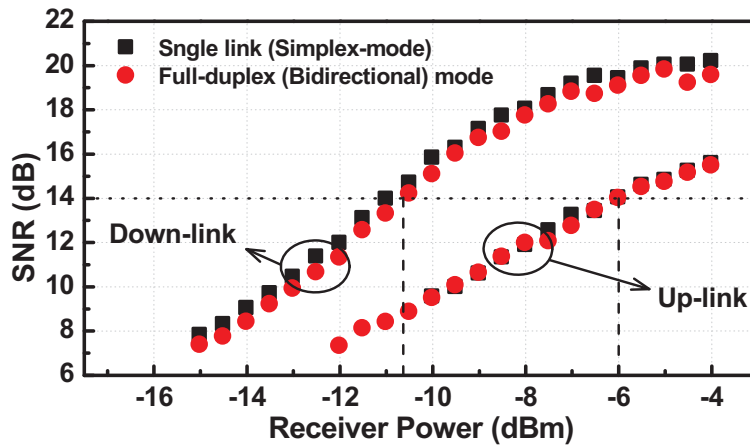


FIG. 5.25. Receiver performance with simplex and full-duplex modes with perpendicular antenna polarization.

on the performance of the system.

To assess the performance of the full-duplex RoF system over the wireless channel, the performances of the downlink and the uplink were first measured individually with the other link turned off. Afterwards, the performance of both links was measured in terms of the received signal SNR and optical sensitivity during simultaneous bi-directional transmission. No significant penalty was observed during simultaneous full-duplex wireless signal transmission as shown in FIG. 5.25. However, FIG. 5.25 shows that the downlink performed better in terms of the optical receiver sensitivity and the achieved peak average SNR. For instance the receiver sensitivity for 14 dB average SNR was -11 dBm for the downlink, which was 5 dB better than that of the up-link (-6 dBm). The major reason for the difference in the performances of the two links is the large difference in the carrier-to-sideband optical power ratio (OPR), which is evident in FIG. 5.24 (A) and (B). The OPR was 3.4 dB for the downlink, compared with 18.3 dB for the uplink. The source of the poor OPR in the uplink is a matter for a separate discussion.

Since the proposed full-duplex bidirectional IMDD RoF system employed DSB

and no optical filtering in both links, chromatic dispersion induced RF fading was expected. To verify the impact of fiber dispersion on the performance of the system, the down-link and up-link optical signals were transmitted over 2 separate 500 m lengths of standard signal mode fiber between the HEU and the RAU, with 2.5m wireless transmission distance between the RAU and the WTU. FIG. 5.26 (A) shows the down-link SNR curves for BTB and 500 m fiber transmission. A received power penalty of 2 dB was observed due to dispersion-induced RF fading. Down-link constellation diagrams with -6 dBm received optical power for BTB and 500 m fiber transmission are shown in FIG. 5.27 (a) and (b) with corresponding average SNRs of 19.1 and 17.9 dB, respectively.

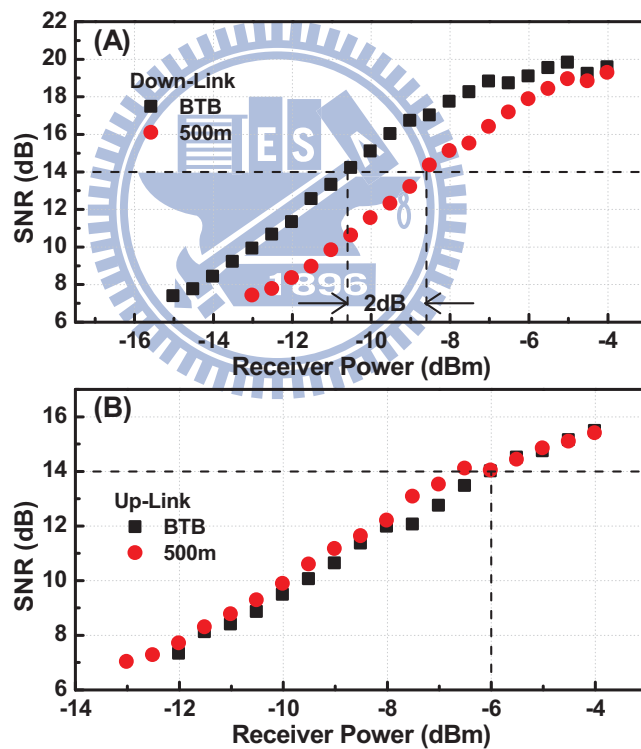


FIG. 5.26. SNR curves transmission at BTB and with 500m fiber transmission for (A) down-link; (B) up-link.

The up-link SNR curves at BTB and 500 m are shown in FIG. 5.26 (B). Com-

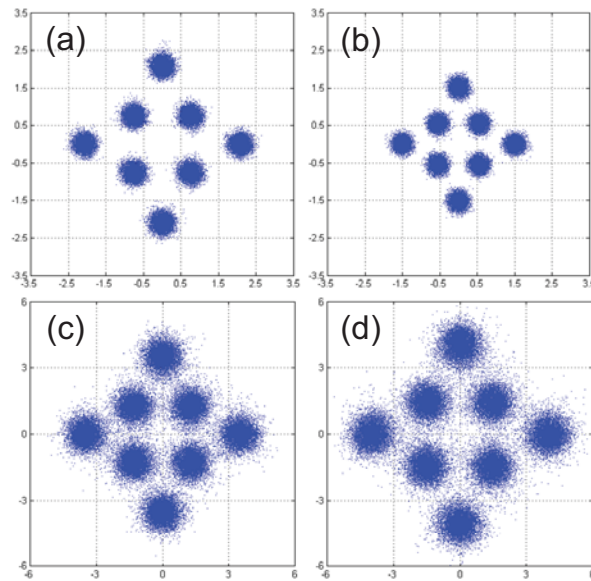


FIG. 5.27. Constellations with -6 -dBm received optical power for (a) Down-link at BTB; (b) Down-link with fiber transmission; (c) Up-link at BTB; (d) Up-link with fiber transmission.

pared to the down-link signal, no significant received power penalty was observed for the up-link. The up-link constellation diagrams for -6 dBm received optical power for BTB and 500m fiber transmission are shown in FIG. 5.27 (c) and (d), with both having an SNR equal to 14 dB, which is sufficient for FEC-coded error-free transmission. The difference in the penalties suffered by the downlink and the uplink over the same fiber transmission distance is attributed to the difference in the bias conditions and the extinction ratios of the two optical modulators employed.

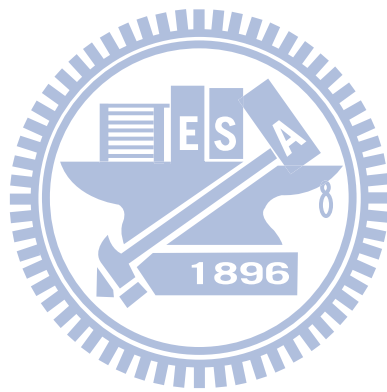
5.6.3 Summary

A symmetrical 2×21 Gbps full-duplex bidirectional RoF system using simple double-sideband IMDD links was successfully demonstrated at 60 GHz. High speed single-electrode MZM and R-EAM were employed in the downlink and uplink transmission, respectively. 8QAM-OFDM signal modulation format was used. At least

500 m fiber transmission and 2.5 m wireless transmission distances were achieved, without any dispersion compensation or optical filtering. The proposed full-duplex RoF system is very simple and fully transparent, making it ideal for in-building high data-rate wireless applications, which are characterized by short fiber spans.

5.7 Conclusion

60-GHz millimeter-wave system is a promising solution for the future Gbps wireless communication. In this chapter, the feasibility of broadband 60-GHz RoF techniques with data-rate beyond 10 Gbps using OFDM modulation formats was experimentally demonstrated using optical up-conversion and one-step electrical up-conversion. Optical up-conversion systems, including TSSB and frequency sextupling systems, can reduce the bandwidth requirement of the transmitter and provides better receiver performances. However, the system complexities are higher. Although the receiver performance is not as good as the optical up-conversion systems, the IMDD systems provide a very simple architecture and practical solutions. In addition, a 2×21 Gbps bidirectional full-duplex RoF system using IMDD techniques was experimentally demonstrated.



Chapter 6

MULTI-SERVICE HYBRID ACCESS NETWORK

Fiber to the x (FTTx) have been widely constructed for high data rate wired services to provide triple play services including voice, data, and video [74]. On the other hand, RoF techniques have become a potential candidate for the future broadband wireless system. Due to the requirement of high bandwidth, high flexibility and high mobility in the next generation access networks, the convergence of FTTx and RoF systems on an identical optical distributed infrastructure to provide wired and wireless access services at the same time are highly desired. Recently, simultaneous generation and transmission of FTTx baseband (BB) and RoF RF vector signals using external modulators have been intensively investigated [14–17]. However, narrow band optical filters at remote nodes are required in these proposed systems to separate BB and RF signal for wired and wireless applications [14–17], which severely hinders the implementation in WDM systems and is not compatible with the existing passive optical network (PON) system. Moreover, DSB-CS modulation schemes have been utilized in most of the proposed systems for RF signals [14–17, 75]. As a result, only on-off-keying (OOK) modulation format with lower spectral efficiency can be used for RF wireless signals.

In this chapter, two architectures for multi-service hybrid access network which simultaneously provide BB FTTx and RF Wireless services will be proposed. Since

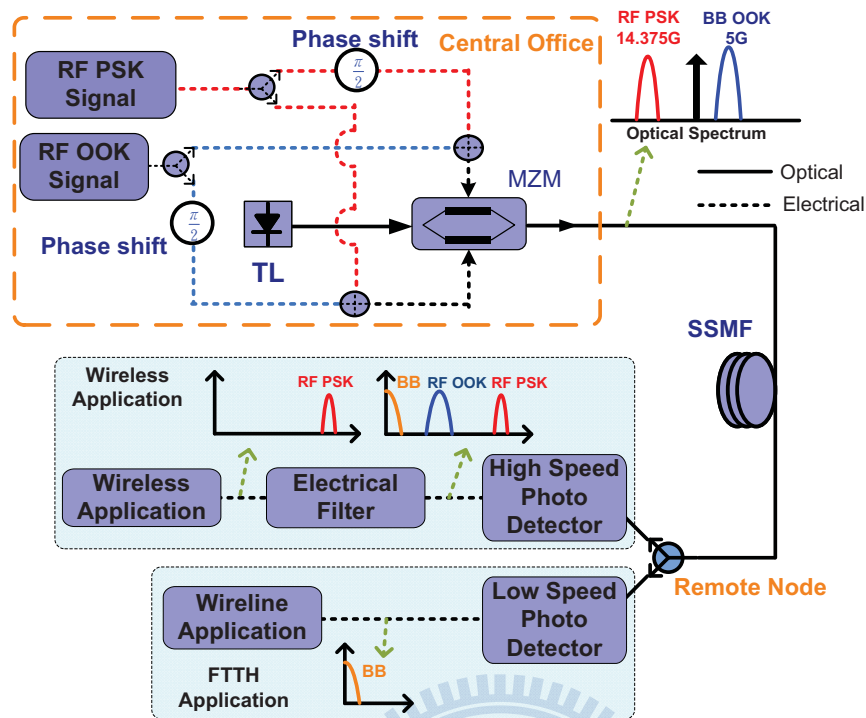


FIG. 6.1. Conceptual diagram of a multi-service hybrid access network system.

the wired and wireless services share an identical optical network, the construction and maintenance costs can be reduced. No narrow band optical filter is required at remote nodes in these systems to separate the BB and RF signals. Furthermore, the proposed scheme does not suffer from the RF performance fading issue and it can carry vector signals which are of utmost important for wireless applications.

6.1 Multi-Services Hybrid Access Network System Using A Dual-Electrode MZM

6.1.1 Concept

Figure 6.1 illustrates the conceptual diagram of a multi-service hybrid access network system. A dual-electrode MZM is employed to simultaneously generate RF and BB signals. The bias of MZM is set at the quadrature point $V_{\pi}/2$, where V_{π} is the

half-wave voltage of the MZM. The electrical OOK RF signal is generated by mixing a BB OOK signal with a sinusoidal signal using an electrical mixer. At the same time, the PSK signal is generated and up-converted to the RF frequency. Both the RF OOK and RF PSK signals are divided into two identical signals by electrical power dividers. The two driving signals of the dual-electrode MZM are the combination of the divided RF OOK and RF PSK signals, except that the RF PSK signal of the upper arm driving signal is delayed with 90° phase shift and the RF OOK signal of the lower arm driving signal is delayed with 90° phase shift.

These two driving signals result in two optical SSB signals with the generated optical spectrum on the different side of the optical carrier. At the remote nodes, no optical filter is required to separate the BB OOK and RF PSK signals. As shown in FIG. 6.2, the RF PSK signal and the optical carrier contribute only DC terms to the BB signal after the PD square-law detection and cause negligible interference on the BB OOK signal after being removed by an electrical DC block. Thus, the BB OOK signal can be easily recovered with a typical low speed receiver. The RF PSK signal is obtained from the beating term of the optical carrier and PSK optical sideband after the PD square-law detection. Therefore, the RF PSK signal can be recovered using a high speed receiver with an electrical filter without interference from the BB signals.

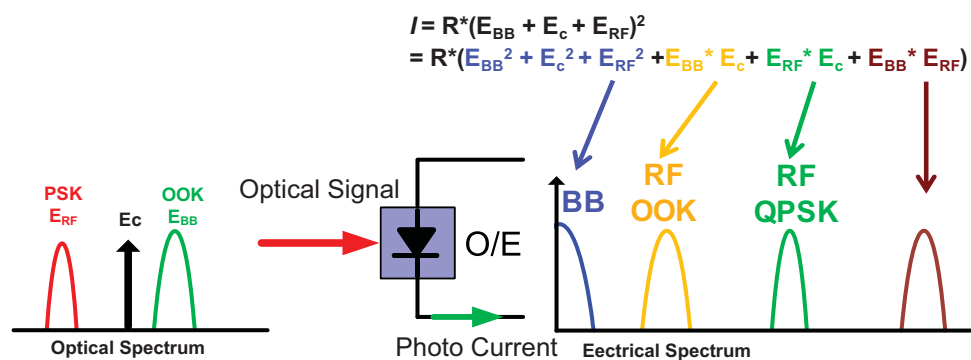


FIG. 6.2. Conceptual diagram of a square-law detection of the proposed system.

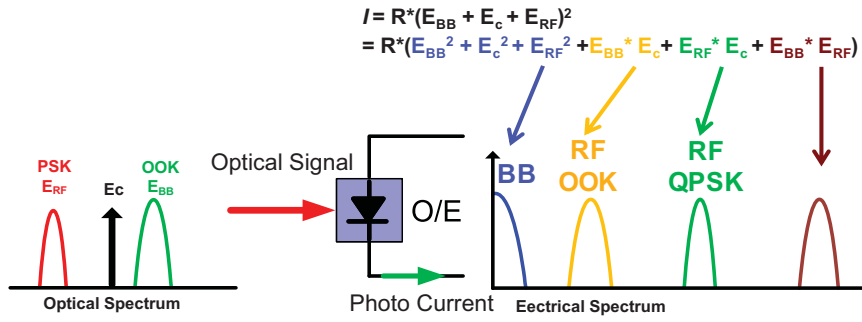


FIG. 6.3. Experimental setup for RF and BB signal generation and transmission.

6.1.2 Experimental setup

Figure 6.3 illustrates the experimental setup of the proposed system. A BPSK signal is utilized for the RF signal in this demonstration. The RF BPSK signal is a 625-Mb/s pseudo random binary sequence (PRBS) signal with word length of $2^{31} - 1$ and up-converted using a 14.375-GHz sinusoidal signal. The RF OOK signal is a 1.25-Gb/s PRBS with the word length of $2^{31} - 1$ and up-converted with a 5-GHz sinusoidal signal. A CW laser is generated by a tunable laser. A dual-electrode MZM which is biased at the quadrature point is employed to modulate the CW laser. After the MZM, a fiber Bragg grating is used to adjust the optical carrier power for receiver sensitivity optimization. Before transmission over 25-km SSMF, the hybrid optical signal is amplified by an EDFA. At the remote node, the hybrid optical signal is separated for different applications just using an optical coupler. For FTTx BB application, the BB OOK signal is directly detected by using a commercial 2.5-Gb/s optical receiver. For RoF applications, the RF BPSK signals are detected by using a high speed photo receiver, down-converted to BB with 14.375-GHz sinusoidal signal, and then pass through low-pass filters with 3 dB bandwidth of 625 MHz.

6.1.3 Results and discussion

The optical power ratio between BPSK subcarrier and optical carrier is an important parameter which influences the receiver sensitivity of BPSK signal. To optimize the RF BPSK receiver sensitivity, the OOK signal is turned off first. Only the 14.375-GHz BPSK RF signal is modulated on the optical subcarrier. The system sensitivities are measured with optical carrier to subcarrier power ratio of -6 dB, 0 dB and 6 dB. FIG. 6.4 plots the bit error rate (BER) curve for different optical carrier to subcarrier power ratio. The inset within FIG. 6.4 shows the sensitivity penalties versus the power ratio of optical carrier power to RF BPSK subcarrier power at the BER of 10^{-9} . The corresponding optical spectra and eye diagrams are shown in FIG. 6.5. The best receiver sensitivity is obtained when the optical carrier to subcarrier power ratio is 0 dB.

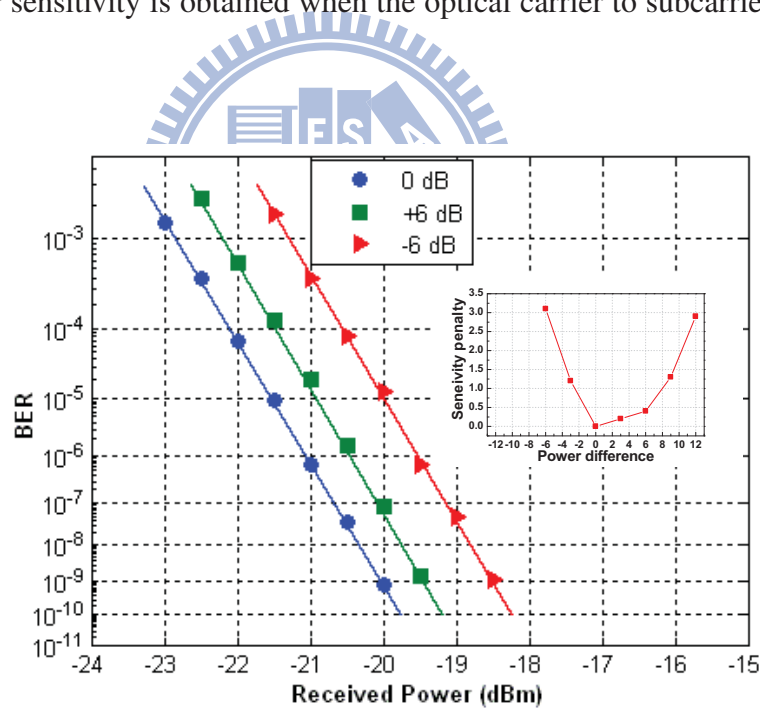


FIG. 6.4. BER curves of BPSK signals.

Compared with wireline transmission media (i.e. fiber), wireless signal is more susceptible to the environment (the presence of radio-opaque obstacles, multipath in-

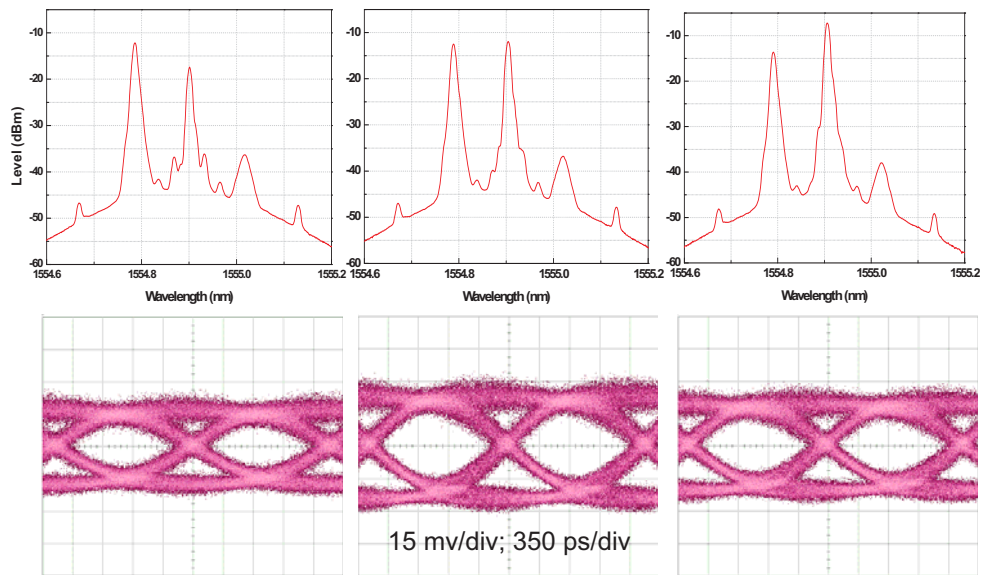


FIG. 6.5. Spectra (Resolution 0.01 nm) and eye diagrams of BPSK signals. (a) -6dB; (b) 0dB; (c) +6dB

interference etc.) Therefore, system operators need to be able to freely adjust the power ratio between wireline and wireless services according to geographic variation. The proposed system provides an easily adjustable power splitting scheme to adapt different geographic landscapes. FIG. 6.6 illustrates the receiver sensitivity of both RF BPSK and BB OOK signals at BER of 10^{-9} with different RF OOK subcarrier to RF BPSK subcarrier optical power ratio (P_{OOK}/P_{BPSK} , P_{OOK} and P_{BPSK} are the powers of RF OOK subcarrier and RF BPSK subcarrier, respectively). A receiver sensitivity trade-off between the BB OOK and down-converted RF BPSK signals is observed. The sensitivities of BB OOK and RF BPSK signals can be adjusted according to the needs of various environments. In this work, the BB and RF signals with the same receiver sensitivities are set as the optimal condition, where the optical power of OOK subcarrier is 1 dB higher than that of the RF BPSK subcarrier, as shown in FIG. 6.7. At the optimal condition, there is about 3-dB penalty when the RF BPSK subcarrier is turned on or off. Among this 3-dB penalty, 1.3-dB is due to the RF BPSK subcarrier

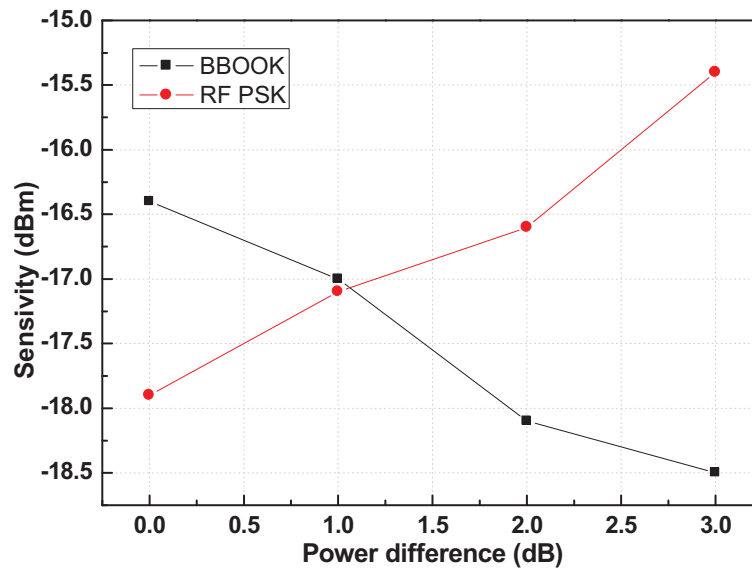


FIG. 6.6. BB OOK and RF BPSK sensitivities with different RF OOK to RF BPSK optical subcarrier power ratios.

power and 1.7-dB is due to channel crosstalk and noises.

Figure 6.8 shows the receiving sensitivities of both the BB OOK and down-converted RF BPSK signals at BTB and following 25 km SSMF transmission. For BB signals, there are three terms of signals after the square-law photo-diode detection: the optical carrier, the RF BPSK subcarrier, and the OOK subcarrier. Although the optical carrier and the RF BPSK subcarrier contribute DC power to BB signals, noises of these three carriers accumulate on BB signals after photo-diode detection. Therefore, the BB OOK signal is noisier than the RF BPSK signal. However, the sensitivities are still good enough for corresponding applications. The power penalties of both the RF PSK and BB OOK signals at BER of 10^{-9} are less than 0.5 dB.

6.1.4 Summary

Simultaneous generation and transmission of FTTx BB and wireless RF signals by using a dual-electrode MZM for hybrid access is experimentally demonstrated in

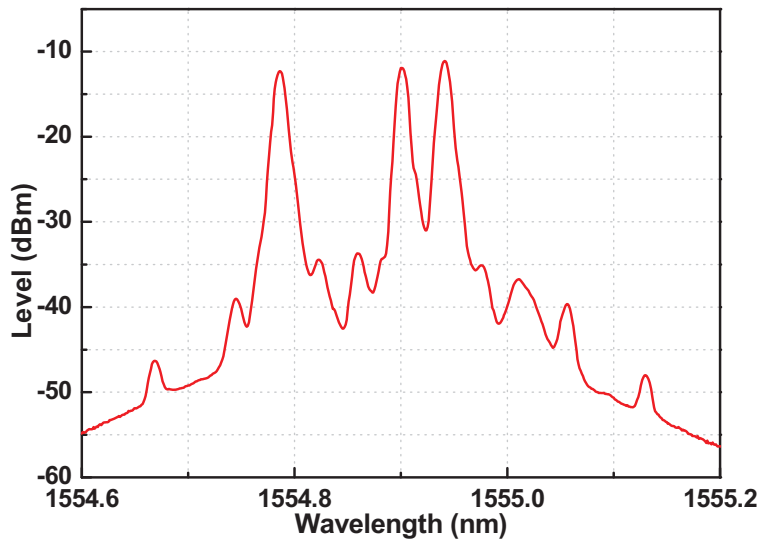


FIG. 6.7. Optimized BTB optical spectrum. (Resolution: 0.01 nm)

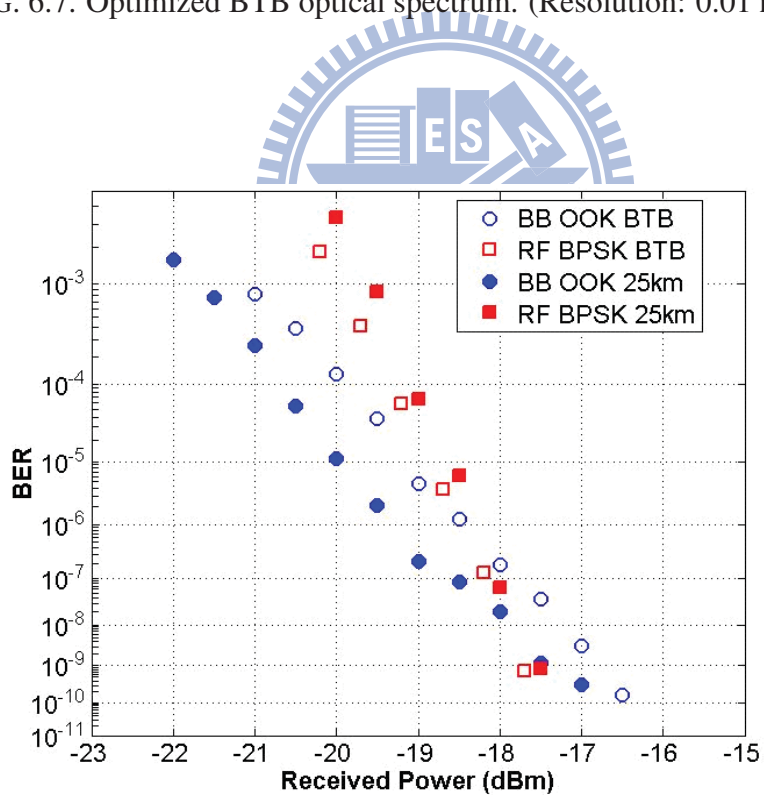


FIG. 6.8. BER curves of BB OOK and RF BPSK BTB and after transmission over 25km.

this section. No optical filter is needed at remote nodes for separating BB and RF signals. The proposed system provides an easily adjustable receiver sensitivity scheme to adapt different geographic landscapes. Following 25 km of SSMF, the receiver sensitivity penalties of both RF and BB signals are less than 0.5 dB.

6.2 Multi-Services Hybrid Access Network System Using A DP-MZM

In last section, a multi-service hybrid access network system using a dual-electrode MZM was proposed. However, a narrow band optical filter is still required in the HEU to control the OPR between the PSK sideband and the optical carrier. In this section, another multi-service hybrid access network system using a DP-MZM will be proposed. All of the optical sidebands in this system are generated from different driving signals. Therefore, the OPR between the optical sidebands can be freely adjusted by controlling the driving signals and no narrow band optical filter is required to suppress the optical carrier power.

6.2.1 Experimental setup

Figure 6.9 shows the experimental setup of the multi-services hybrid access network system using a DP-MZM. A DFB laser is used as the optical source. Both 8PSK and QPSK modulation formats with 312.5-MSymbol/s symbol rates are demonstrated for the RF signals. The M-ary PSK signals are generated from an AWG with 2.5-GHz carrier frequency and up-converted to 10-GHz using an electrical mixer with a 7.5-GHz LO signal. The 1.25-Gb/s OOK PRBS signal with word length of $2^{31} - 1$ is generated using a pattern generator and up-converted to 5-GHz. A 10-GHz sinusoidal signal is also employed for the generation of new optical subcarrier. The signals are separated using 90° hybrid couplers. The 90° phase delays are added on the upper path of OOK and PSK to generate USB signals, and the 90° phase delay is added on

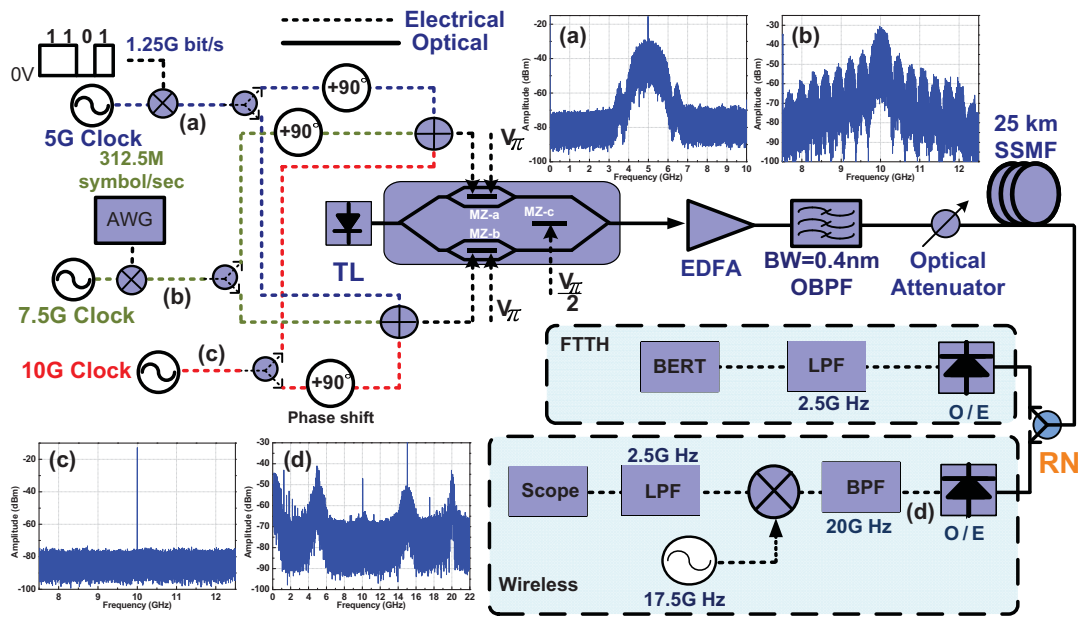


FIG. 6.9. Experimental setup of the multi-services hybrid access network system using a DP-MZM.

the lower path of the 10-GHz sinusoidal signal to generate LSB signal. The half-wave voltages (V_π) of MZ-a and MZ-b in the DP-MZM are 2.9 volts. In addition, the modulation indices (V_m/V_π , V_m is the amplitude of the driving signal) for all the driving signals are about 0.1.

At the output of the modulator, an EDFA is utilized to boost the optical power and adjust to 0 dBm before sent into fiber. After transmission over 25-km SSMF, only an optical coupler is employed to separate the optical power of the hybrid signal for different applications. For FTTx BB application, the BB OOK signal is directly detected using a commercial 2.5-Gb/s photo receiver and sent into a bit error rate tester (BERT) for performance analysis. For radio-over-fiber applications, the 20-GHz M-ary PSK signal is detected using a high speed photo receiver, down-converted with a 17.5-GHz sinusoidal signal, and then sent into a real time scope to capture the time domain waveform for off-line analysis. In this work, 1024 symbols of PSK

signals are captured. The BER of the Gray-coded M-ary PSK are calculated using $BER = (1/\log_2 M) \times \text{erfc}[\sqrt{E/N_0} \sin(\pi/M)]$ [76, 77]. Where M is the order of the M-ary PSK signal, E is the energy of the modulation symbol and N_0 is the noise power spectrum density.

6.2.2 Results and discussion

In this system, all of the optical sidebands are generated from different driving signals. Therefore, the OPR between the optical sidebands can be freely adjusted. To optimize the RF PSK signal, the RF OOK signal is turned off first. Only PSK and the 10-GHz sinusoidal signals are sent into the dual-parallel MZM. FIG. 6.10 illustrate the $-\log(\text{BER})$ of both the 8PSK and QPSK signals with different PSK optical sideband to optical carrier OPR. The BER values of RF 8PSK and QPSK signals are obtained with -18.5 and -17-dBm optical power, respectively. The best receiver sensitivity of both the 8PSK and QPSK signals are obtained when the OPRs are 0 dB.

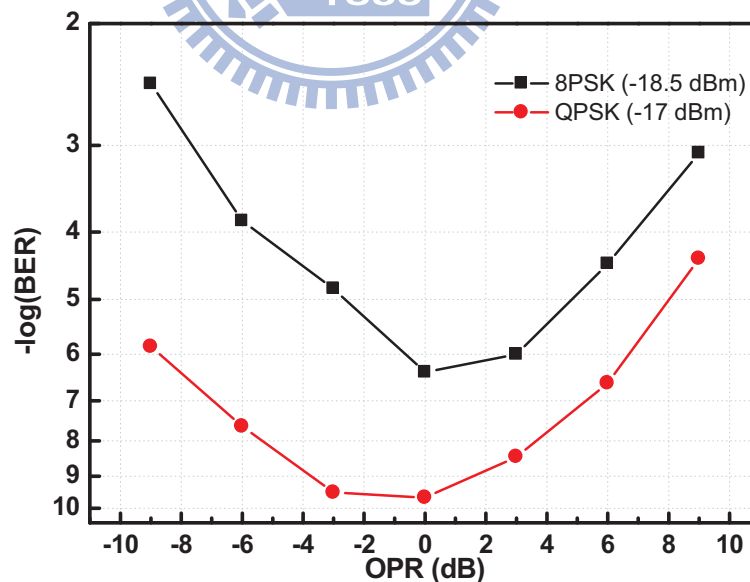


FIG. 6.10. $-\log(\text{BER})$ versus Optical Power Ratio between PSK optical sideband and new carrier.

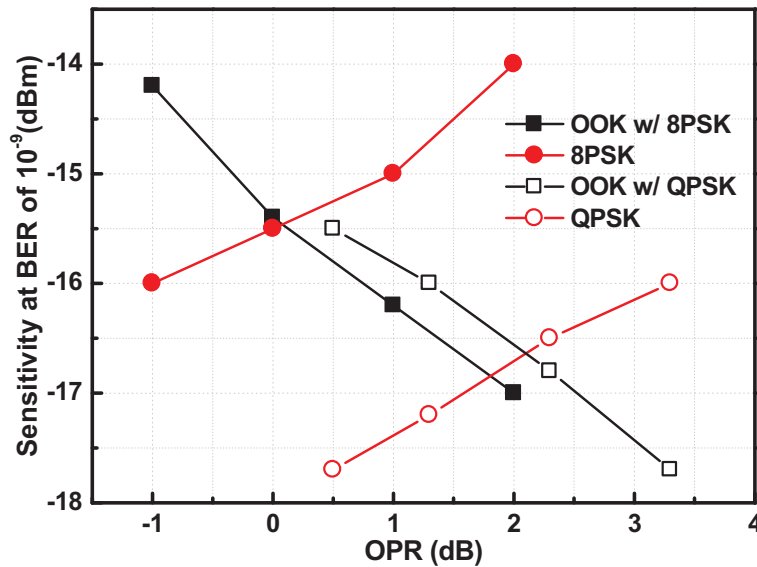


FIG. 6.11. Optical Power Ratio between 8PSK and new carrier.

After optimization of the OPR between PSK and new optical carrier sidebands, the OPR between the RF OOK and optical carrier sidebands are also needed to be optimized. Compared with wired transmission media, wireless signal is more sensitive to the transmission environment. Therefore, system operators need to be able to freely adjust the power ratio between wired and wireless services according to geographic variation. FIG. 6.11 illustrates the receiver sensitivity of both RF PSK and BB OOK signals at BER of 10^{-9} with different new carrier to OOK signals OPR. The receiver sensitivity trade-off between the RF PSK and BB OOK signals are observed. In this work, RF and BB signals with equal receiver sensitivities are set as the optimal condition, where the 8PSK and QPSK to OOK OPR are about 0 dB and 2 dB.

Figure 6.12 shows the $-\log(\text{BER})$ curves of both the 8PSK-OOK and QPSK-OOK systems at BTB and following 25-km transmission of SSMF. No significant receiver power penalties of both the RF and BB signals in 8PSK-OOK and QPSK-OOK systems are observed after the transmission. The constellations of the RF 8PSK and QPSK signals, the eye diagrams of the BB OOK signals in 8PSK-OOK and QPSK-

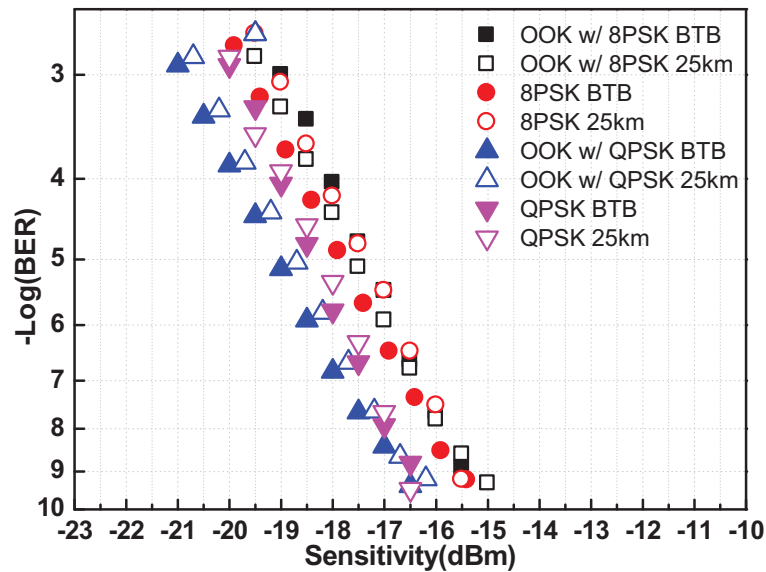


FIG. 6.12. BER curves of OOK (w/ 8PSK), 8PSK, OOK (w/ QPSK) and QPSK.

OOK systems are also shown in FIG. 6.13. After the transmission, no significant distortions are observed in both the RF and BB signals.

6.2.3 Summary

Simultaneous generation and transmission of wireless RF M-ary PSK vector signal and FTTx BB OOK signals for hybrid access networks are experimentally demonstrated. No additional narrow-band optical filter is needed in the proposed system to separate the RF and BB signals. Only a typical low-speed photo receiver is required to recover the BB OOK signal. Therefore, the proposed system is compatible with the existing WDM PON system.

In addition, frequency doubling is also achieved in the proposed system. Generations of 20-GHz RF signals are experimentally demonstrated using 10-GHz RF components in this work. Moreover, high spectral efficiency QPSK and 8PSK modulation formats can be used in the proposed system which is compatible with the existing wireless communication system. After the transmission over 25-km SSMF,

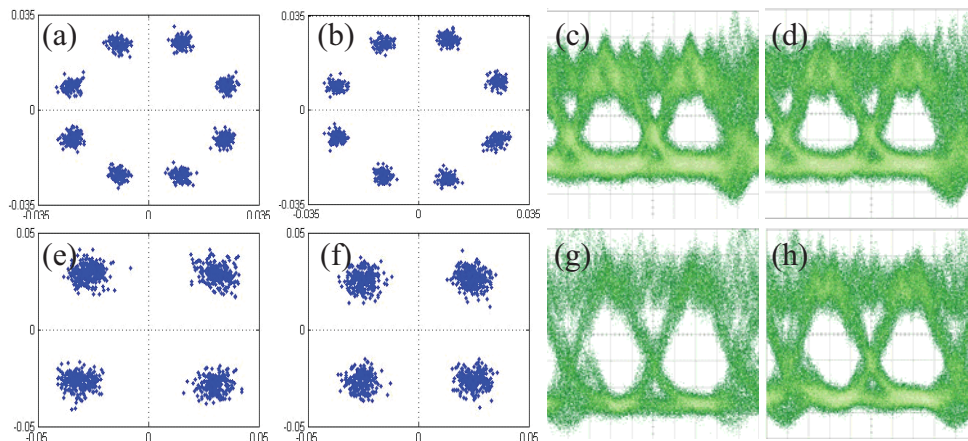


FIG. 6.13. Constellations and eye diagrams. (a) 8PSK BTB; (b) 8PSK 25km; (c) OOK w/ 8PSK BTB; (d) OOK w/ 8PSK 25km; (e) QPSK BTB; (f) QPSK 25km; (g) OOK w/ QPSK BTB; (h) OOK w/ QPSK 25km. (Eye diagrams 100 mV/div; 200 ps/div)

no significant receiver penalties are observed in both RF and BB signals.

6.3 Conclusion

Two architectures for multi-service hybrid access network were proposed in this chapter. Simultaneous generation and transmission BB OOK signal for FTTx and RF PSK signal for RoF applications were achieved. No narrow band optical filter which severely hinders the implementation in WDM systems and is not compatible with the existing passive optical network (PON) system is required at remote node to separate the BB and RF signals. In summary, the proposed systems provide attractive and cost-effective solutions for the next generation hybrid access networks.

Chapter 7

CONCLUSIONS

The demand and concept of optical millimeter-wave signal generation has been discussed in the thesis. Conventional optical millimeter-wave signal generations based on DSB, SSB and DSB-CS modulation schemes are discussed. DSB modulation is the simplest architecture, but chromatic dispersion induced RF fading issue restricts the fiber transmission distance. SSB modulation scheme has no chromatic dispersion induced RF fading issue. However, the weak MI and high optical carrier power limit the OMI of SSB signal. Because the high-OMI and no chromatic dispersion induced RF fading issue, DSB-CS modulation scheme becomes a popular choice for optical millimeter-wave signal generation. Moreover, frequency doubling can be achieved in DSB-CS modulation scheme.

An optical millimeter-wave signal generation system with frequency quadrupling was proposed in this thesis. The impact of the imbalance of the DP-MZM was investigated. 40-GHz optical millimeter-wave signal with 38-dB carrier and undesired optical sideband suppression was experimentally demonstrated. Since no optical filter is needed, the proposed approaches can be adopted for optical up-conversion in WDM radio-over-fiber systems and continuously tunable millimeter-wave signal systems. Four channels WDM up-conversion of 1.25-Gbps OOK signals were experimentally demonstrated. Additionally, receiver sensitivity degradation due to MZM bias drifts

is also investigated for 20-GHz WDM signals. The receiver power penalty can be less than 1 dB when bias deviation ratios are less than 20% of the half-wave voltage, which can be achieved using a bias feedback control system. After transmission over a 50-km SSMF, the receiver power penalties of both the BB and 20-GHz RF OOK signals are less than 1 dB. The 40- and 60-GHz WDM up-conversion using 10- and 15-GHz RF driving signals are also demonstrated. The proposed system is compatible with existing WDM PON system. Since only low-frequency RF components and equipment are required, the proposed system is a potential solution for future WDM up-conversion system.

Optical millimeter-wave generation with frequency octupling was theoretically analyzed and experimentally demonstrated. Two commercially available DP-MZMs are keys to the proposed system. V-band 60-GHz and W-band 80-GHz optical MMW signal are experimentally generated from 7.5- and 10-GHz driving signals with 30-dB undesired sideband suppression ratios. Time domain waveform with a 50% duty cycle is observed. After transmission of 25-km SSMF, no significant signal distortion is observed. Optical MMW signal with frequency up to 320-GHz can be generated using the state-of-the-art 40-GHz DP-MZMs. The proposed frequency octupling optical MMW generation is a potential solution for the future ultra-high frequency MMW applications. W-band wireless communication based on the frequency octupling system was experimentally demonstrated. Single-carrier 1.25-GSymbol/sec QPSK and 8QAM wireless data transmission at 102.5-GHz under direct bias modulation and 9-mA photocurrent can be achieved with 170-cm wireless transmission distance.

Optical millimeter-wave signal generation with frequency 12-tupling was proposed. The key to the proposed system is the optical high-purity millimeter-wave signal generation with frequency quadrupling using a commercially available dual-parallel MZM. 40- and 70-GHz high purity two-tone optical signals were experimentally demonstrated from 10- and 17.5-GHz RF driving signals. Modulation depth trim-

ming between MZ-a and MZ-b are employed to compensate the amplitude imbalance between the MZM arms and improve the optical carrier suppression ratio. Following optical frequency quadrupling, optical four-wave mixing was promoted utilizing an SOA. Since the excellent optical carrier and harmonic distortion suppression ratio of the FWM pump signals, only the second and sixth order sidebands were obtained at the output of the SOA. After filtering out the undesired sidebands using optical interleavers, high-purity optical two-tone signals separated by 120 and 210 GHz were obtained. The optical carrier and harmonic distortion ratios of the generated 210- and 120-GHz optical two-tone signals were 20 and 30 dB, respectively. The frequency of the generated optical millimeter-wave signal is 12 times that of the RF driving signal. Millimeter-wave signals with frequency beyond 100 GHz can be easily achieved using low frequency RF equipments and components. Since the frequency response of the state-of-the-art MZM is up to 40 GHz, the proposed system provides a reliable and cost-effective solution for optical millimeter-wave generation with frequencies of up to 480 GHz.

To demonstrate the feasibility of 60-GHz RoF system, several 60-GHz RoF architecture were proposed. Frequency doubling, high spectral efficiency vector signal, and full-duplex systems were achieved in the TSSB system. The TSSB system does not suffer from dispersion induced performance fading issue. An-symmetrical full-duplex with 13.75-Gbps down-link and 1.25-Gbps up-link transmissions was achieved in the TSSB RoF system. No significant receiver power penalties was observed after transmission of 25-km SSMF.

To reduce the bandwidth of the transmitter, an 60-GHz RoF system with frequency sextupling was proposed based on a modified SSB modulation scheme and optical up-conversion system with frequency quadrupling. The generation and transmission of 13.75-Gb/s QPSK-OFDM and 20.625-Gb/s 8QAM-OFDM signals occupying the full 7-GHz license-free band at 60 GHz was experimentally demonstrated.

After transmission over 25-km of standard single-mode fiber, no significant received power penalty was observed with both OFDM signal formats. Based on the frequency sextupling, the bandwidth requirement of the transmitter is only 10-GHz.

To demonstrate the symmetrical full-duplex system, 60-GHz RoF system based on very simple IMDD architecture was proposed. A symmetrical 2×21 Gbps full-duplex bidirectional RoF system using simple double-sideband IMDD links was successfully demonstrated at 60 GHz. High speed single-electrode Mach Zehnder and Reflective Electro-Absorption modulators were employed in the downlink and uplink transmission, respectively. OFDM-8QAM signal modulation format was utilized. At least 500m fiber transmission and 2.5m wireless transmission distances were achieved, without any dispersion compensation or optical filtering. The proposed full-duplex RoF system is very simple and fully transparent, making it ideal for in-building high data-rate wireless applications, which are characterized by short fiber spans.

To achieve the multi-service hybrid access network, simultaneous generation and transmission of wireless RF M-ary PSK vector signal and FTTx BB OOK signals for hybrid access networks were experimentally demonstrated. No additional narrow-band optical filter is needed in the proposed system to separate the RF and BB signals. Therefore, the proposed system is compatible with the existing WDM PON system. After the transmission of 25-km SSMF, no significant receiver penalties are observed in both RF and BB signals in the proposed systems. In summary, the proposed system provides an attractive and cost-effective solution for the next generation hybrid access networks.

Appendix A

IMBALANCE OF CONVENTIONAL MZM

Due to the manufacturing imperfection, the power splitting ratios of the Y-splitters are usually imbalanced and provide limited extinction ratio in a real MZM. FIG. A.1 shows a conceptual diagram of a conventional MZM with imbalanced Y-splitters. γ_1 and γ_2 denote the couple factors of the input and output Y-splitters, respectively. Assume that the optical field at the input of the integrated MZM is defined as $E_{in}(t) = E_o \cos(\omega_o t)$. The upper and lower arm optical field after the input Y-splitter can be expressed as

$$\begin{aligned} E_1 &= \sqrt{1-\gamma_1} \cdot E_o \cdot \exp[j\omega_o t] \\ E_2 &= \sqrt{\gamma_1} \cdot E_o \cdot \exp[j\omega_o t] \end{aligned} \quad (\text{A.1})$$

When driving voltages are applied to the MZM, optical carrier phase shifts of ϕ_1 and

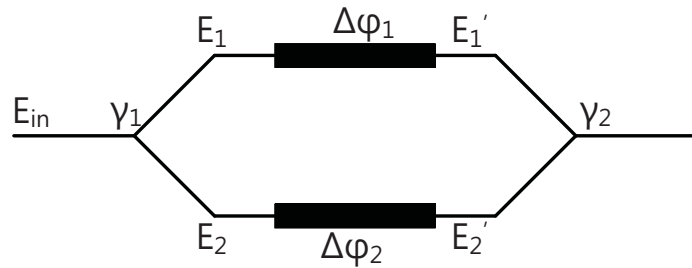


FIG. A.1. Conceptual diagram of an imbalanced MZM.

ϕ_2 are introduced to the upper and lower arms signals. The phase shifts are

$$\begin{aligned}\phi_1 &= \frac{\pi}{2} \frac{1}{V_\pi} (V_{bias_1} + V_{RF_1}) \\ \phi_2 &= \frac{\pi}{2} \frac{1}{V_\pi} (V_{bias_2} + V_{RF_2})\end{aligned}\quad (\text{A.2})$$

,where V_π is the half-wave voltage of the MZM, V_{bias_n} are the bias voltages, and V_{RF_n} are the RF driving voltages. In a single-electrode MZM, $\Delta\phi_1 = -\Delta\phi_2 = \Delta\phi$. After modulation of the electrodes, the optical fields in the upper and lower arms can be expressed as

$$\begin{aligned}E'_1 &= \sqrt{1 - \gamma_1} \cdot E_o \cdot \exp(j\omega_o t) \cdot \exp(j\Delta\phi_1) \\ E'_2 &= \sqrt{\gamma_1} \cdot E_o \cdot \exp(j\omega_o t) \cdot \exp(j\Delta\phi_2)\end{aligned}\quad (\text{A.3})$$

These two optical fields are combined at the output Y-splitter. Then, the output optical field becomes

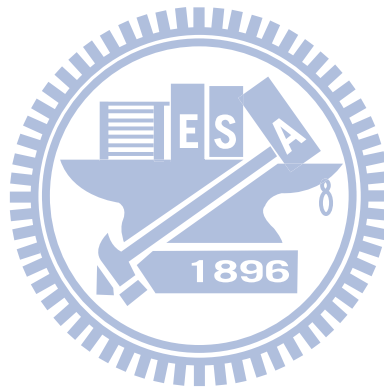
$$\begin{aligned}E_{out} &= j \cdot \sqrt{\gamma_2} \cdot E'_1 + \sqrt{1 - \gamma_2} \cdot E'_2 \\ &= E_o \cdot \exp(j\omega_o t) \cdot [j \cdot \sqrt{1 - \gamma_1} \cdot \sqrt{\gamma_2} \cdot \exp(j\Delta\phi_1) \\ &\quad + j \cdot \sqrt{\gamma_1} \cdot \sqrt{1 - \gamma_2} \cdot \exp(j\Delta\phi_2)] \\ &= E_{in} \cdot [j \cdot \sqrt{1 - \gamma_1} \cdot \sqrt{\gamma_2} \cdot \exp(j\Delta\phi) + j \cdot \sqrt{\gamma_1} \cdot \sqrt{1 - \gamma_2} \cdot \exp(-j\Delta\phi)]\end{aligned}\quad (\text{A.4})$$

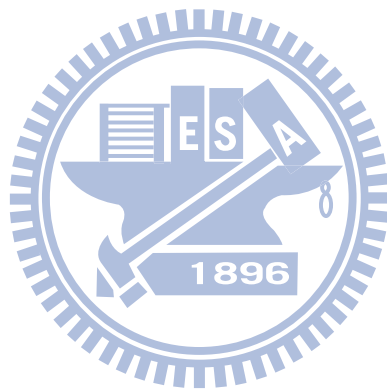
Besides, the extinction ratio (ER) of this MZM is defined as

$$ER = \left[\frac{\sqrt{\gamma_1} \cdot \sqrt{\gamma_2} + \sqrt{1 - \gamma_1} \cdot \sqrt{1 - \gamma_2}}{\sqrt{\gamma_1} \cdot \sqrt{\gamma_2} - \sqrt{1 - \gamma_1} \cdot \sqrt{1 - \gamma_2}} \right]^2 \quad (\text{A.5})$$

With an ideal case, the couple factors are $\gamma_1 = \gamma_2 = 0.5$. Therefore, the optical field after the modulation of the MZM can be presented as

$$\begin{aligned}
 Re\{E_{out}\} &= Re\left\{\frac{1}{2} \cdot E_{in}[j \cdot \exp(j\Delta\phi) + j \cdot \exp(-j\Delta\phi)]\right\} \\
 &= Re\{j \cdot E_o \cdot \exp(j\omega_o t) \cdot \cos(\Delta\phi)\} \\
 &= -E_o \cdot \sin(\omega_o t) \cdot \cos\left(\frac{\pi}{2} \frac{1}{V_\pi}(V_{bias} + V_{RF})\right)
 \end{aligned} \tag{A.6}$$





Appendix B

CHROMATIC DISPERSION INDUCED RF FADING IN DSB MODULATION SCHEME

Due to the chromatic dispersion in a dispersive SSMF, the group velocity of an optical signal transmitting in an optical fiber is wavelength dependent. The wavelength dependent group velocity causes a phenomenon referred to as group-velocity dispersion (GVD). When an optical millimeter-wave signal is transmitted over a SSMF, different phase shifts are introduced to each optical sidebands due to the chromatic dispersion. When a DSB optical signal is transmitted over the SSMF, the generated millimeter-wave signal fades out with the increasing of the fiber distance due to the chromatic dispersion.

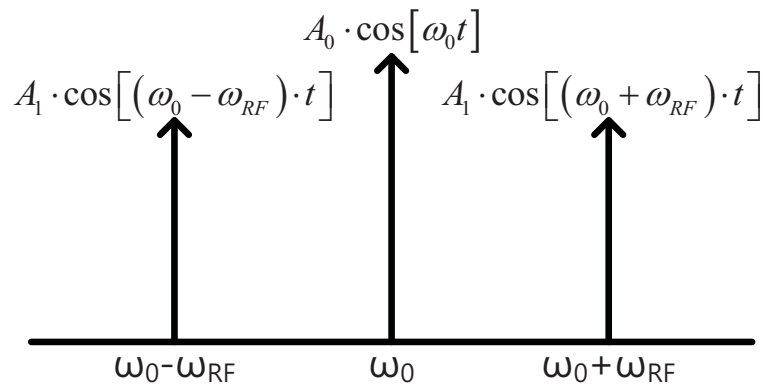


FIG. B.1. Conceptual diagram of a DSB optical spectrum.

When an optical signal with wavelength of ω transmits over a SSMF, the propagation constant of the signal can be expressed as

$$\begin{aligned}\beta(\omega) &= n(\omega) \frac{\omega}{c} \\ &= \beta_0 + \beta_1(\omega - \omega_o) + \frac{1}{2}\beta_2(\omega - \omega_o)^2 + \dots\end{aligned}\quad (\text{B.1})$$

where $\beta_m = (d^m \beta / d\omega^m)|_{\omega=\omega_o}$ is the derivative of the propagation constant evaluated at a angular frequency of $\omega = \omega_o$, and c is the speed of light. To simplify the analysis, the high order terms can be ignored at 1550 nm. For a DSB signal as shown in FIG. B.1, the propagation constants for the sidebands with frequencies of $\omega = \omega_o \pm \omega_{RF}$ are

$$\beta(\omega_o \pm \omega_{RF}) \cong \beta_0 \mp \beta_1(\omega_o)\omega_{RF} + \frac{1}{2}\beta_2(\omega_o)\omega_{RF}^2 \quad (\text{B.2})$$

and

$$\beta_2(\omega_o) = -\frac{c}{2\pi f_o^2} \cdot D(\omega_o) \quad (\text{B.3})$$

, where D is the chromatic dispersion parameter, f_o is the frequency of the optical carrier, ω_{RF} is the angular frequency of the millimeter-wave signal. For the SSMF, D is 17 ps/(nm · km).

After the transmission over a SSMF of distance z , the electrical fields of the DSB tones can be written as

$$\begin{aligned}\text{OpticalCarrier} &: A_0 \cdot \cos[\omega_o t - \beta_0] \cdot t \\ \text{LowerSideband} &: A_1 \cdot \cos\left[(\omega_o - \omega_{RF}) \cdot t - \beta_0 + \beta_1 \cdot \omega_{RF} \cdot z - \frac{1}{2} \cdot \beta_2 \cdot \omega_{RF}^2 \cdot z\right] \\ \text{UpperSideband} &: A_1 \cdot \cos\left[(\omega_o + \omega_{RF}) \cdot t - \beta_0 - \beta_1 \cdot \omega_{RF} \cdot z - \frac{1}{2} \cdot \beta_2 \cdot \omega_{RF}^2 \cdot z\right]\end{aligned}\quad (\text{B.4})$$

After the PD square-law detection, the millimeter-wave with the frequency of ω_{RF} are the combination of the beating term of the optical carrier and lower optical sideband,

and the beating term of the optical carrier and the upper sideband. The photo-current with the frequency of ω_{RF} becomes

$$I_{\omega_{RF}} = R \cdot \frac{A_0 \cdot A_1}{2} \cdot \cos \left[\omega_{RF} \cdot t - \beta_1 \cdot \omega_{RF} \cdot z - \frac{1}{2} \cdot \beta_2 \cdot \omega_{RF}^2 \cdot z \right] + R \cdot \frac{A_0 \cdot A_1}{2} \cdot \cos \left[\omega_{RF} \cdot t - \beta_1 \cdot \omega_{RF} \cdot z + \frac{1}{2} \cdot \beta_2 \cdot \omega_{RF}^2 \cdot z \right] \quad (\text{B.5})$$

Let $a = \omega_{RF} \cdot t - \beta_1 \cdot \omega_{RF} \cdot z$ and $b = \frac{1}{2} \cdot \beta_2 \cdot \omega_{RF}^2 \cdot z$. Then, the generated photo-current with frequency of ω_{RF} can be simplified as

$$\begin{aligned} I_{\omega_{RF}} &= R \cdot \frac{A_0 \cdot A_1}{2} \cdot [\cos(a - b) + \cos(a + b)] \\ &= R \cdot \frac{A_0 \cdot A_1}{2} \cdot 2 \cdot \cos(a) \cdot \cos(b) \\ &= R \cdot A_0 \cdot A_1 \cdot \cos(a) \cdot \cos(b) \end{aligned} \quad (\text{B.6})$$

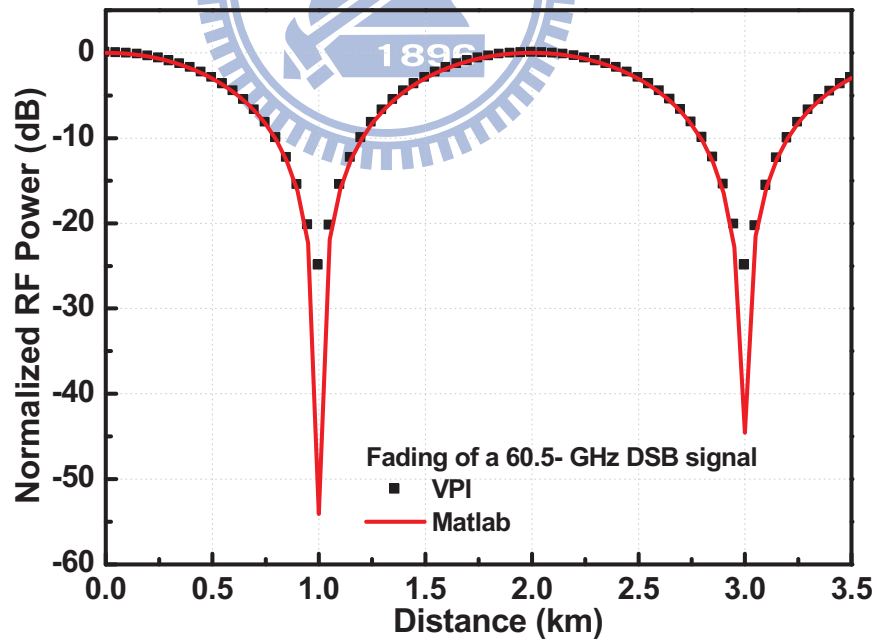


FIG. B.2. Simulation results of dispersion induced fading of a 60.5-GHz DSB optical millimeter-wave signal.

Due to the chromatic dispersion, the generated photo-current with the frequency of ω_{RF} is related to $\cos [(1/2) \cdot \beta_2 \cdot \omega_{RF}^2 \cdot z]$. Therefore, the generated millimeter-wave signal fades out with a certain distance of fiber transmission distance.

Figure B.2 shows the analytical (Matlab) and numerical (VPI) simulation fading results of a 60.5-GHz DSB optical millimeter-wave signal. The analytical and numerical results are matched to each other. After transmission over 1-km SSMF, the 60.5-GHz millimeter-wave signal fades out. In addition, a fading period of 2 km is observed from the simulation results.



REFERENCES

- [1] J. Wells, “Faster than fiber: The future of multi-g/s wireless”, *IEEE Microw. Magazine*, vol. 10, no. 3, pp. 104–122, 2009.
- [2] H. Y. Chang and H. Wang, “A 98/196 ghz low phase noise voltage controlled oscillator with a mode selector using a 90 nm cmos process”, *IEEE Microw. Wirele. Compo. Lett.*, vol. 19, no. 3, pp. 170–172, 2009.
- [3] C. Cao, E. Seok, and K.K. O, “192 ghz push-push vco in 0.13 μm cmos”, *IEEE Electro. Lett.*, vol. 42, no. 4, pp. 208–210, 2006.
- [4] B. Heydari, M. Bohsali, E. Adabi, and A. M. Niknejad, “Low-power mm-wave components up to 104ghz in 90nm cmos”, in *International Solid-State Circuits Conference*, 2007, pp. 200–201.
- [5] H. K. Chen, H. J. Chen, D. C. Chang, Y. Z. Juang, and S. S. Lu, “A 0.6 v, 4.32 mw, 68 ghz low phase-noise vco with untrinsic-tuned technique in 0.13 μm cmos”, *IEEE Microw. Wirele. Compo. Lett.*, vol. 18, no. 7, pp. 467–469, 2008.
- [6] J. Yao, “Microwave photonics”, *IEEE J. Lightw. Technol.*, vol. 27, no. 3, pp. 314–335, 2009.
- [7] K. T. Lau, “Narrow-band modulation of semiconductor lasers at millimeter wave frequencies (≤ 100 ghz) by mode locking”, *IEEE J. Quantum Electro.*, vol. 26, no. 2, pp. 250–261, 1990.
- [8] K. H. Lee, W. Y. Choi, Y. A. Leem, and K. H. Park, “Harmonic millimeter-wave generation and frequency up-conversion using a passively mode-locked

- multisection dfb laser under external optical injection”, *IEEE Photon. Technol. Lett.*, vol. 19, no. 3, pp. 161–163, 2007.
- [9] W. W. Hsiang, C. Y. Lin, N. K. Sooi, and Y. Lai, “Long-term stabilization of a 10 ghz 0.8 ps asynchronously mode-locked er-fiber soliton laser by deviation-frequency locking”, *Opt. Express*, vol. 14, no. 5, pp. 1822–1828, 2006.
- [10] C. Williams, F. Quinlan, and P. J. Delfyett, “Injection-locked mode-locked laser with long-term stabilization and high power-per-combine”, *IEEE Photon. Technol. Lett.*, vol. 21, no. 2, pp. 94–96, 2009.
- [11] J. Yu, Z. Jia, L. Yi, G. K. Chang, and T. Wang, “Optical millimeter-wave generation or up-conversion using external modulator”, *IEEE Photon. Technol. Lett.*, vol. 18, no. 1, pp. 265–267, 2006.
- [12] H. Chi and J. Yao, “Frequency quadrupling and upconversion in a radio over fiber link”, *IEEE J. Lightw. Technol.*, vol. 26, pp. 2706–2711, 2008.
- [13] M. Mohamed, X. Zhang, B. Hraimel, and K. Wu, “Frequency sixupler for millimeter-wave over fiber systems”, *Opt. Express*, vol. 16, no. 14, pp. 10141–10151, 2008.
- [14] J. Yu, Z. Jia, L. Yi, Y. Su, G. K. Chang, and T. Wang, “Optical millimeter-wave generation or up-conversion using external modulators”, *IEEE Photon. Technol. Lett.*, vol. 18, no. 1, pp. 265–267, 2006.
- [15] Z. Jia, J. Yu, A. Chowdhury, G. Ellinas, and G. K. Chang, “Simultaneous generation of independent wired and wireless services using a single modulator in millimeter-wave-band radio-over-fiber systems”, *IEEE Photon. Technol. Lett.*, vol. 19, no. 20, pp. 1691–1693, 2007.

- [16] Q. Chang and Y. Su, "A radio over fiber system for simultaneous generation and transmission of multiband signals", in *European Conf. on Optical Communication (ECOC 2007)*, 2007, p. P091.
- [17] Y. Tian and Y. Su, "A wdm-pon system providing quadruple play service with converged optical and wireless access", in *European Conf. on Optical Communication (ECOC 2007)*, 2007, p. P.6.07.
- [18] <http://www.wirelesshd.org>, ”.
- [19] <http://www.ieee802.org/15/pub/TG3c.html>, ”.
- [20] Behzad Razavi, "Gadgets gab at 60 ghz", *IEEE Spectrum*, pp. 46–58, 2008.
- [21] M. Weiß, M. Huchard, A. Stöhr, B. Charbonnier, S. Fedderwitz, and D. S. Jager, "60-ghz photonic millimeter-wave link for short- to medium-range wireless transmission up to 12.5gb/s", *IEEE J. Lightw. Technol.*, vol. 26, pp. 2424–2429, 2008.
- [22] Y. X. Guo, B. Luo, C.S. Park, L. C. Ong, M.-T. Zhou, and S. Kato, "60 ghz radio-over-fiber for gbps transmission", in *Global Symposium on Millimeter Waves (GSMM)*, 2008, p. Invited.
- [23] J. J. V. Olmos, T. Kuri, T. Sono, K. Tamura, H. Toda, and K. Kitayama, "Reconfigurable 2.5-gb/s baseband and 60-ghz (155-mb/s) millimeter-waveband radio-over-fiber (interleaving) access network", *IEEE J. Lightw. Technol.*, vol. 26, pp. 2506–2512, 2008.
- [24] T. Taniguchi, N. Sakurai, K. Kumozaki, and T. Imai, "Full-duplex 1.0 gbit/s data transmission over 60 ghz radio-on-fiber access system based on the loop-back optical heterodyne technique", *IEEE J. Lightw. Technol.*, vol. 26, pp. 1765–1776, 2008.

- [25] J. H. Seo, C. S. Choi, Y. S. Kang, Y. D. Chung, J. Kim, and W. Y. Choi, "Soa-eam frequency up/down-converters for 60-ghz bi-directional radio-on-fiber systems", *IEEE Trans. on Microw. Theory and Tech.*, vol. 54, pp. 959–966, 2006.
- [26] T. Kuri, K. Kitayama, and Y. Takahashi, "A single light-source configuration for full-duplex 60-ghz-band radio-on-fiber system", *IEEE Trans. on Microw. Theory and Tech.*, vol. 51, pp. 431–439, 2003.
- [27] H. C. Chien, A. Chowdhury, Z. Jia, Y. T. Hsueh, and G. K. Chang, "60 ghz millimeter-wave gigabit wireless services over long-reach passive optical network using remote signal regeneration and upconversion", *Opt. Express*, vol. 17, pp. 3036–3041, 2009.
- [28] M. Huchard, M. Weiß, A. Pizzinat, S. Meyer, P. Guignard, and B. Charbonnier, "Ultra-broadband wireless home network based on 60-ghz wpan cells interconnected via rof", *IEEE J. Lightw. Technol.*, vol. 26, no. 15, pp. 2364–2372, 2008.
- [29] G. H. Nguyen, B. Cabon, and Y. Le Guennec, "Generation of 60-ghz mb-ofdm signal-over-fiber by up-conversion using cascaded external modulators", *IEEE J. Lightw. Technol.*, vol. 27, pp. 1496–1502, 2009.
- [30] W. K. Kim, S. W. Kwon, W. J. Jeong, G. S. Son, K. H. Lee, W. Y. Choi, W. S. Yang, H. M. Lee, and H. Y. Lee, "Integrated optical modulator for signal up-conversion over radio-on-fiber link", *Opt. Express*, vol. 17, pp. 2638–2645, 2009.
- [31] Y. T. Hsueh, Z. S. Jia, H. C. Chien, J. J. Yu, and G. K. Chang, "A novel bidirectional 60-ghz radio-over-fiber scheme with multiband signal generation using a single intensity modulator", *IEEE Photon. Technol. Lett.*, vol. 21, pp. 1338–1340, 2009.

- [32] C. S. Park, Y. Guo, Y. K. Yeo, Y. Wang, L. C. Ong, and S. Kato, “Fiber-optic 60-ghz wireless downlink using cross-absorption modulation in an eam”, *IEEE Photon. Technol. Lett.*, vol. 20, pp. 557–559, 2008.
- [33] A. Ng’oma, M. Sauer, D. Thelen, and J. George, “Data throughput tripling by feed-forward equalization and photonic qpsk in a 7 gbps single-carrier rof link at 60 ghz”, in *International Topical Meeting on Microwave Photonics Asia-Pacific Microwave Photonics Conference (2008)*, 2008, pp. 213–216.
- [34] Y. Le Guennec, G. Maury, J. P. Yao, and B. Cabon, “New optical microwave up-conversion solution in radio-over-fiber networks for 60-ghz wireless applications”, *IEEE J. Lightw. Technol.*, vol. 24, pp. 1277–1282, 2006.
- [35] A. Hirata, T. Kosugi, H. Takahashi, R. Yamaguchi, F. Nakajima, T. Furuta, H. Sugahara H. Ito, Y. Sato, and T. Nagatsuma, “120-gh-band millimeter-wave photonic wireless link for 10-gb/s data transmission”, *IEEE Trans. Microw. Theory Tech.*, vol. 54, no. 5, pp. 1937–1944, 2005.
- [36] J. F. Cliche, B. Shillue, M. Tetu, and M. Poulin, “A 100-ghz-tunable photonic millimeter wave synthesizer for the atacama large millimeter array radiotelescope”, in *International Microw. Theory and Tech. Society*, Honolulu, Hawaii, 2007, pp. 349–352.
- [37] A. Sasaki and T. Nagatsuma, “Reflection-type cw-millimeter-wave imaging with a high-sensitivity waveguide-mounted electro-optic sensor”, *Jpn. J. Appl. Phys.*, vol. 41, no. 1A/B, pp. L83–L86, 2002.
- [38] J. Yu, Z. Jia, L. Yi, G. K. Chang, and T. Wang, “Optical millimeter-wave generation or up-conversion using external modulators”, *IEEE Photon. Technol. Lett.*, vol. 18, no. 1, pp. 265–267, 2006.

- [39] T. Ohno, F. Nakajima, T. Furuta, and H. Ito, “A 240-ghz active mode-locked laser diode for ultra-broadband fiber-radio transmission systems”, in *Optical Fiber Communication Conf. (OFC 2005)*, 2005, p. PDP13.
- [40] T. Ohno, F. Nakajima, T. Furuta, and H. Ito, “A 240-ghz active mode-locked laser diode for ultra-broadband fiber-radio transmission systems”, in *Optical Fiber Communication Conf. (OFC 2005)*, 2005, p. PDP13.
- [41] F. V. Dijk, A. Enard, X. Buet, F. Lelarge, and G. H. Duan, “Quantum dash mode-locked laser for millimeter-wave coupled opto-electronic oscillator”, in *Int. Topic Meeting on Microwave Photonics (MWP 2007)*, 2007, pp. 66–69.
- [42] J. Kondo, K. Aoki, Y. Iwata, A. Hamajima, T. Ejiri, O. Mitomi, and M. Minakata, “76-ghz millimeter-wave generation using mz linbo3 modulator with drive voltage of 7 vp-p and 19 ghz signal input”, in *Int. Topic Meeting on Microwave Photonics (MWP 2005)*, 2005, pp. 1–4.
- [43] J. Yu, Z. Jia, L. Yi, T. Wang, and G. K. Chang, “Centralized lightwave radio-over-fiber system with photonic frequency quadrupling for high-frequency millimeter-wave generation”, *IEEE Photon. Technol. Lett.*, vol. 19, no. 19, pp. 1499–1501, 2007.
- [44] Z. Pan, S. Chandel, and C. Yu, “160 ghz optical pulse generation using a 40 ghz phase modulator and two stages of delayed mz interferometers”, in *Conf. Lasers Electro-Optics (CLEO 2006)*, 2006, p. CFP2.
- [45] A. Wiberg, P. Perez-Millan, M. V. Andres, and P. O. Hedekvist, “Microwave-photonic frequency multiplication utilizing optical four-wave mixing and fiber bragg gratings”, *IEEE J. Lightw. Technol.*, vol. 24, no. 1, pp. 329–334, 2006.

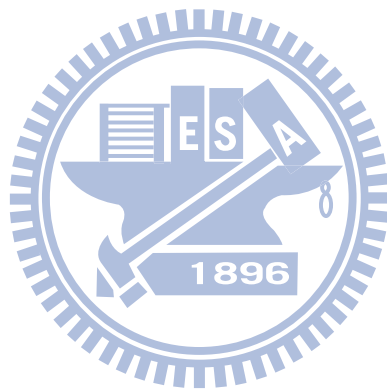
- [46] C. Yu, Z. Pan, T. Luo, Y. Wang, L. Christen, and A. E. Willner, “Beyond 40-ghz return-to-zero optical pulse-train generation using a phase modulator and polarization-maintaining fiber”, *IEEE Photon. Technol. Lett.*, vol. 19, no. 1, pp. 42–44, 2007.
- [47] T. Wang, M. Chen, H. Chen, J. Zhang, and S. Xie, “Millimeter-wave signal generation using two cascaded optical modulators and fwm effect in semiconductor optical amplifier”, *IEEE Photon. Technol. Lett.*, vol. 19, no. 16, pp. 1191–1193, 2007.
- [48] M. Mohamed, X. Zhang, B. Hraimel, and K. Wu, “Analysis of frequency quadrupling using a single mach-zehnder modulator for millimeter-wave generation and distribution over fiber systems”, *Opt. Express*, vol. 16, no. 14, pp. 10786–10802, 2008.
- [49] X. Wei, J. Leuthold, and L. Zhang, “Delay-interferometer-based optical pulse generator”, in *Optical Fiber Communication Conf. 2004 (OFC 2004)*, 2004, p. WL6.
- [50] G. Qi, J. Yao, Joe S., S. Paquet, and C. Belisle, “Optical generation and distribution of continuously tunable millimeter-wave signals using an optical phase modulator”, *IEEE J. Lightwave Technol.*, vol. 23, pp. 2687–2695, 2005.
- [51] G. Qi, J. Yao, J. Seregelyi, S. Paquet, and C. Belisle, “Generation and distribution of a wide-band continuously tunable millimeter-wave signal with an optical external modulation technique”, *IEEE Trans. on Microwave Theory and Tech.*, vol. 53, no. 10, pp. 3090–3097, 2005.
- [52] A. Wiberg, P. Perez-Millan, M. V. Andres, and Per Olof Hedekvist, “Microwave-photonic frequency multiplication utilizing optical four-wave mixing and fiber bragg gratings”, *IEEE J. Lightwave Technol.*, vol. 24, no. 1, pp. 329–334, 2006.

- [53] Q. Wang, H. Rideout, F. Zeng, and J. Yao, “Millimeter-wave frequency tripling based on four-wave mixing in a semiconductor optical amplifier”, *IEEE Photon. Technol. Lett.*, vol. 18, no. 23, pp. 2460–2462, 2006.
- [54] Z. Pan, S. Chandel, and C. Yu, “160 ghz optical pulse generation using a 40 ghz phase modulator and two stages of delayed mz interferometers”, in *Conf. Lasers and Electro-Optics (CLEO 2006)*, 2006, p. CFP2.
- [55] C. Yu, Z. Pan, T. Luo, T. Wang, L. Christen, and A. E. Willner, “Beyond 40-ghz return-to-zero optical pulse-train generation using a phase modulator and polarization-maintaining fiber”, *IEEE Photon. Technol. Lett.*, vol. 19, no. 1, pp. 42–44, 2007.
- [56] Z. Xu, X. Zhang, and J. Yu, “Frequency upconversion of multiple rf signals using optical carrier suppression for radio over fiber downlinks”, *Opt. Express*, vol. 15, no. 25, pp. 16737–16747, 2007.
- [57] A. Hirata, H. Takahashi, R. Yamaguchi, T. Kosugi, K. Murata, T. Nagatsuma, N. Kukutsu, and Y. Kado, “Transmission characteristics of 120-ghz-band wireless link using radio-on-fiber technologies”, *IEEE J. Lightw. Technol.*, vol. 26, pp. 2338–2344, 2008.
- [58] H. C. Chien, A. Chowdhury, Z. Jai, Y. T. Hsueh, and G. K. Chang, “Long-reach 60-ghz mm-wave optical-wireless access network using remote signal regeneration and upconversion”, in *European Conf. on Optical Communication (ECOC 2008)*, 2008, pp. 137–138.
- [59] J. Y. Kim, C. S. Choi, W. Y. Choi, H. Kamitsuna, M. Ida, and K. Kurishima, “Characteristics of inp-ingaas hpt-based optically injection-locked self-oscillating optoelectronic mixers and their influence on radio-over-fiber system performance”, *IEEE Photon. Technol. Lett.*, vol. 19, pp. 155–157, 2007.

- [60] M. Tsuchiya and T. Hosida, “Nonlinear photodetection scheme and its system applications to fiber-optic millimeter-wave wireless down-links”, *IEEE Trans. Microwave Theory Tech.*, vol. 47, 1999.
- [61] A. Hirata, T. Furuta, H. Ito, and T. Nagatsuma, “10-gb/s millimeter-wave signal generation using photodiode bias modulation”, *IEEE J. Lightw. Technol.*, vol. 24, pp. 1725–1731, 2006.
- [62] H. Fushimi, T. Furuta, T. Ishibashi, and H. Ito, “Photoresponse nonlinearity of a uni-traveling-carrier photodiode and its application to optoelectronic millimeter-wave mixing in 60ghz band”, *Jpn. J. Appl. Phys*, vol. 43, pp. L966–L968, 2004.
- [63] J. W. Shi, Y. S. Wu, and Y. S. Lin, “Near-ballistic uni-traveling-carrier photodiode based v-band optoelectronic mixers with internal up-conversion-gain, wide modulation bandwidth, and very high operation current performance”, *IEEE Photon. Technol. Lett.*, vol. 20, pp. 939–941, 2008.
- [64] F. M. Kuo, Y. S. Wu, and J. W. Shi, “Near-ballistic unitraveling-carrier photodiode-based v-band optoelectronic mixers with low upconversion loss and high operation current performance under optical if signal injection”, *IEEE Electron Device Lett.*, vol. 30, pp. 21–23, 2009.
- [65] J. W. Shi, C. Y. Wu, Y. S. Wu, P. H. Chiu, and C. C. Hong, “High-speed, high-responsivity, and high-power performance of near-ballistic uni-traveling-carrier photodiode at 1.55 μm wavelength”, *IEEE Photon. Technol. Lett.*, vol. 17, pp. 1929–1931, 2005.
- [66] Y. S. Wu and J. W. Shi, “Dynamic analysis of high-power and high-speed near-ballistic unitraveling carrier photodiodes at w-band”, *IEEE Photon. Technol. Lett.*, vol. 20, pp. 1160–1162, 2008.

- [67] H. Ito, S. Kodama, Y. Muramoto, T. Furuta, T. Nagatsuma, and T. Ishibashi, “High-speed and high-output inp-ingaas unitraveling-carrier photodiodes”, *IEEE J. of Sel. Topics in Quantum Electronics*, vol. 10, pp. 709–727, 2004.
- [68] R. Nagarajan, C. H. Joyner, R. P. Schneider, J. S. Bostak Jr., T. Butrie, A. G. Dentai, V. G. Dominic, P. W. Evans, M. Kato, M. Kauffman, D. J. H. Lambert, S. K. Mathis, A. Mathur, R. H. Miles, M. L. Mitchell, M. J. Missey, S. Murthy, A. C. Nilsson, F. H. Peters, S. C. Pennypacker, J. L. Pleumeekers, R. A. Salvatore, R. K. Schlenker, R. B. Taylor, H. S. Tsai, M. F. Van Leeuwen, J. Webjorn, M. Ziari, D. Perkins, J. Singh, S. G. Grubb, M. S. Reffle, D. G. Mehuys, F. A. Kish, and D. F. Welch, “Large-scle photonic integrated circuits”, *IEEE J. Sel. Top. Quan. Electron.*, vol. 11, no. 1, pp. 50–65, 2005.
- [69] J. Yu, Z. Jia, L. Xu, L. Chen, T. Wang, and G. K. Chang, “Dwdm optical millimeter-wave generation for radio-over-fiber using an optical phase modulator and an optical interleaver”, *IEEE Photon. Technol. Lett.*, vol. 18, no. 13, pp. 1418–1420, 2006.
- [70] C. Lim, M. Attygalle, A. Nirmalathas, D. Novak, and R. Waterhouse, “Analysis of optical carrier-to-sideband ratio for improving transmission performance in fiber-radio links”, *IEEE Trans. on Microw. Theory and Tech.*, vol. 54, no. 5, pp. 2181–2187, 2006.
- [71] C. T. Lin, S. P. Dai, J. Chen, P. T. Shih, P. C. Peng, and S. Chi, “A novel direct detection microwave photonic vector modulation scheme for radio-over-fiber system”, *IEEE Photon. Technol. Lett.*, vol. 20, pp. 1106–1108, 2008.
- [72] C. T. Lin, E. Z. Wong, W. J. Jiang, P. T. Shih, J. Chen, and S. Chi, “28-gb/s 16-qam ofdm radio-over-fiber system within 7-ghz license-free band at 60 ghz

- employing all-optical up-conversion”, in *The Conference on Lasers and Electro-Optics (CLEO 2009)*, 2009, pp. PDP, CPDA8.
- [73] G. H. Nguyen, B. Cabon, and Y. L. Guennec, “Generation of 60-ghz mb-ofdm signal-over-fiber by up-conversion using cascaded external modulators”, *IEEE J. Lightw. Technol.*, vol. 27, no. 11, pp. 1496–1502, 2009.
- [74] V. Shukla, “Fiber to the home: a carrier perspective”, in *European Conf. on Optical Communication (ECOC 2008)*, 2008, p. Tu.1.F.1.
- [75] J. B. Jensen, X. Yu, I. T. Monroy, C. Peucheret, and P. Jeppesen, “Combined transmission of baseband nrz-dqpsk and phase modulated radio-over-fibre”, in *European Conf. on Optical Communication (ECOC 2008)*, 2007, p. Tu.4.F.3.
- [76] F. Xiong, “Digital modulation techniques ed. 2nd”, *Artech House, INC.*, 2006.
- [77] V. J. Urick, J. X. Qie, and F. Bucholtz, “Wide-band qam-over-fiber using phase modulation and interferometric demodulation”, *IEEE Photon. Technol. Lett.*, vol. 16, no. 10, pp. 2374–2376, 2004.



PUBLICATION LIST

International Journals (SCI Journal Paper)

1. W. J. Jiang, C. T. Lin, **P. T. Shih**, L. Y. Wang-He, J. Chen, and S. Chi, "Simultaneous generation and transmission of 60 GHz wireless and baseband wireline signals with uplink transmission using an RSOA," Accepted by *IEEE Photonics Technology Letters*.
2. C. T. Lin, J. Chen, **P. T. Shih**, W. J. Jiang, and S. Chi, "Ultra-high data-rate (>10 Gb/s) 60 GHz radio-over-fiber systems employing optical frequency multiplication and OFDM formats," Accepted by *Journal of Lightwave Technology*. (Invited Paper)
3. W. J. Jiang, C. T. Lin, A. Ng'oma, **P. T. Shih**, J. Chen, M. Sauer, F. Annunziata, and S. Chi, "Simple 14 Gbps short-range radio-over-fiber system employing a single-electrode MZM for 60 GHz wireless applications," Accepted by *Journal of Lightwave Technology*.
4. **P. T. Shih**, C. T. Lin, W. J. Jiang, H. S. Huang, J. Chen, A. Ng'oma, M. Sauer, and S. Chi, "Transmission of 20-Gb/s OFDM signals occupying 7-GHz license-free band at 60 GHz using a RoF system employing frequency sextupling optical up-conversion," *OSA Optics Express*, vol. 18, No. 12, pp. 12752–12755, Jun. 7, 2010.
5. W. J. Jiang, C. T. Lin, **P. T. Shih**, Y. H. Chen, J. Chen, and S. Chi, "Transmission of wireless and wired services employing a simple system architecture," *IEEE Photonics Technology Letters*, vol. 22, No. 8, pp. 532–534, Apr. 15, 2010.
6. W. J. Jiang, C. T. Lin, **P. T. Shih**, J. Chen, P. C. Peng, and S. Chi, "A full duplex radio-over-fiber link with multi-level OFDM signal via a single-electrode MZM

- and wavelength reuse with a RSOA,” *OSA Optics Express*, vol. 18, No. 3, pp. 2170–2718, Feb. 1, 2010.
7. ***P. T. Shih***, C. T. Lin, W. J. Jiang, J. Chen, H. S. Huang, P. C. Peng, and S. Chi, “Optical millimeter-wave signal generation beyond 100 GHz via frequency 12-tupling,” *IEEE Journal of Lightwave Technology*, vol. 28, No. 1, pp. 71–78, Jan. 1, 2010.
 8. C. T. Lin, ***P. T. Shih***, W. J. Jiang, J. Chen, P. C. Peng, and S. Chi, “A continuously tunable and filterless optical millimeter-wave generation via frequency octupling,” *OSA Optics Express*, vol. 17, No. 22, pp. 19749–19756, Oct. 26, 2009.
 9. ***P. T. Shih***, C. T. Lin, W. J. Jiang, Y. H. Chen, J. Chen, and S. Chi, “Full duplex 60-GHz RoF link employing tandem single sideband modulation scheme and high spectral efficiency modulation format,” *OSA Optics Express*, vol. 17, No. 22, pp. 19501–19508, Oct. 26, 2009.
 10. F. M. Kuo, J. W. Shi, S. N. Wang, N. W. Chen, ***P. T. Shih***, C. T. Lin, W. J. Jiang, E. Z. Wong, J. Chen, and S. Chi, “W-band wireless data transmission by the integration of a near-ballistic unitraveling-carrier photodiode with a horn antenna fed by a quasi-Yagi radiator,” *IEEE Electron Device Letters*, vol. 30, No. 11, pp. 1167–1169, Nov., 2009.
 11. J. W. Shi, F. M. Kuo, Y. S. Wu, N. W. Chen, ***P. T. Shih***, C. T. Lin, W. J. Jiang, E. Z. Wong, J. Chen, and S. Chi, “A W-band photonic transmitter-mixer based on high-power near-ballistic uni-traveling-carrier photodiodes for BPSK and QPSK data transmission under bias modulation,” *IEEE Photonics Technology Letters*, vol. 21, No. 15, pp. 1039–1041, Aug. 15, 2009.
 12. C. T. Lin, ***P. T. Shih***, J. Chen, S. P. Dai, P. C. Peng, Y. L. Ho, and S. Chi, “Optical millimeter-wave up-conversion employing frequency quadrupling without optical

- filtering,” *IEEE Transactions on Microwave Theory and Techniques*, vol. 57, No. 8, pp. 2084–2092, Aug., 2009 .
13. C. T. Lin, ***P. T. Shih***, W. J. Jiang, E. Z. Wong, J. Chen, and S. Chi, “Photonic vector signal generation at microwave/millimeter-wave band employing optical frequency quadrupling scheme,” *OSA Optics Letters*, vol. 34, No. 14, pp. 2171–2173, Jul. 15, 2009.
 14. ***P. T. Shih***, C. T. Lin, W. J. Jiang, Y. H. Chen, J. Chen, and S. Chi, “Hybrid access network integrated with wireless multi-level vector and wired baseband signals using frequency doubling and no optical filtering,” *IEEE Photonics Technology Letters*, vol. 21, No. 13, pp. 857–859, Jul. 1, 2009.
 15. P. C. Peng, F. M. Wu, W. J. Jiang, R. L. Lan, C. T. Lin, J. Chen, ***P. T. Shih***, G. R. Lin, and S. Chi, “RF phase shifter using a distributed feedback laser in microwave transport systems,” *OSA Optics Express*, vol. 17, No. 9, pp. 7609–7614, Apr. 27, 2009.
 16. J. Chen, C. T. Lin, ***P. T. Shih***, W. J. Jiang, S. P. Dai, Y. M. Lin, P. C. Peng, and S. Chi, “Generation of optical millimeter-wave signals and vector formats using an integrated optical I/Q modulator,” *OSA Journal of Optical Networking*, vol. 8, No. 2, pp. 188–200, Feb., 2009. (Invited Paper)
 17. ***P. T. Shih***, C. T. Lin, J. Chen, H. S. Huang, Y. H. Chen, P. C. Peng, and S. Chi, “WDM optical up-conversion system providing wired and wireless services employing frequency quadrupling technique,” *OSA Optics Express*, vol. 17, No. 3, pp. 1726–1733, Feb. 2, 2009.
 18. C. T. Lin, Y. M. Lin, J. Chen, S. P. Dai, ***P. T. Shih***, P. C. Peng, and S. Chi, “Optical direct-detection OFDM signal generation for radio-over-fiber link using frequency

- doubling scheme with carrier suppression,” *OSA Optics Express*, vol. 16, No. 9, pp. 6056–6063, Apr. 28, 2008.
19. C. T. Lin, S. P. Dai, J. Chen, ***P. T. Shih***, P. C. Peng, and S. Chi, “A novel direct detection microwave photonic vector modulation scheme for radio-over-fiber system,” *IEEE Photonics Technology Letters*, vol. 20, No. 13, pp. 1106–1108, Jul. 1, 2008.
20. C. T. Lin, ***P. T. Shih***, J. Chen, W. Q. Xue, P. C. Peng, and S. Chi, “Optical millimeter-wave signal generation using frequency quadrupling technique and no optical filtering,” *IEEE Photonics Technology Letters*, vol. 20, No. 12, pp. 1027–1029, Jun. 15, 2008.
21. C. T. Lin, ***P. T. Shih***, J. Chen, P. C. Peng, S. P. Dai, W. J. Jiang, W. Q. Xue, and S. Chi, “Cost-effective multi-services hybrid access networks with no optical filter at remote nodes,” *IEEE Photonics Technology Letters*, vol. 20, No. 10, pp. 812–814, May. 15, 2008.
22. C. T. Lin, P. C. Peng, ***P. T. Shih***, J. Chen, and S. Chi, “Distributed feedback laser in external light injection scheme for tunable slow light,” *Japanese Journal of Applied Physics*, vol. 47, No. 6, pp. 4600–4601, 2008.
23. P. C. Peng, F. M. Wu, C. T. Lin, J. H. Chen, W. C. Kao, ***P. T. Shih***, W. J. Jiang, H. C. Kuo, and S. Chi, “40 GHz phase shifter based on semiconductor laser,” *IEE Electronics Letters*, vol. 44, No. 8, pp. 520–521, Apr., 2008.
24. P. C. Peng, C. T. Lin, W. J. Jiang, J. Chen, F. M. Wu, ***P. T. Shih***, and S. Chi, “Improvement of transmission in fiber wireless system using semiconductor laser amplifier,” *IEE Electronics Letters*, vol. 44, No. 4, pp. 298–299, Feb., 2008.

25. C. T. Lin, W. J. Jiang, J. Chen, ***P. T. Shih***, P. C. Peng, E. Z. Wong, and S. Chi, “Novel optical vector signal generation with carrier suppression and frequency multiplication based on a single-electrode mach-zehnder modulator,” *IEEE Photonics Technology Letters*, vol. 20, No. 24, pp. 2060–2062, Dec. 15, 2008.
26. C. W. Luo, C. C. Hsieh, Y.-J. Chen, ***P. T. Shih***, M. H. Chen, K. H. Wu, J. Y. Juang, J.-Y. Lin, T. M. Uen, and Y. S. Gou, “Spatial dichotomy of quasiparticle dynamics in underdoped thin-film $\text{YBa}_2\text{Cu}_3\text{O}_{7-\delta}$ superconductors,” *Physical Review B*, vol. 74, No. 18, 184525, Nov. 22, 2006.
27. C. W. Luo, ***P. T. Shih***, Y.-J. Chen, M. H. Chen, K. H. Wu, J. Y. Juang, J.-Y. Lin, T. M. Uen, and Y. S. Gou, “Spatially resolved relaxation dynamics of photoinduced quasiparticles in underdoped $\text{YBa}_2\text{Cu}_3\text{O}_{7-\delta}$,” *Physical Review B*, vol. 72, No. 9, 092506, Sep. 15, 2005.

International conferences

1. W. J. Jiang, C. T. Lin, ***P. T. Shih***, L. Y. Wang He, J. Chen, and S. Chi, “Hybrid signal generation and transmission of 60 GHz wireless and baseband wireline system,” *OptoElectronics and Communications Conference 2010 (OECC 2010)*, No. 8P-07, Sapporo, Japan, 2010.
2. A. Ng’oma, ***P. T. Shih***, J. George, F. Annunziata, M. Sauer, C. T. Lin, W. J. Jiang, J. Chen, and S. Chi, “21 Gbps OFDM wireless signal transmission at 60 GHz using a simple IMDD radio-over-fiber system,” *2010 Optical Fiber Communication Conference (OFC 2010)*, OTuF4, San Diego, California, March 21–25, 2010.
3. A. Ng’oma, M. Sauer, F. Annunziata, W. J. Jiang, ***P. T. Shih***, C. T. Lin, J. Chen, and S. Chi, “14 Gbps 60 GHz RoF link employing a simple system architecture and OFDM modulation,” *2009 International Topical Meeting on Microwave Photonics (MWP 2009)*, Fr1.3, Valencia, Spain, October 14–16, 2009.

4. **P. T. Shih**, C. T. Lin, H. S. Huang, W. J. Jiang, J. Chen, A. Ng'oma, M. Sauer, and Sien Chi, "13.75-Gb/s OFDM signal generation for 60-GHz RoF system within 7-GHz license-free band via frequency sextupling," *35nd European Conference on Optical Communication (ECOC 2009)*, Paper 4.5.4, Vienna, Austria, September 20–24, 2009.
5. **P. T. Shih**, C. T. Lin, H. S. Huang, W. J. Jiang, D. Z. Hsu, J. Chen, F. M. Kuo, N. W. Chen, J. W. Shi, and S. Chi, "W-band 3.75-Gb/s 8PSK wireless signal generation and transmission via optical frequency octupling and bias modulation of NBUTC-PD with feed-forward equalizer," *35nd European Conference on Optical Communication (ECOC 2009)*, Paper P3.14, Vienna, Austria, September 20–24, 2009.
6. W. J. Jiang, C. T. Lin, E. Z. Wong, **P. T. Shih**, J. Chen, and S. Chi, "A novel optical direct-detection I/Q up-conversion with I/Q imbalance compensation via gram-schmidt orthogonalization procedure," *35nd European Conference on Optical Communication (ECOC 2009)*, Paper 10.5.2, Vienna, Austria, September 20–24, 2009.
7. W. J. Jiang, C. T. Lin, Y. H. Chen, **P. T. Shih**, D. Z. Hsu, J. Chen, and S. Chi, "Simultaneous generation and transmission of 60-GHz RF and baseband signals employing only a simple single electrode MZM," *35nd European Conference on Optical Communication (ECOC 2009)*, Paper 4.5.2, Vienna, Austria, September 20–24, 2009.
8. C. T. Lin, E. Z. Wong, W. J. Jiang, **P. T. Shih**, J. Chen, S. Chi, "28-Gb/s 16-QAM OFDM radio-over-fiber system within 7-GHz license-free band at 60 GHz employing all-optical up-conversion," *Conference on Lasers and Electro-Optics (CLEO/QELS 2009)*, CPDA8, Maryland, Baltimore, May 31–June 5, 2009. (Post-

deadline Paper)

9. **P. T. Shih**, C. T. Lin, Y. H. Chen, W. J. Jiang, J. Chen, and Sien Chi, "Hybrid access network integrated with multi-level RF vector signal and baseband signal without optical filtering," *2009 Optical Fiber Communication Conference (OFC 2009)*, OTuB5, San Diego, California, Mar. 24–26, 2009.
10. **P. T. Shih**, C. T. Lin, W. J. Jiang, E. Z. Wong, J. Chen, S. Chi, Y. S. Wu, F.M. Kuo, N. W. Chen, and J. W Shi, "W-Band vector signal generation via optical millimeter-wave generation and direct modulation of NBUTC-PD," *2009 Optical Fiber Communication Conference (OFC 2009)*, OWP4, San Diego, California, Mar. 24–26, 2009.
11. C. T. Lin, **P. T. Shih**, Y. H. Chen, W. J. Jiang, J. Chen, and S. Chi, "Experimental demonstration of 10-Gb/s OFDM-QPSK signal at 60 GHz using frequency-doubling and tandem SSB modulation," *2009 Optical Fiber Communication Conference (OFC 2009)*, OMV7, San Diego, California, Mar. 24–26, 2009.
12. W. J Jiang, C.T. Lin, H. S. Huang, **P. T. Shih**, J. Chen, and S Chi, "Experimental demonstration of a novel filterless frequency quadrupling technique for colorless WDM millimeter-wave up-conversion systems," *2009 Optical Fiber Communication Conference (OFC 2009)*, JWA75, San Diego, California, Mar. 24–26, 2009.
13. W. J Jiang, C. T Lin, H. S. Huang, **P. T. Shih**, J. Chen, and S. Chi, "60-GHz photonic vector signal generation employing frequency quadrupling scheme for radio-over-fiber link," *2009 Optical Fiber Communication Conference (OFC 2009)*, OWF1, San Diego, California, Mar. 24–26, 2009.
14. A. Ng'oma, M. Sauer, F. Annunziata, W. J. Jiang, C. T. Lin, J. Chen, **P. T. Shih**, and S. Chi, "Simple multi-Gbps 60 GHz radio-over-fiber links employing optical and

- electrical data up-conversion and feed-forward equalization,” *2009 Optical Fiber Communication Conference (OFC 2009)*, OWF2, San Diego, California, Mar. 24–26, 2009.
15. P. C. Peng, S. K. Yeh, F. M. Wu, J. Chen, C. T. Lin, W. J. Jiang, ***P. T. Shih***, H. C. Kuo, and S. Chi, “Tunable photonic microwave filter using slow light in vertical cavity surface emitting laser,” *2009 Optical Fiber Communication Conference (OFC 2009)*, JWA58, San Diego, California, Mar. 24–26, 2009.
 16. Y. S. Wu, F. M. Kuo, S. N. Wang, N. W. Chen, J. Wei Shi, ***P. T. Shih***, C. T. Lin, W. J. Jiang, E. Z. Wong, J. Chen, and Sien Chi, “A W-band photonic transmitter-mixer based on high-power near-ballistic uni-traveling-carrier photodiode (NBUTC-PD) for 1.25-Gb/s BPSK data transmission under bias modulation,” *2009 Optical Fiber Communication Conference (OFC 2009)*, OWX3, San Diego, California, Mar. 24–26, 2009.
 17. ***P. T. Shih***, C. T. Lin, J. Chen, P. C. Peng, and S. Chi, “Hybrid access networks integrated with wireline and wireless signals without optical filtering at remote nodes,” *34th European Conference on Optical Communication (ECOC 2008)*, Tu.4.F.7, Brussels, Belgium, Sep. 21–25, 2008.
 18. ***P. T. Shih***, C. T. Lin, J. Chen, P. C. Peng, and S. Chi, “WDM optical millimeter-wave up-conversion using external modulator with frequency quadrupling,” *34th European Conference on Optical Communication (ECOC 2008)*, P.3.3, Brussels, Belgium, Sep. 21–25, 2008.
 19. C. T. Lin, S. P. Dai, W. J. Jiang, J. Chen, Y. M. Lin, ***P. T. Shih***, P. C. Peng, and S. Chi, “Experimental demonstration of optical colorless direct-detection OFDM signals with 16- and 64-QAM formats beyond 15 Gb/s,” *34th European Conference on Optical Communication (ECOC 2008)*, Mo.3.E.1, Brussels, Belgium, Sep.

- 21–25, 2008.
20. C. T. Lin, W. J. Jiang, J. Chen, E. Z. Wong, S. P. Dai, Y. M. Lin, ***P. T. Shih***, P. C. Peng, and S. Chi, “Experimental demonstration of optical 5-Gb/s 16-QAM OFDM signal generation and wavelength reuse for 1.25-Gbit/s uplink signal,” *34th European Conference on Optical Communication (ECOC 2008)*, We.1.F.3, Brussels, Belgium, Sep. 21–25, 2008.
 21. P. C. Peng, W. C. Kao, J. Chen, F. M. Wu, C. T. Lin, ***P. T. Shih***, and S. Chi, “Tunable slow light in semiconductor optical amplifier without external pump laser,” *34th European Conference on Optical Communication (ECOC 2008)*, P.7.1, Brussels, Belgium, Sept. 21–25, 2008.
 22. P. C. Peng, F. M. Wu, W. J. Jiang, C. T. Lin, J. H. Chen, ***P. T. Shih***, W. C. Kao, and S. Chi, “Slow light in distributed feedback laser for all-optical inverter,” *2008 Slow and Fast Light Topical Meeting (SL 2008)*, JMB29, Boston, Massachusetts, Jul. 13–16, 2008.
 23. C. T. Lin, W. J. Jiang, E. Z. Wong, J. Chen, ***P. T. Shih***, P. C. Peng, and S. Chi, “Optical vector signal generation using double sideband with carrier suppression and frequency multiplication,” *Conference on Lasers and Electro-Optics (CLEO/QELS 2008)*, CThR5, San Jose, California, May. 4–9, 2008.
 24. P. C. Peng, F. M. Wu, C. T. Lin, J. Chen, ***P. T. Shih***, W. C. Kao, W. J. Jiang, H. C. Kuo, and S. Chi, “Tunable slow light in quantum well vertical-cavity surface-emitting laser at 40 GHz,” *Conference on Lasers and Electro-Optics (CLEO/QELS 2008)*, JThA2, San Jose, California, May. 4–9, 2008.
 25. C. T. Lin, Y. M. Lin, J. Chen, S. P. Dai, P. C. Peng, ***P. T. Shih***, and S. Chi, “Generation of direct-detection optical OFDM signal for radio-over-fiber link using fre-

- quency doubling scheme with carrier suppression,” *2008 Optical Fiber Communication Conference (OFC 2008)*, OMM5, San Diego, California, Feb. 24–28, 2008.
26. C. T. Lin, ***P. T. Shih***, J. Chen, P. C. Peng, S. P. Dai, W. Q. Xue, and S. Chi, “Generation of carrier suppressed optical mm-wave signals using frequency quadrupling and no optical filtering,” *2008 Optical Fiber Communication Conference (OFC 2008)*, JThA73, San Diego, California, Feb. 24–28, 2008.
27. P. C. Peng, C. T. Lin, W. J. Jiang, J. Chen, ***P. T. Shih***, F. M. Wu, and S. Chi, “Transmission improvement in fiber radio links using semiconductor laser,” *2008 Optical Fiber Communication Conference (OFC 2008)*, JThA68, San Diego, California, Feb. 24–28, 2008.
28. P. C. Peng, W. C. Kao, C. T. Lin, J. Chen, ***P. T. Shih***, and S. Chi, “Fast light improvement using periodic bending of erbium-doped fiber,” *2008 Optical Fiber Communication Conference (OFC 2008)*, JThA2, San Diego, California, Feb. 24–28, 2008.

